Coordination Chemistry Reviews 523 (2025) 216147

Contents lists available at ScienceDirect

Coordination Chemistry Reviews

journal homepage: www.elsevier.com/locate/ccr

Utilizing the metal coordination and supramolecular chemistry of macrocycles to tackle medicinal issues

Carl Redshaw *

Chemistry, School of Natural Sciences, The University of Hull, Cottingham Rd, Hull HU6 7RX, UK

ARTICLE INFO

Keywords:
Macrocycle
Metal
Health
Calixarene
Cucurbituril
Pillarene
Cyclodextrin
Schiff-base

ABSTRACT

In this review, recent (post-2018) prominent examples of metal coordination and/or supramolecular chemistry of macrocycles, which have been employed against a variety of diseases are highlighted. The broad range of macrocycles available as well as their facile modification and, in some cases, the ability to act as hosts is leading to a growth in the use of macrocyclic metal-based agents against a number of common health issues as well as some of the lesser-known ailments. The focus here is mostly on the use of systems comprised of either calixarenes or cucurbiturils, but we also note some of the highlights that have emerged from the use of other metal-containing macrocyclic systems such as those based on pillarenes, cyclodextrins, crown ethers, and Schiff-base macrocycles. Much of the work is centered around improving the delivery and effectiveness of metal-containing anti-cancer drugs, particularly those based on platinum, however, there have also been advances in a number of other areas such as their use as agents against bacteria, TB or HIV. A significant body of work has also been conducted in conjunction with nanoparticles, where the surface of the nanoparticles has been modified with a view to subsequent use in medicine.

1. Introduction

Over recent decades, much use has been made of macrocycles and organic derivatives thereof in the medicinal arena. For some areas such as medical imaging, macrocyclic research has made great strides in developing new metal agents capable of impressive medical intervention, and such work has been reviewed elsewhere [1–4]. Indeed, the use of metal agents, both macrocyclic and acyclic, against a range of specific diseases has been reviewed, including cancer [5–8], tuberculosis [9,10], HIV [11], Parkinson's Disease [12], as well as their use as antibiotics [13], and as antibacterial and antimicrobial agents [14–16]. A number of recent reviews covering the use of particular macrocycles for medical applications have also appeared and these include 'Applications of Cucurbiturils in Medicinal Chemistry', 'Role of Calixarene in Chemotherapy Delivery Strategies', 'Challenges and Opportunities of Functionalized Cucurbiturils for Biomedical Applications', 'Functionalized Calixarenes as Promising Antibacterial Drugs to Face Antimicrobial Resistance', 'Cucurbituril-Based Supramolecular Assemblies: Prospective on Drug Delivery, Sensing, Separation, and Catalytic Applications' and 'Pharmaceutical properties of macrocyclic Schiff base transition metal complexes: Urgent need in Today's World' [17–40]. The use of supramolecular chemistry has also been reviewed by a number of groups for a variety of applications related to medical issues [41–62]. However, with the exception of radionuclide work, and breakthroughs such as cisplatin [63], far less attention has been given to utilizing the ability of macrocycles to either capture metals or to use bound metal species in medicine. Only in recent times has the host-guest chemistry and the coordination chemistry of macrocycles began to capture the imagination of researchers.

The ability to tune the properties of a metal center by modifying its coordination sphere has proved to be of crucial importance across a range of applications including battling diseases [64], where the steric and electronic properties of the ligands present can help dictate not only the degree of nuclearity of the system, but can also help to improve stability under various environments as well as enhance the ability of the metal agent to target specific species/regions. Moreover, properties such as solubility and thermal stability can readily be modified by judicious choice of ligand set. The same is true in supramolecular chemistry, where the formation of host-guest complexes has proved to be useful and has led to enhanced stability, lower toxicity and a lowering of drug resistance. Issues relating to drug resistance have been highlighted in a number of recent reviews [65–69]. The desirable features outlined

* Corresponding author.
E-mail address: C.Redshaw@hull.ac.uk.

https://doi.org/10.1016/j.ccr.2024.216147
Received 27 June 2024; Received in revised form 6 August 2024; Accepted 7 August 2024
Available online 11 October 2024

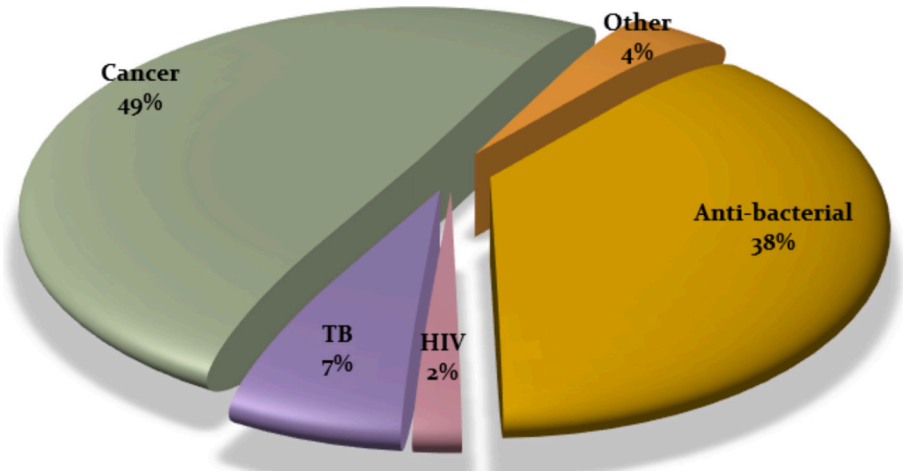

Chart 1. Breakdown of the medical issues tackled by the macrocyclic/metal systems described in this review. Others include Alzheimer's, anti-epidemic, pain killer, eye lens protection.

above have led to a growth in interest in the design and use of metal-based agents that utilize macrocyclic ligation and/or host-guest chemistry, with the overall aim being to improve the performance of metal-based drugs.

Herein, we discuss some of the metal-based macrocyclic systems that have been reported over the last 5 years and have been utilized against a range of diseases (Chart 1). This includes systems where the metal can be used as part of a drug, or embedded in the macrocycle, employed as an imaging system or as a support in functionalized metal nanoparticles. It is hoped that this review will stimulate other researchers by highlighting how the use of coordination and/or supramolecular chemistry of macrocycles has the potential to open-up new opportunities to contribute to our understanding of, and ultimately the defeat of, many diseases. The structure of the review is such that macrocyclic metal agents are discussed in terms of application, starting with drug performance enhancement, and then where possible each section is sub-divided into macrocyclic type.

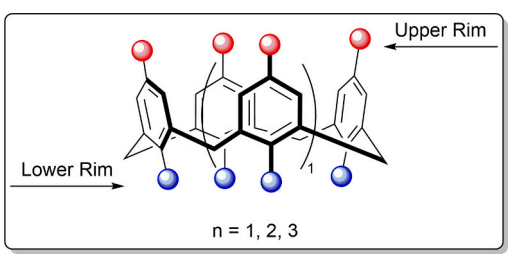

Fig. 1. Depiction of the structure of calix[4]arene. In this review, methylene bridged calix[4, 5 and 6]arenes (*i.e.* $n = 1$–3 above) and sulfonyl-bridged calix[4]arenes are discussed. A variety of upper rim groups are employed including H, *t*Bu, SO_3H, SO_3Na, $CH_2PO_3H_2$, $NHC(NH)NH_3^+$, $CH_2 = CHC_5H_4NMe^+$, vinylpyridinium and lower rim substituents including hexyl, dodecyl, acetoymethyl.

2. Supramolecular enhancement of platinum-based drug performance

The use of macrocyclic host-guest chemistry to enhance the performance of drug molecules *via*, for example, extending their lifetime was reviewed back in 2017 [70]. Since that time, a number of other exciting supramolecular systems have been reported that can improve the properties of metal-based drugs and e.g. Fig. 2.

2.1. Calixarenes

Calixarenes are phenolic macrocycles with between 4 and 20 phenol groups typically linked with methylene bridges, and possess hydrophobic cavities, Fig. 1. Although dating back to the mid-19th century and the work of von Baeyer, modern calixarene chemistry stems for the work of Gutsche in the 1970s [71]. Most reports involve the use of the more common and readily accessible (and hence cheaper) calix[4]arene system.

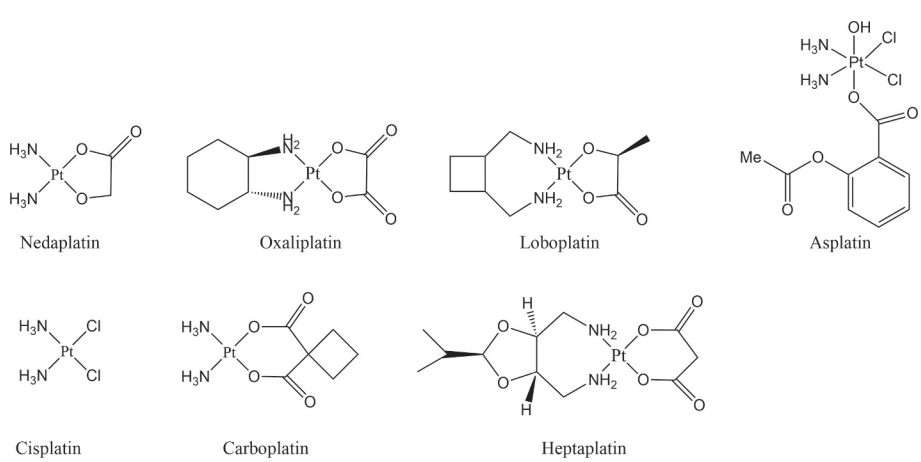

Fig. 2. The range of Pt-based drug complexes discussed herein.

2.1.1. Calix[4]arenes

Much work utilizing calixarenes and platinum-containing complexes was conducted prior to 2019 [72–78]. In more recent studies, Mo et al. showed that the phosphonated calixarene scaffold **1**, shown in Fig. 3, was capable of simultaneously capturing carboplatin (within the cavity) and paclitaxel (within the lower rim hexyl groups). The assembly was found to exhibit better cytotoxicity than either carboplatin (Fig. 2, bottom center) or paclitaxel alone against two colon cancer cell lines, and in mice exhibited HT-29 inhibition in tumors [79].

El-Said Azzazy et al. combined *p*-sulfocalix[4]arene (SC4) with asplatin (Fig. 2, top right) to form a 1:1 complex, and studied its drug release properties at pH 5.5. High cytotoxic activity was observed against MCF-7, HeLa (cervical) and A-549 (lung cancer cells) *in vitro*, with IC_{50} values of 0.75, 2.15 and 3.60 μg/mL, respectively; note that for free asplatin the corresponding values are 1.54, 5.05 and 3.91 μg/mL. The potential of the *p*-sulfocalix[4]arene@asplatin was further demonstrated by comparison with *p*-sulfocalix[4]arene@oxaliplatin and *p*-sulfocalix[4]arene@carboplatin, with stronger anticancer activity against MCF-7 cells exhibited by the asplatin host-guest complex (Table 1) [80].

Zhao, Gao et al. have investigated the use of nitrobenzooxadiazole glycocalix[4]arenes **2** as bio-probes and drug carriers (Fig. 4). Three derivatives were prepared utilizing glucose, galactose and mannose; the anomeric stereochemistry of the sugar was that of a single isomer (β-anomers for the glycose and galactose derivatives and an α-anomer for the mannose derivative). The scaffold acted as a targeting agent for the GLUT1 protein and was capable of delivering drugs such as cisplatin for selective tumor targeting. Excitation (375 nm) resulted in an emission peak at 510 nm allowing for the use of such systems as probes in diagnostic tumor imaging studies. *In vitro* studies (using HEK-293FT cells and GLUT1 transfected GLUT1-293FT cell lines) indicated that cellular uptake followed a concentration-dependent pathway, and best results were observed when using the mannose derivative. Using this mannose derivative, confocal microscopy studies revealed that internalization of **2** was based on a tumor specific Warburg effect/GLUT1-dependent recognition. The mannose derivative was then utilized for *in vivo* fluorescence imaging of tumor bearing mice (Fig. 5). The results revealed image contrast tumor-to-background ratios as high as 6.96:1, with fluorescent signals lasting up to 48 h in tumor tissues [81].

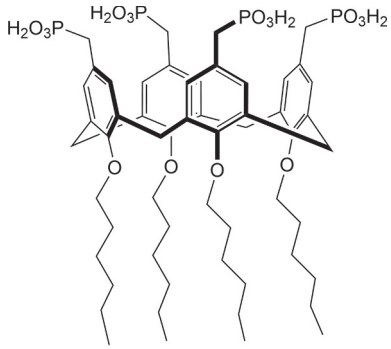

1

Fig. 3. Phosphonated calix[4]arene scaffold **1**.

Table 1
In vitro anti-cancer activity of *p*-sulfocalix[4]arene (SC4) in combination with a variety of Pt-based drugs.

Agent	IC_{50} (μg/mL) MCF-7	IC_{50} (μg/mL) A549
Oxaliplatin/SC4	1.56 ± 0.07	–
Carboplatin/SC4	4.3 ± 0.2	5. ± 0.4
Asplatin/SC4	0.75 ± 0.05	3.60 ± 0.32

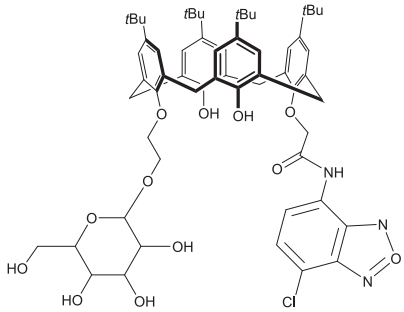

2

Fig. 4. Nitrobenzooxadiazole glycocalix[4]arenes **2** as bio-probes and drug carriers.

2.1.2. Calix[4]resorcinol

Calix[4]resorcinol consists of four resorcinol units arranged in cyclic form linked by a methylene bridge, Fig. 6 [82]. Kashapov et al. reported a metallosurfactant, which was comprised of two 4-aza-1-hexadecylazoniabicyclo[2.2.2]octane bromides and lanthanum nitrate, combined with a sulfonated calix[4]resorcinol (ratio 3:2). The resulting aggregate was capable of encapsulating cisplatin, and subsequent cells studies revealed increased cytotoxicity against M-HeLa tumor cells, but less cytotoxicity toward Chang liver cells [83].

2.1.3. Calix[5]arenes

Guo et al. utilized a pegylated guanidinium-modified calix[5]arene pentadodecyl ether **3** (Fig. 7) to form a nanosystem that is capable of tightly binding a variety of drug molecules *via* host-guest chemistry including the likes of oxaliplatin (Fig. 2, top, middle-left). Encapsulation and drug loading efficiency was better than that of liposomes, and better anticancer efficacy, *versus* the free drugs, was noted [84].

Other macrocycles have also been utilized to bring about improvement in cisplatin-type drug performance. Of these, cucurbituril-based systems are showing real potential and these are discussed in the next section.

2.2. Cucurbit[n]urils

Cucurbit[*n*]urils, abbreviated here as Q[*n*]s (some literature prefers the use of CB), being relatively new, are described as 4th generation macrocyclic hosts. They are comprised of glyoxal units linked *via* methylene bridges; n represents the number of glyoxylate units present, Fig. 8 [85]. The cytotoxicity of the Q[*n*]s (for $n = 5$, 6 and 7) has been evaluated against HaCat cells, and over 24 h, good biocompatibility was noted for the n = 5 and 6 systems (Table 2) [86].

Much work has been done recently on the use of Q[*n*]s as hosts for platinum-based drugs, and such systems tend to be based on either the Q[7] macrocycle or, to a lesser extent, the Q[8] system.

2.2.1. Cucurbit[7]urils

It has recently been shown using mononuclear cells obtained from donated blood that the host-guest complex formed between Q[7] and carboplatin (Fig. 2, bottom, middle) can decrease both the number of $FoxP3^+$ regulatory T cells present and the expression of CTLA-4 (compared to controls, *e.g.* Q[7] alone) [87].

The same cucurbituril was shown to form a host-guest complex with lobaplatin and was found to reduce the toxicity of lobaplatin (Fig. 2, top, middle-right) toward normal human intestinal cells at concentrations as high as 100.0 μM. Given the binding constant of lobaplatin with Q[7] is lower than that of spermine, it proved possible to displace the guest lobaplatin in the Q[7]@lobaplatin complex when in spermine solution. The host-guest system thus enabled the spermine to act as an *in vitro* biomarker tumor [88].

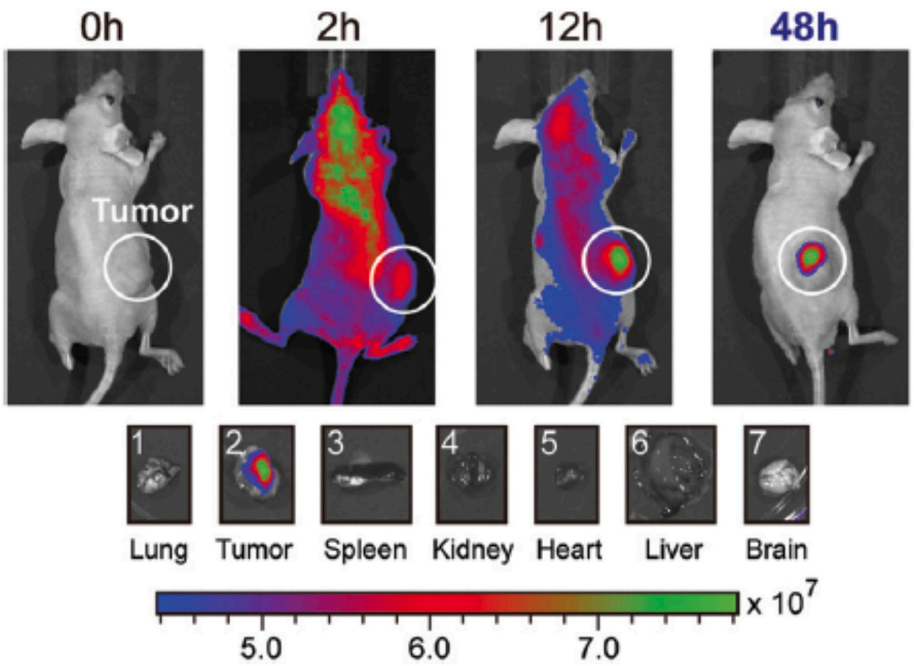

Fig. 5. *In vivo* fluorescent imaging using the mannose derivative of **2** on MDA-MB-468 tumor bearing BALB/c mice. Reproduced from reference 81 with permission from the Royal Society of Chemistry.

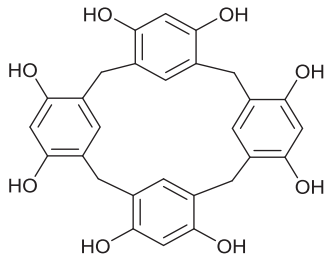

Fig. 6. Representation of the structure of calix[4]resorcinol.

Similarly, when the inclusion complex Q[7]@heptaplatin is exposed to a tumor environment (pH 6.0) where spermine is over expressed, the heptaplatin (Fig. 2, bottom right) is released from the Q[7] cavity. Indeed, use of the host-guest complex led to better results in terms of anti-tumor activity and cytotoxicity on colorectal normal cells than observed when using the heptaplatin on its own. Investigation of the *modus operandi* of the host-guest complex suggested that it exerted an inhibitory response during the cell cycle (at the G_1 phase) [89].

Earlier work by Sun, Zhang et al. showed how it was possible to employ a polymeric Q[7]-containing system **5** (see Fig. 9), whereby Q[7]s were linked *via* Click chemistry using an α,ω-diazide-PEG. It then proved possible to encapsulate oxaliplatin within the Q[7] cavities, and utilize the resulting polymeric complex for cell studies [90]. In the presence of cancer cells possessing excess spermine, for example colorectal cancer cells, the typical cytotoxicity of oxaliplatin was evident, whereas for normal cells, the polymeric system displayed lower cytotoxicity. By contrast, for cancer cells, the polymeric system **4** was more cytotoxic than oxaliplatin, which was thought to arise from reduced spermine local to the cancer cell combined with the presence of the released platinum drug. Furthermore, the polymeric species exhibited enhanced circulation *in vivo versus* the host-guest complex Q[7]@oxaliplatin.

Wang et al. reported the use of the Q[7] derived fluorescent AIE photosensitizer **5** (Fig. 10). This AIE photosensitizer was synthesized *via* the CuAAC-catalyzed Click coupling of the alkyne appended Q[7] and

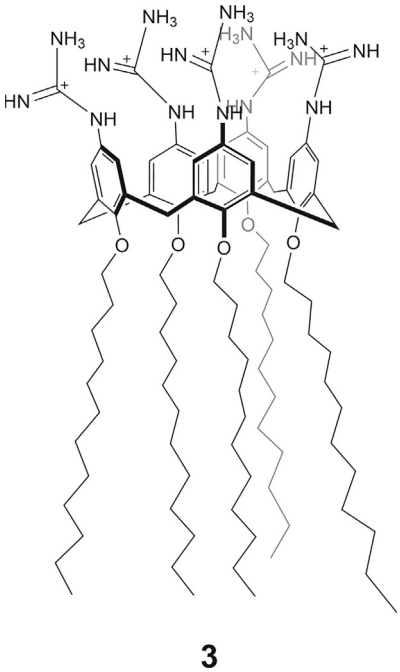

Fig. 7. Pegylated guanidinium-modified calix[5]arene pentadodecyl ether **3**.

the particular azide shown in the figure. The combination of hydrophilic and hydrophobic properties of this system led to its ability to form a transparent colloidal aqueous solution, *i.e.* it could spontaneously self-assemble in aqueous solution. This system was stable at ambient temperature for 3 days or more. The inherent fluorescence of the system allowed its cellular internalization to be monitored in A549 cells; efficient take up was evident (37 °C over 8 h) with localization predominantly in the lysosome. Under slightly acidic conditions, singlet oxygen generation could be enhanced, and this demonstrates the Photodynamic Therapy (PDT) potential of the system. Of more relevance to this review,

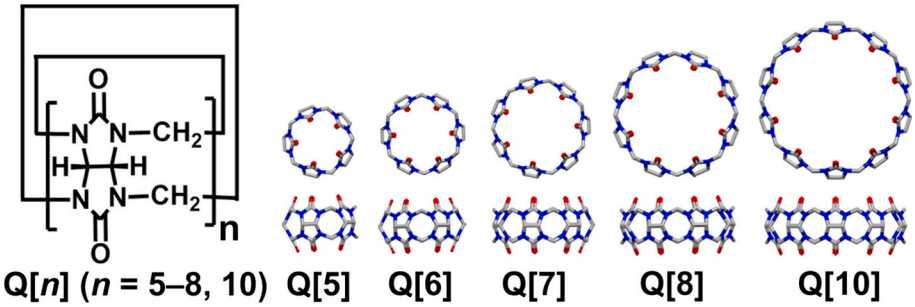

Fig. 8. Structures of cucurbit[*n*]urils Q[*n*]s (n = 5, 6, 7, 8, 10).

Table 2
Cytotoxicity of Q[*n*]s measured by flow cytometry.

Compound	Concentration mg/mL	Healthy cells (/%)	Apoptopic cells (%)	Dead cells (%)
Q[5]	15	85.7	4.8	9.5
Q[6]	30	89.5	4.4	6.1
Q[7]	7.5	67.9	24.3	7.8
(−)ve control		93.5	3.4	3.1
(+) control		56.8	32.9	10.3

the presence of the Q[7] cavity again allowed for the encapsulation of oxaliplatin; the loading efficiency was >96% (by ICP-MS). When employing cells with excess spermine present, the oxaliplatin could be efficiently displaced from the Q[7] cavity, and as evidenced for A549 cells, could then kill the majority of the cells. The anti-tumor efficacy of the system was as good as, if not better than, that of stand-alone oxaliplatin. Synergic PDT and chemotherapy effects (increased anti-cancer activity) were evident when the system was exposed to light irradiation [91].

Gao et al. have reported the 1:1 host-guest complex formed between Q[7] and nedaplatin, and found that it affords superior (up to 3-fold) cytotoxicity toward both A549 and HCT116 cells *versus* free nedaplatin (Fig. 2, top, left) (see Table 3) [92].

By appending a hexanoate group, Chen et al. not only were able to greatly increase the solubility of Q[7] (>600 mg/mL), but found that this Q[7]-$(CH_2)_5CO_2Na$ (**6**, Fig. 11) was capable of efficient and controlled drug release [93]. Guests used in the study included Lobaplatin and Oxaplatin for which the binding affinities were $(1.8 \pm 0.3) \times 10^4$ and $(9.3 \pm 0.4) \times 10^6$, respectively in 10 mM phosphate buffer at pH 7.4.

The *in-vitro* cytotoxicity and anti-tumor activity of systems involving Q[7] and oxaliplatin and carboplatin have been investigated using the tumor cell lines B16 and K562, as well as T cells and B cells as animal melanoma models. In the case of the cell lines B16 and K562, the presence of the Q[7]@oxaliplatin inclusion complex led to increased cytotoxicity *versus* free oxaliplatin, whereas little difference was noted between the two species *in vivo*; the acute toxicity of oxaliplatin improved upon complexation *in vivo*. For carboplatin, when mixed with Q[7], some beneficial effects such as more pronounced anti-tumor effects (*versus* free carboplatin) were noted on the murine B16 melanoma cell line, and the acute toxicity of the carboplatin was increased *in vivo* [94].

Xu et al. have also employed a Q[7]-based nanocarrier which incorporates a redox-responsive disulfide linkage, which, on reduction to thiol, triggered drug release *via* a self-inclusion process [95]. The system, **7** (Fig. 12. top) involved alkyl ammonium motifs bridged by a central disulfide. The ability of the system to self-include was demonstrated by use of the model compound **8** (Fig. 12, bottom). On addition of *p*-xylylenediamine, the released viologen proton signals could readily be seen, indicating that it had been displaced from the Q[7] cavity. It was found that the system was capable of binding oxaliplatin (1:2) with a binding constant of 9.46×10^6 M^{-1} (by ITC experiments), however this was not as high as the binding constant for the self-inclusion species. The self-inclusion could be triggered by reduction, for example, on addition of tris(2-carboxyethyl)phosphine, which led to the release of >80% of oxaliplatin over 2 min. (and 95% over 5 min.).

2.2.2. *Cucurbit[8]urils*

Stang et al. employed a water soluble system comprised of Q[8], curcumin (an anti-cancer drug) and a hexagonal platinum(II)-based metallocycle, which was capable of improved *in vitro* anticancer activity for human melanoma (C32) and breast cancer cells (MDA-MB231) *versus* free curcumin [96]. The combination of the self-assembled (*via* metal–pyridyl bonding) Pt(II) metallacycle bearing tri(ethylene glycol) groups and the encapsulation ability of the Q[8] allowed for the effective delivery of curcumin to cancerous cells. In this system, the Q[8] formed a water soluble heteroternary host-guest complex with methyl viologen and curcumin (1:1:1), which exhibited much improved IC_{50} values. This host-guest complex exhibited concentration dependent features such as vesicles, fibers and honeycomb networks as evidenced by TEM experiments.

Fuentealba et al. noted cytotoxicity/phototoxicity cooperative

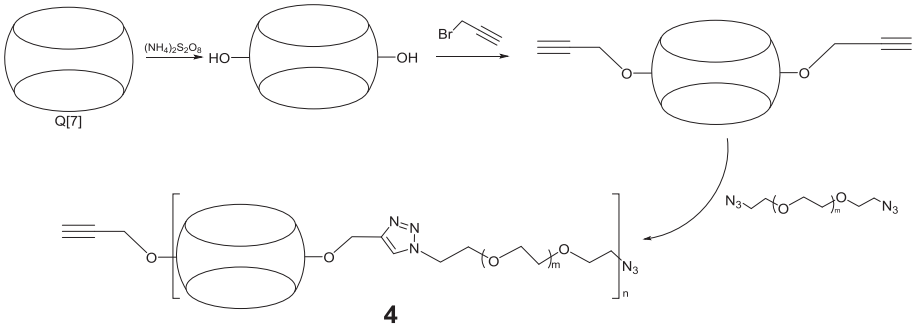

Fig. 9. Preparation of polymeric Q[7] system **4**.

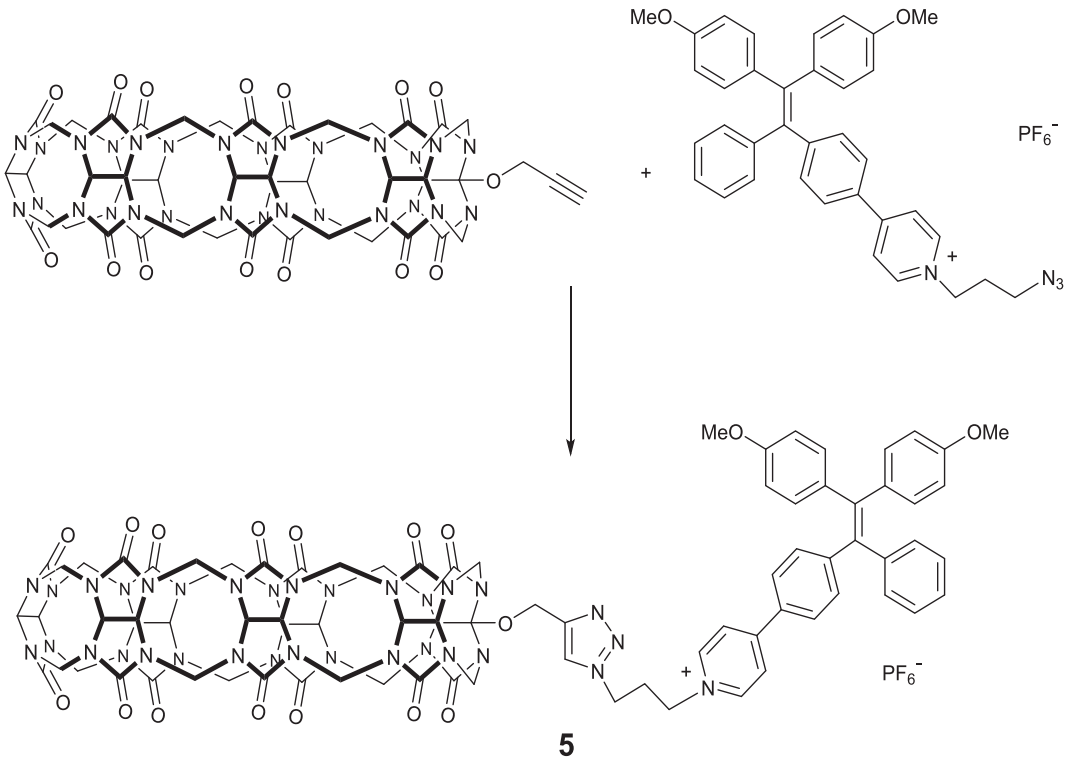

Fig. 10. Preparation of the fluorescent AIE photosensitizer **5**.

Table 3
Nedaplatin and nedaplatin@Q[7] cytotoxicity in three human cancer cell lines.

Compound	IC_{50} (μM) A549	IC_{50} (μM) HCT116	IC_{50} (μM) MCF-7
Nedaplatin	28.8 ± 0.5	5.2 ± 0.7	>50
Nedaplatin@Q[7]	9.9 ± 0.4	3.0 ± 0.2	39.1 ± 0.8

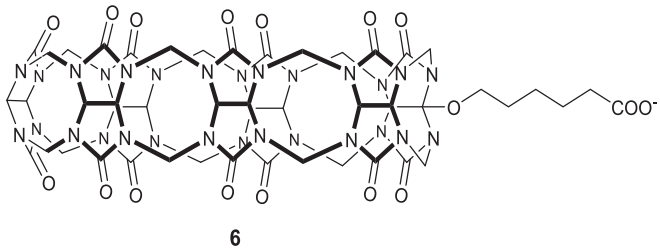

Fig. 11. Structure of Q[7]C_5CO_2Na **6**.

effects when investigating the behaviour of the inclusion complexes Q[8]@acridine orange and Q[8]@oxaliplatin on HeLa cells [97]. Given the binding constant for acridine orange was, as determined by ITC, six times greater than that for oxaliplatin, little displacement was observed at low concentrations of oxaliplatin. Cells studies revealed that the Q[8]@acridine orange inclusion complex was phototoxic whilst Q[8]@oxaliplatin, following a 24 h incubation period, was cytotoxic. Interestingly, if cells were pre-treated (over 24 h) with Q[8]@oxaliplatin, then following subsequent treatment with Q[8]@acridine orange, photodynamic behavior was not observed. More promising results were obtained when both species were co-incubated over 90 min., as this led to a 30% increase in the cytotoxicity/phototoxicity effects, *i.e.* cooperativity.

Other Q[8]-based studies include work by Yu, Lui et al. who employed a polymer derived from modified (with a mitochondrion-targeting peptide and 4-bromophenylpyridium) hyaluronic acid [98]. For this system, the Q[8] formed a homoternary complex with the 4-bromophenylpyridium (2:1) with a binding constant of 6.24×10^{12} M^{-2}. It proved possible to employ this system for both imaging of mitochondrial behavior in living cells and to improve the *in vitro* and *in vivo* antitumor efficiency of cisplatin (using MCF-7 cells) *versus* cisplatin alone.

In a recent review by Shukla et al., the working mechanisms for Q[*n*] complexation of biologically relevant guests is discussed, including the use of Q[7] with a number of platinum-based agents such as cisplatin [99]. The behavior of Q[7] toward a number of platinum drugs has also been reviewed by Pashking et al. [100].

2.3. Pillar[n]arenes

Pillar[*n*]arenes are a relatively new class of macrocycles that were first reported by Ogoshi *et al* in 2008 and are composed of between 5 and 10 dialkoxybenzene or hydroquinone units linked by methylene bridges [101].

Sessler, Meng, Li et al. have utilized a carboxylatopillar[6]arene to encapsulate and deliver both oxaliplatin and doxorubicin, the former in the form of a Pt(IV) analogue, namely **9** as shown in Fig. 13. In this system, drug release can be achieved simply by pH change; release occurs under acidic conditions (pH 5.0). *In vitro* studies using CCK-8 assays, together with positive controls, on the HepG-2 and LO2 cell lines revealed a synergic effect in terms of cytotoxicity resulting from use of the host-guest supramolecular complex DOX@**9** ⊂ CP6A *versus* the parent drugs alone. It was concluded from confocal laser scanning microscopy and flow cytometry that internalization was an energy-dependent endocytosis mechanism. The anti-tumor efficacy of the system was investigated *in vivo* using HepG-2 derived subcutaneous tumor xenograft mouse models. Results revealed that the system was capable of not only efficiently retarding tumor growth, but also reducing side effects in BALB/c nude mice [102].

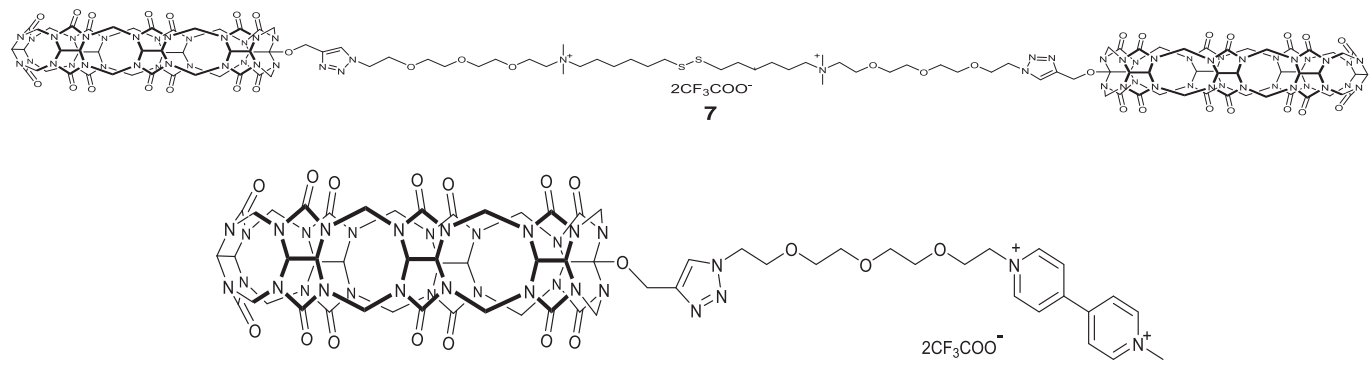

Fig. 12. Structure of **7** and model compound **8**.

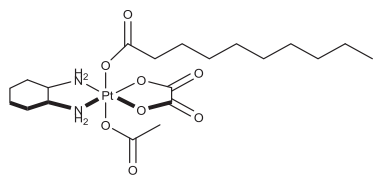

Fig. 13. Structure of **9**.

2.4. Cyclodextrins

Cyclodextrins date back to the time of Villiers in the late 19th century and are comprised of glucose units (6 to 8) linked by α-1,4-glycosidic bonds, *i.e.* cyclic oligosaccharides [103].

Tian, Stang et al. employed orthogonal coordination-driven [2 + 2] self-assembly combined with the host-guest chemistry of β-cyclodextrin (Fig. 14) to access a Pt(II) macrocyclic assembly **10** comprising spherical nanoparticles that was capable of responding to both nitric oxide (*via* amide cleavage) and redox stimulation (*via* H_2O_2 addition). The spherical nanoparticles were constructed in a way that allowed for doxorubicin loading and given the presence of the platinum-containing motif, the system was able to co-deliver both drugs in synergic fashion *in vitro* to liver tumor (HepG2) sites [104].

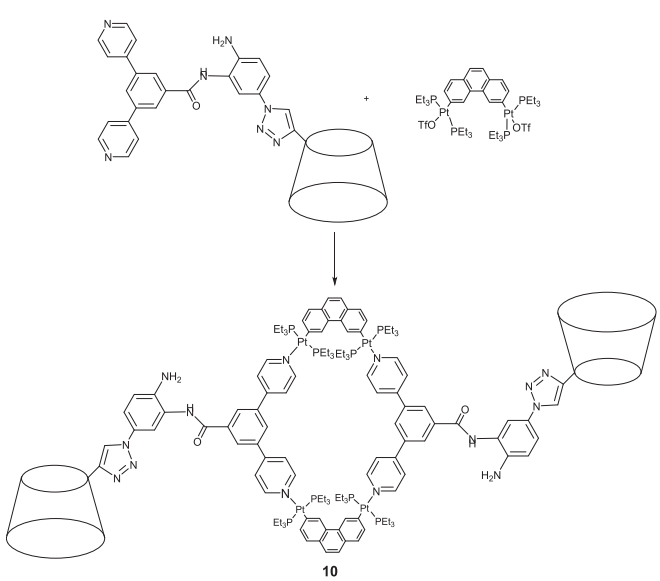

Fig. 14. Pt(II) macrocyclic assembly **10** *via* orthogonal coordination-driven self-assembly.

Zhang et al. constructed the β-CD-containing nanodrug GOx&Pt@FcNV (GOx = glucose oxidase, Pt = cisplatin, FcNV = ferrocene-containing nanovesicle), which utilized cascade reactions involving H_2O_2 and •OH generation to overcome multi-drug resistance in various tumors as demonstrated by both *in vitro* and *in vivo* studies. Indeed, it was noted that the system exhibited tumor inhibitory rates (TIRs) of up to 79.1% and 72.8% against A549/DDP and MCF-7/ADR double-tumor-bearing nude mice, respectively; note for free cisplatin (TIRA549/DDP: 9.7%; TIRMCF-7/ADR: 8.4%) and Pt@FcNV (TIRA549/DDP: 23.7%; TIRMCF-7/ADR: 17.1%) [105].

2.5. Crown ethers

Crown ethers are macrocyclic polyethers possessing 4 or more oxygen atoms each separated by 2 or 3 carbon atoms, and their synthesis dates to the work of Pedersen in the 1960s [106,107].

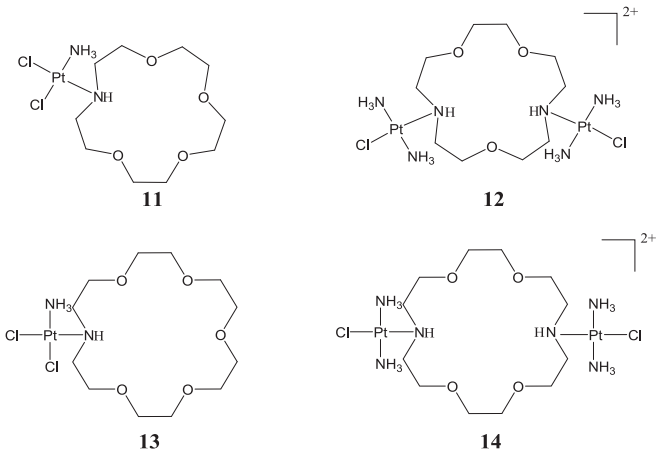

Fig. 15. Structures of Oxa-aza crown ethers **11–14**.

Table 4
Cytotoxicity of **11–14** in human ovarian cancer (A2780) and cisplatin-resistant A2780cisR.

Complex	IC_{50} (μM) A2780	IC_{50} (μM) A2780cisR
11	66	>100
12	21	>100
13	>100	>100
14	>100	>100
Cisplatin	0.37	2.4

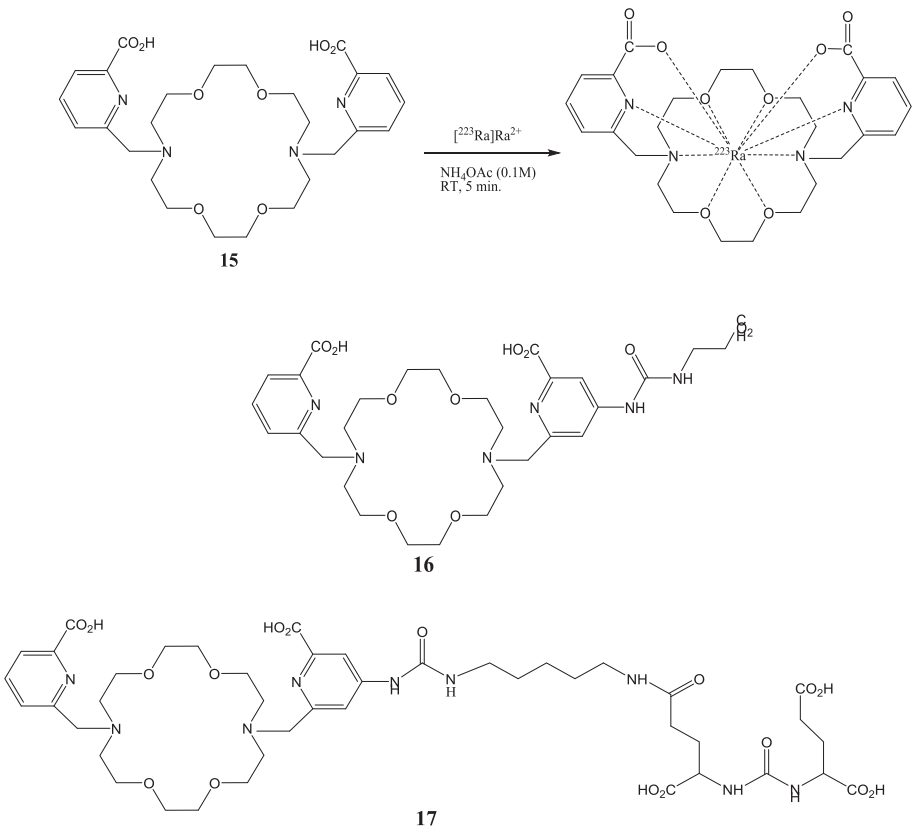

Fig. 16. Top: labelling of macrocycle **15** with [^{223}Ra]Ra^{2+}; Middle: conjugation of **15** to β-alanine to afford **16**; Bottom: conjugation of **15** to DUPA to afford **17**.

2.5.1. Oxa-aza crown ethers

Reedijk et al. have investigated the cisplatin-type coordination chemistry of a series of oxa-aza crown ethers, see **11**–**14** in Fig. 15. Cytotoxicity studies against A2780 human ovarian cancer revealed that *cis*-[$PtCl_2(NH_3)$(1,4,7,10-tetraoxa-13-azacyclopentadecane-N)] (**11**) possessed the highest cytotoxicity, albeit lower than that of cisplatin (Table 4). For both neutral and cationic species, the 15-membered ring systems exhibited the greater binding to intracellular DNA. The results suggested that the shape of the linker played a part in the ability of such systems to enter cells [108].

Oxa-aza crown ethers have also shown potential for targeted α-particle therapy. Wilson, Thorek et al. showed that it was possible to label the macrocycle **15** (Fig. 16, top) with [^{223}Ra] Ra^{2+} at ambient temperature over 5 min., with efficiency >95% and stability *in vitro* (under physiological conditions) and *in vivo* (in murine models) [109]. Moreover, when conjugated to the amino acid β-alanine or the peptide 2-[3-(1,3-dicarboxypropyl)ureido]pentanedioic acid (DUPA), *i.e.* compounds **16** and **17** (Fig. 16, middle and bottom), the resultant radium [^{223}Ra] complexes exhibited rapid clearance in mice with low bone absorption. The results of this work suggest this type of macrocycle has potential to expand the possibilities for radium around targeted α-particle therapy.

In a meeting report, the synthesis of an oxa-aza crown-6, namely crown-1paMe, was mentioned, which was labelled with ^{155}Tb under mild conditions (ambient temperature) with $\geq 10^{-6}$ M chelator concentrations. It was proposed that such a system will be of use in dual modality probes [110].

2.5.2. Calix[4]arene-1,3-crown[6]ether

Mamat et al. have investigated the coordination chemistry of the calix[4]arene 1,3-crown[6]ether **18** (Fig. 17) with a view to its use as a chelator in radiopharmaceutical chemistry. Complexation studies (titrations, NMR and UV/Vis spectroscopic experiments) revealed a high selectivity for lead(II) ions as well as heavy alkaline earth metal ions [111].

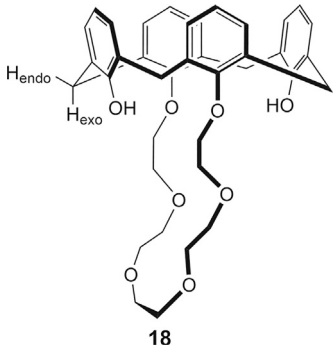

Fig. 17. Calix[4]arene 1,3-crown[6]ether **18.**

2.6. Aza macrocycles

We note that heterometallic platinum-containing complexes are also attracting interest [112]. Adams and Meade reported heterometallic platinum(IV)-containing gadolinium complexes **19** and **20**, which were based on cisplatin or carboplatin ligation, see Fig. 18 [113]. Both complexes proved to be magnetic resonance imaging (MRI) contrast agents as well as being capable of chemotherapy. The cisplatin-like complex exhibited superior cellular toxicity (see Table 5) and performed better as an MR contrast agent *in vitro*.

Finally, in terms of platinum-based drugs, we note that a useful guide from a chemist's perspective regarding side effects has been published by Wheate et al. [114].

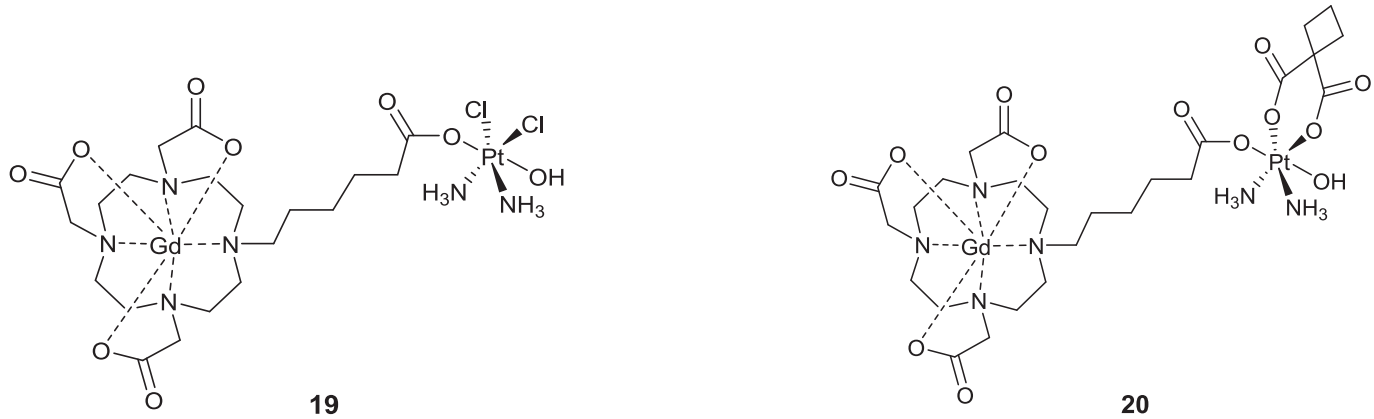

Fig. 18. Heterometallic platinum(IV)-containing gadolinium(III) complexes **19** and **20**.

Table 5
Anti-cancer activity of **19** and **20** *versus* carboplatin and cisplatin.

Complex	IC_{50} (μg/mL)	IC_{50} (μg/mL)	IC_{50} (μg/mL)
	A2780	HeLa	MCF-7
19	29.8 ± 2.5	49.3 ± 1.3	113 ± 4
20	55.0 ± 2.9	258 ± 5.0	382 ± 6
Carboplatin	15.3 ± 5.8	71.2 ± 4.9	124 ± 4
Cisplatin	7.6 ± 2.3	14.7 ± 1.2	22.4 ± 2.0

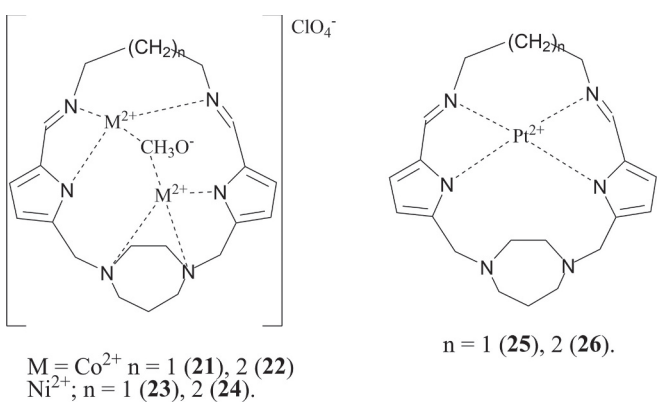

Fig. 19. Ni(II), Co(II) and Pt(II) complexes **21** to **26**.

Table 6
Cytotoxicity studies on macrocycles with $n = 1$, 2 and complexes **21**–**26**.

Compound	IC_{50} (μM) HT29 cells	IC_{50} (μM) HeLa cells	IC_{50} (μM) A549 cells	IC_{50} (μM) Fibroblast
Macrocycle n = 1	>100	12	10	>100
Macrocycle $n = 2$	>100	15	10	>100
21	>100	>100	9	>100
22	>100	>100	8	>100
23	>100	>100	>100	>100
24	>100	>100	>100	>100
25	>100	11	7	>100
26	>100	11	6	>100

2.7. Schiff-base macrocycles

Schiff-bases date back to the mid-19th century and to the work of Hugo Schiff on primary amines and carbonyls [115]. Work has been extended to include many types of Schiff-base macrocycles derived from dicarbonyls and a variety of diamines/dianilines [116].

Biologically relevant Schiff base macrocyclic complexes reported between 2005 and 2021 have been highlighted in a review by Sikha et al. [117].

In more recent times, Keypour et al. have prepared two new Schiff-base macrocycles using the dialdehyde *N*,*N*′-bis(5-formylpyrrol-2-ylmethyl) homopiperazine and the diamines 1,3-diaminopropane or 1,4-diaminobutane in methanol (Fig. 19). Complexes of Co(II) (**21**,**22**), Ni(II) (**23**, **24**) and Pt(II) (**25**, **26**) were prepared, and the crystal structure of the complex $[Ni_2L^2(CH_3O)]ClO_4$ determined, where L^2 is the macrocycle derived from 1,4-diaminobutane; the methoxide ligand bridges the two nickel centers. Cytotoxicity studies (Table 6) of both macrocycles and complexes against A549, HeLa cells, and HT29 cells afforded mixed results. Whilst the cobalt complexes performed poorly, the platinum complex of L^2 afforded the best results with an IC_{50} of 6 μM for A549 cells [118].

2.8. Other macrocyclic systems

Dey et al. reported the macrocyclic complexes **27**–**30**, shown in Fig. 20, that were isolated from the reaction of $[M(P\cap P)(X)_2]$ (M = Pt, X = NO_3, OTf; M = Pd, X = OTf) and 4,4′-dipyridyldiselenide or *via* the use of the phosphine PEt_3 (**31**) Interestingly from MTT and clonogenic assays using breast (MCF7), lung (A549), bone (U2OS) and ovarian (SKOV3) cancer cell lines, it was found that a key factor was the diphosphine (P∩P) ligand bite angle, with complexes bearing a wide bite angle exhibiting cisplatin-like cytotoxicity, *i.e.* similar IC_{50} values (see Table 7) [119].

Texaphyrins are extended porphyrins and contain two Schiff-base motifs. A recent example of their use is a Pt(IV) texaphyrin system, which involves the addition of oxaliplatin to a gadolinium metallotexaphyrin core bearing oxalate and diaminocyclohexyl motifs [120]. The diaminocyclohexyl grouping was incorporated to provide an oxaliplatin-like environment. The system was capable of not only delivering Pt(II) to solid tumors, but could also overcome some of the platinum resistance associated with the tumor suppressor p53. Indeed, in vivo studies revealed that this Pt(IV) texaphyrin system could be added at three times the dose of oxaliplatin without any observable side effects.

3. Non-platinum based anti-cancer activity

3.1. β-cyclodextrin

Huang, Gao et al. have prepared the Ir(III) complex **32** by the route shown in Fig. 21, and then encapsulated it within β-cyclodextrin. The cyclodextrin was modified with Cyanine7 and this resulted in a ratiometric oxygen fluorescence probe. *In vitro* studies revealed a rapid response to O_2, whilst *in vivo* work revealed the mapping potential of the

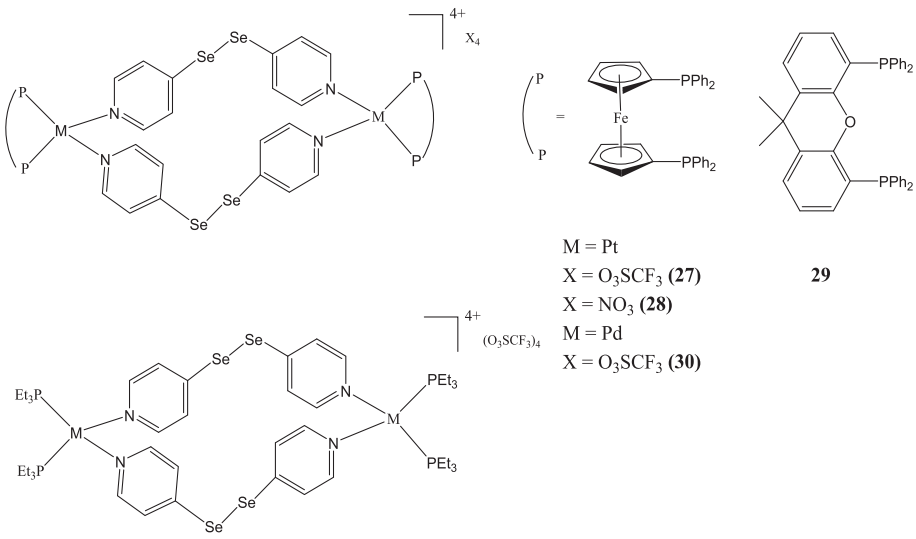

Fig. 20. Macrocyclic complexes **27**–**31**.

Table 7
IC_{50} values for complexes **27**–**31** and Cisplatin.

Compound	IC_{50} (μM) MCF7 cells	IC_{50} (μM) U2OS cells	IC_{50} (μM) A549 cells	IC_{50} (μM) SKOV3	IC_{50} (μM) Vero
27	10 ± 1.7	2.8 ± 0.1	6 ± 0.8	4 ± 0.8	19 ± 1
28	–	2.8 ± 0.4	3.5 ± 0.9	4 ± 0.3	8 ± 0.9
29	9 ± 0.7	2.5 ± 0.1	8 ± 1	6 ± 0.9	20.5 ± 1.2
30	6 ± 1.0	16 ± 0.6	>25	>25	>25
31	4 ± 0.3	4.8 ± 0.3	13 ± 1	12 ± 1.5	19 ± 0.3
Cisplatin	6.5 ± 1.0	8 ± 0.9	13 ± 1.2	14 ± 1.8	15 ± 1.3

probe for hypoxia microenvironment when deployed on solid tumors For example, see Fig. 22 for the photoluminescent images of mice bearing with tumors grown from the colorectal cancer cell line LS180 [121].

3.2. Schiff-base macrocycles

Keypour et al. reacted 2-((4-(2-aminobenzyl)-1,4-diazepan-1-yl) methyl)benzenamine with either 2,6-diacetylpyridine or 2,6-pyridinedicarbaldehyde to afford macrocycles of type **33**, see Fig. 23. Metal complexes were prepared by further reaction with perchlorate salts (R = H, M = Cd, **34**, Mn **35**, Zn **36**; R = Me, M = Cd, **37**, Mn **38**, Zn **39**). The cytotoxicity of the complexes against the cell lines A2780, U37 MG, and H1299 was evaluated *versus* that of doxorubicin (Table 8). Best results were achieved using the manganese species **35**, *e.g.* for U37 MG cells, IC_{50} = 20.73 ± 1.5 μM *vs* 23.3 ± 1.7 μM for doxorubicin) [122].

3.3. Tetra-aza macrocycles

Kothari and Agrawal reported three copper(II) complexes **40**–**42** bearing tetra-aza macrocycles (Fig. 24). The anticancer activity against 7 breast cancer cell lines *versus* that of cisplatin was investigated. Under the conditions employed, the copper complexes were found to have IC_{50}

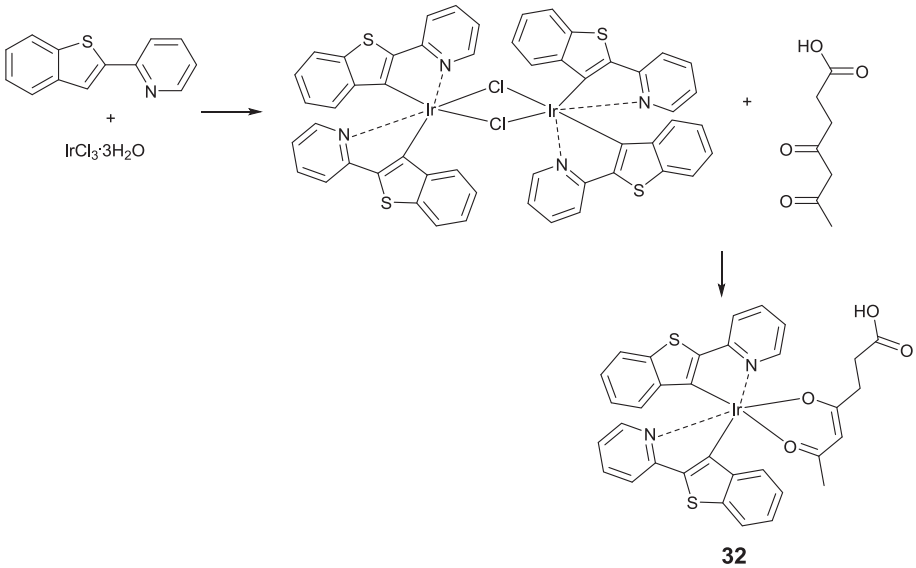

Fig. 21. Preparation of the Ir(III) complex **32**.

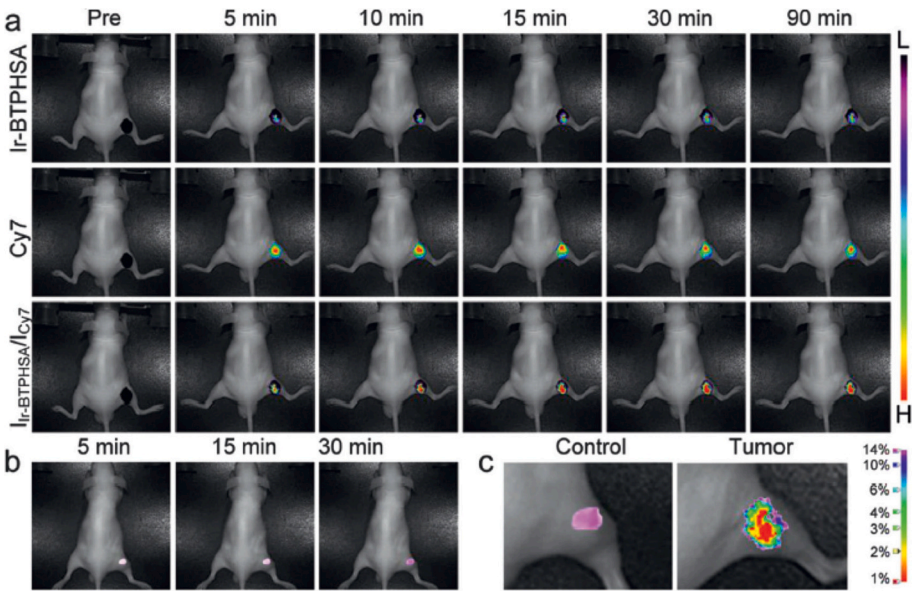

Fig. 22. a) Photoluminescence images of the tumor for tumor-bearing mice at different times post-injection of the probe; b) photoluminescence images of a comparable site for mice with no tumor after injection of the same probe; c) oxygen level mapping for the tumor *versus* control site. Reproduced from reference 121 under the terms of the Creative Commons CC BY license.

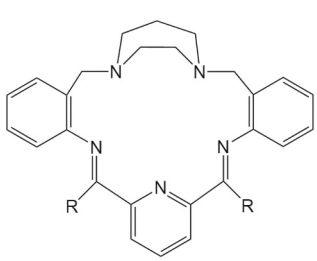

33

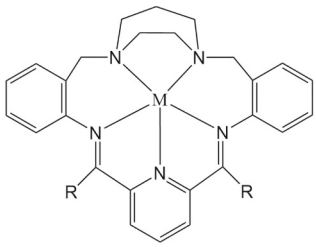

R = H, M = Cd (**34**), Mn (**35**), Zn (**36**)

R = Me, M = Cd (**37**), Mn (**38**), Zn (**39**)

Fig. 23. Macrocycle **33** and complexes **34**–**39** thereof (R = H, M = Cd, Mn, Zn; R = Me, M = Cd, Mn, Zn).

Table 8
Cytotoxicity of complexes **34**–**39** against human carcinoma cell lines.

Compound	IC_{50} (μM) A2780 cells	IC_{50} (μM) H1299 cells	IC_{50} (μM) U37 MG cells
34	150.3 ± 2.36	272 ± 13.6	80.23 ± 14.4
35	58.2 ± 3.7	110 ± 15.3	31.03 ± 2.4
36	81.3 ± 2.9	69.76 ± 1.3	25.9 ± 3.8
37	25.41 ± 1.3	25.41 ± 1.3	20.73 ± 1.5
38	89.6 ± 6.1	119 ± 3.6	39.32 ± 3.2
39	38.6 ± 5.9	78 ± 3.5	28.23 ± 1.2
Doxorubicin	4.2 ± 0.89	27.3 ± 3.9	23.3 ± 1.7

values between 7.21 ± 0.1 μM to 13.10 ± 0.3 μM compared with 1.9 μM for cisplatin (see Table 9) [123].

4. MOF and SOF delivery systems

4.1. Calix[4]arenes

Pellois, Zhou et al. have synthesized a number of coordination cages derived from combinations of sulfonylcalix[4]arenes, tricarboxylic acids, pyridyls and metal nodes based on zinc, cobalt or palladium, see **43**–**45**, Fig. 25. The hydrophobic internal cavities of these cages, together with the presence of, in some cases, net charges, have been employed to load a drug cargo, such as the anticancer drug (+)-Camptothecin. The subcellular distributions of these cages were measured using living mammalian cells, and it was found that charge and affinity were important factors in dictating the cell targeting. Moreover, the use of these cage vectors led to increased anticancer efficacy of the agent been transported, as was evidenced in this work for a DNA topoisomerase inhibitor [124].

In subsequent work, Pellois et al. expanded their studies on the Zn (II)/sulfonylcalix[4]arene/tricarboxylic acid cage system and investigated its cell entry, disassembly and toxicity properties. Results revealed that cell entry rates could be correlated with extracellular concentration, which suggests that despite the size of the cage, it is able to passively diffuse through the membrane. Inside the cells, the cage system decomposes into its constituent parts within hours, and over a period of 1 day, the various parts are cleared from the cells [125].

4.2. Calix[6]arenes

Zhu et al. have post-modified a terbium-based MOF with calix[6]arene, and obtained a composite that maintained its photoluminescent properties for up to 15 days in aqueous solution. In terms of applications, the composite, by making use of the calixarene cavity, was capable of the monitoring of 11β,17,21-trihydroxypregna-1,4-diene-3,20-dione (*Prednis*), the latter is an anti-epidemic drug. Based on the emission studies, the limit of detection was found to be 2.6 ng mL^{-1} [126].

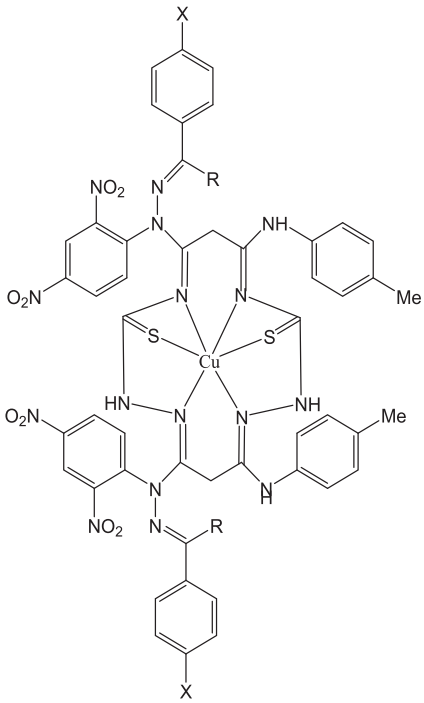

40 - 42

Fig. 24. Tetraaza macrocyclic copper complexes **40**–**42** (X = H, R = H **40**, Me **41**; X = Cl, R = Me **42**).

Table 9
Anti-cancer activity of complexes **40**–**42** against MCF-7 breast cancer cell lines.

Complex	IC_{50} (μg/mL)
40	7.21 ± 0.1
41	9.29 ± 0.1
42	1.01 ± 0.2
Cisplatin	1.9

4.3. Cucurbit[6]uril-based SOFs

Ni et al. have constructed supramolecular organic frameworks (SOFs) by utilizing the host-guest interactions available to cucurbit[6]uril, and studied their potential as drug delivery platforms. For example, the SOF formed in the presence of 2-(cyclohexylamino)ethanol, and using $[ZnCl_4]^{2-}$ anions as the structure inducer, was loaded with ibuprofen. It was found that the system could respond to external stimuli such as temperature or pH to trigger drug release [127].

5. Bioimaging *in-vivo*

5.1. Calixarenes

Zhao, Zeng, Jin et al. synthesized a calix[4]arene system **46** bearing two acetoymethyl groups on the lower rim and two (on the opposite phenyl groups) vinylpyridinium-containing substituents on the upper rim, see Fig. 26. This calixarene system proved to be an excellent chemosensor for Ca(II), Sr(II) and Ba(II), and could even distinguish between these alkaline earth metals *via* their color to the naked eye. Moreover, this calixarene could be employed *in vivo* for the imaging of Zebrafish [128].

5.2. Cucurbiturils

Chen et al. have made used of the self-assembly of tetramethyl cucurbit[6]uril conducted in the presence of 4,4′-biphenyldisulfonic acid and the alkaline earth metal nitrate salts of Ca(II), Sr(II) and Ba(II). The resulting fluorescent coordination polymers were capable of the detection of the antibiotic norfloxacin with detection limits of 9.52×10^{-4} (for the Sr derivative) and 2.55×10^{-4} (for the Ba derivative) [129].

5.3. Schiff-bases

Saha et al. has employed the Robson-type aza-phenol macrocycles of type **47** as multi analyte sensors for a variety of metals including trivalent Cr, Fe and Al (Fig. 27), where the fluorescent enhancement is chelation induced and the LODs are of the order of 10^{-7}–10^{-8} M. Of more relevance to this review is the deployment of such systems for bioimaging, for example against HepG2 cells, where uptake was marked by increased green fluorescence. MTT assays using WI38 cell lines revealed that the macrocycles exhibited little toxicity at a concentration of 100 μg/mL over 24 h [130].

6. PET imaging

As well as delivering conventional drugs to specific sites, macrocyclic systems are also useful scaffolds for radiotracers (radioactive drugs), which allows for detailed 3D images of tissues and organs and can lead to early detection/location of disease. Some recent examples using either cucurbiturils or crown ethers are discussed below.

6.1. Cucurbiturils

Houghton et al. utilized the strong host-guest binding between Q[7] and an amine appended adamantine-containing guest (association constant *ca.* 10^{14} M^{-1}), a typical synthesis of the latter is shown in Fig. 28 (top). Three different guest molecules were prepared which possessed the linkers R1 to R3, and these were labelled with ^{64}Cu to afford **48**–**50** (Fig. 28, bottom). The *in vitro* stability of the resulting host-guest complexes was studied, and high stability was noted over 24 h. Moreover, high tumor uptake was demonstrated for *in vivo* PET imaging (using BxPC3 tumor-bearing nude mice) with retention of complex integrity over 24 h [131].

6.2. Oxa-aza crown ethers

The use of somatosatin (SSTR) type receptors for PET has recently been reviewed [132]. A notable scaffold was formed from the combination of DOTA and Tyr^3-octreotate, which was named DOTATATE [133]. The system ^{177}Lu-DOTATATE (**51**), called Lutathera, received FDA approval early in 2018 for SSTR-positive gastroenteropancreatic neuroendocrine tumor treatment, and was developed/marketed by Advanced Accelerator Applications (they had also previously (in 2016) had the Ga 68 version **52** (Netspot) FDA approved) [134,135]. In 2020, the copper 64 analogue **53**, named Detectnet, also received FDA approval as an imaging agent and was developed/marketed by Curium US LLC [136]. The structures of these FDA-approved radiopharmaceuticals are shown in Fig. 29.

Another scaffold that is showing potential is the 18-membered macrocycle MACROPA **16** (Fig. 17), which was utilized for targeted alpha therapy (^{225}Ac) by Radchenko, Wilson et al. [137].

Building on the successes of DOTATATE and MACROPA, King, Gutsche et al. coupled MACROPA with Tyr3-octreotate to afford the scaffold **54** (Fig. 30) which was named MACROPATATE. Investigations revealed that MACROPATATE, when complexed to ^{225}Ac, exhibited increased stability (x4-fold) *versus* DOTATATE (**55**). However, despite the increased *in vitro* stability *versus* ^{225}Ac-DOTATATE, the latter performed better *in vivo* [138].

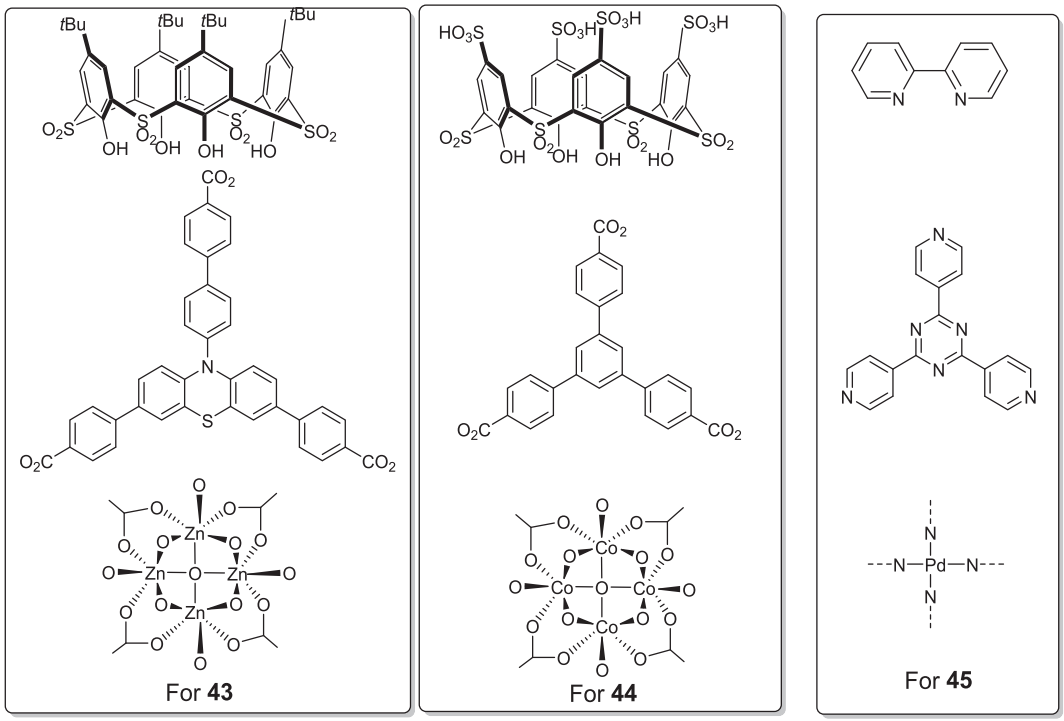

Fig. 25. Nodes and linkers employed to construct the coordination cages **43**–**45**.

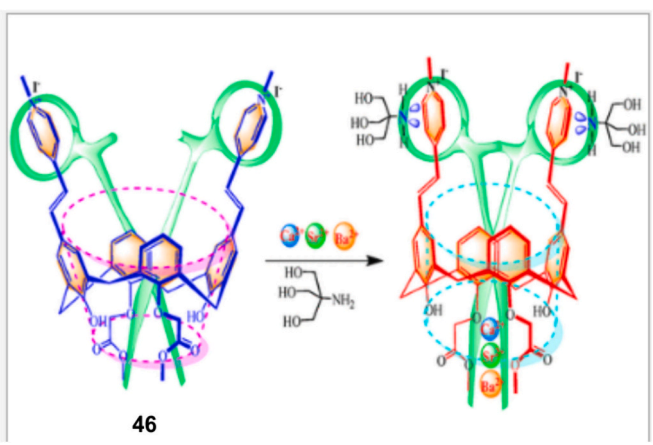

Fig. 26. Calix[4]arene system **46** as a chemosensor for Ca(II), Sr(II) and Ba(II). Reproduced from reference 128 with permission from the American Chemical Society.

6.3. DOTA-type chelators for targeted therapy

The use of DOTA-type chelators (DOTA = 1,4,7,10-tetraazacyclododecane-1,4,7,10-tetraacetic acid) and their use in targeted α-therapy has recently been reviewed with particular emphasis on ^{149}Tb, ^{211}At, $^{212/213}$Bi, ^{212}Pb (for ^{212}Bi), ^{223}Ra, ^{225}Ac, $^{226/227}$Th, and ^{230}U species [139]. The use of macrocyclic chelators for PET has also been recently reviewed [140].

Chi et al. reported a family of potential PSMA target compounds, four of which were labelled with ^{68}Ga which were then employed in PET/CT tumor targeting. One of these compounds, namely that bearing a *p*-iodophenyl moiety, was also subject to ^{177}Lu labelling studies (**56**, Fig. 31). Cold studies revealed that this compound possessed the best PSMA binding ability, whilst its ^{68}Ga derivative exhibited high tumor uptake together with kidney clearance. Use of the ^{177}Lu derivative resulted in effective inhibition of tumors with no adverse effects [141]. From studies on the biodistribution (using *p*-iodophenyl group as an albumin binder), the ^{177}Lu complex **56** revealed blood circulation values of 1 h = 10.32 ± 0.31, 6 h = 2.68 ± 1.07 %ID/g, and was found to be renally excreted. Mice treated with the same complex (4 and 6 MBq) had a survival rate of >61 days, whilst the human effective dose was estimated to be 0.03 mSv/MQq for kidney and 0.07 ± 0.01 mSv/MQq for the body.

Wurzer, Kunert et al. have also employed PSMA ligation to tackle prostate cancer. In their work, the complex **57** (Fig. 32) was highlighted as having potential as a competitive agent for endoradiotherapy based on its favorable pharmacokinetics (low kidney uptake; fast excretion; high tumor accumulation) in mice studies [142].

Hasserodt et al. have reported the pH responsive low spin Fe(III)-based MRI agents **58** and **59** (Fig. 33) in which the pyrrolidene-containing arms can, in aqueous solution, reversibly coordinate with the metal center; the binding being pH dependent. Of note here is that the inactivated forms are essentially MRI silent, whereas on addition of HCl and subsequent de-coordination of the arm, there is a huge increase in the ability of the systems to speed up the rate of longitudinal relaxation of water/hydrogen nuclei. The signal gap compares very favorably with other types of MRI probe, *e.g.* probes of the ^{19}F or CEST type [143].

It is also noteworthy that enzyme responsive peptides can be employed to create a more specific distribution of a contrast agent. Such a methodology was employed by Oh, Shim et al. whereby a macrocyclam system decorated with PEGylated matrix metalloproteinases (MMP)-cleavable peptides was able to form polymeric nanoparticles. When in the presence of tumor tissue, the polymeric system degraded thereby unmasking the metal complex present as well as the cyclam core. The study investigated the use of ^{64}Cu and Gd as contrast agents [144].

7. Antibacterial agents

The search for new metal-based antibacterial agents has recently been reviewed [145].

Of the systems reported in recent years, the majority utilize tetra-aza type macrocyclic ligation and these are covered first below.

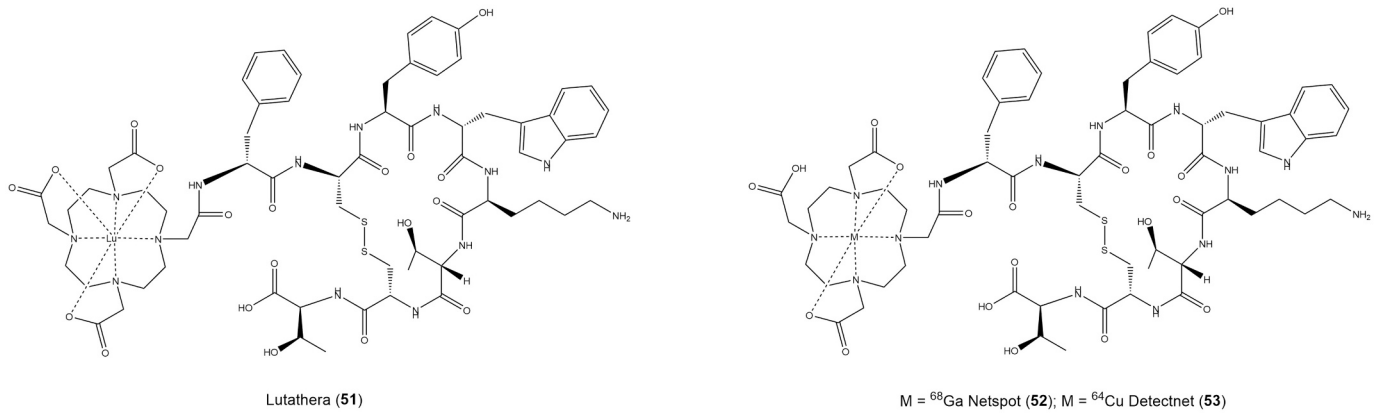

Fig. 27. Robson-type aza-phenol macrocycles **47** as multi analyte sensors. Reproduced from reference 130 with permission of the American Chemical Society under CC-BY-NC-ND 4.0 (Copyright 2024).

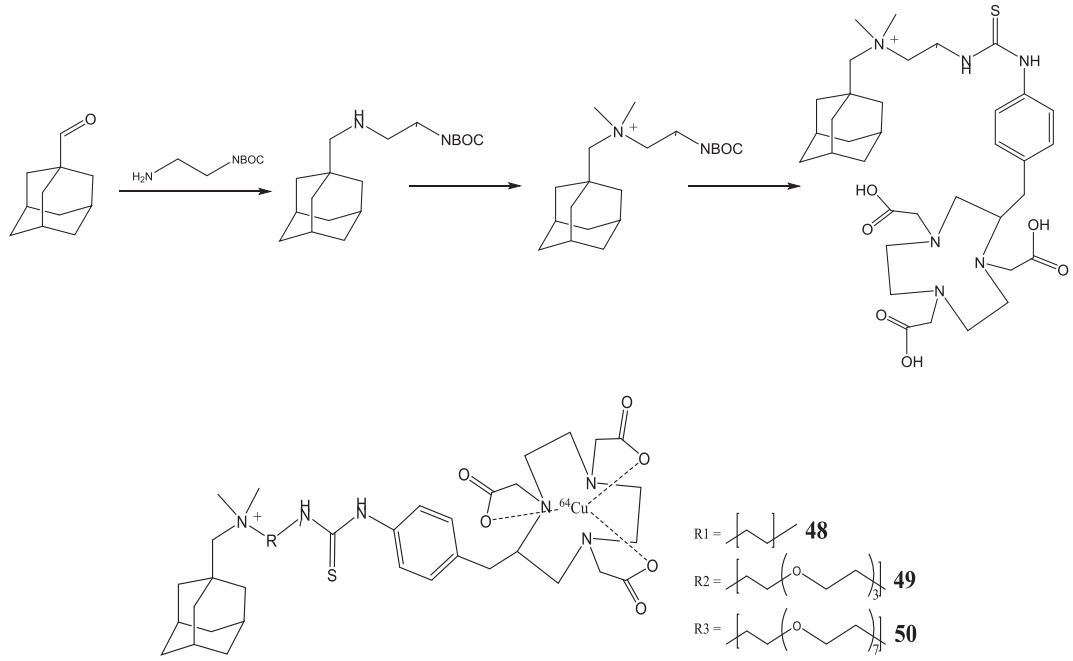

Fig. 28. Synthesis of adamantine-containing guest and structures of **48**–**50**.

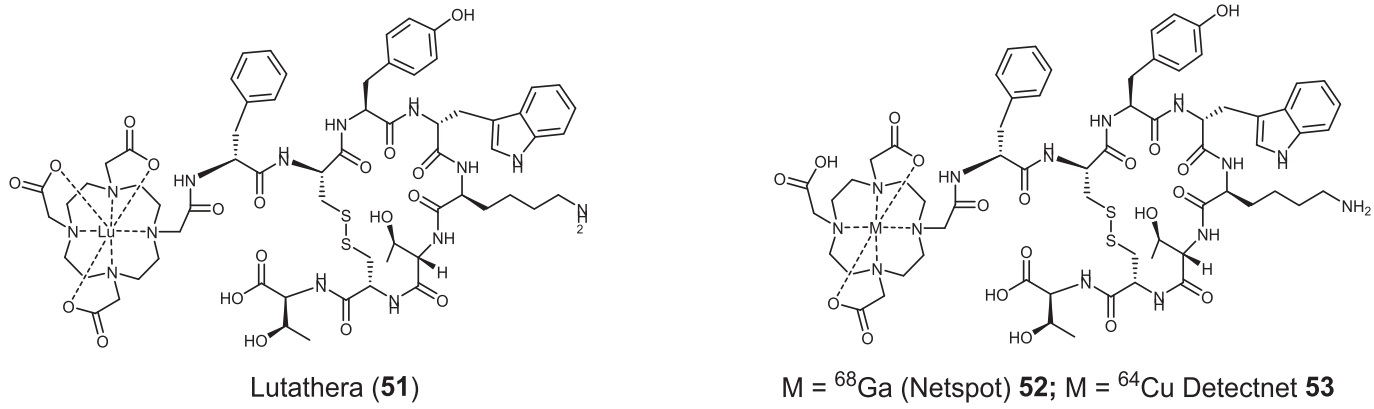

Fig. 29. FDA approved radiopharmaceuticals Netspot, Detectnet and Lutathera.

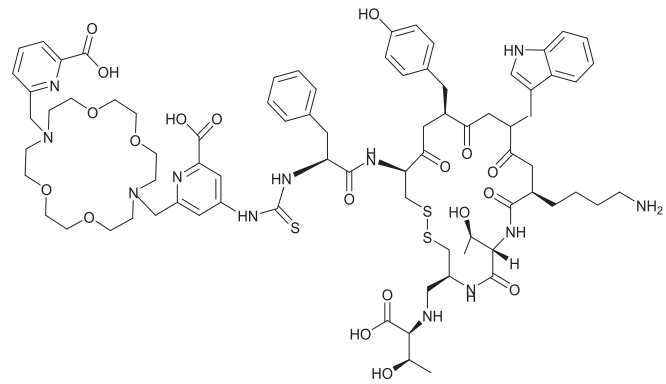

54

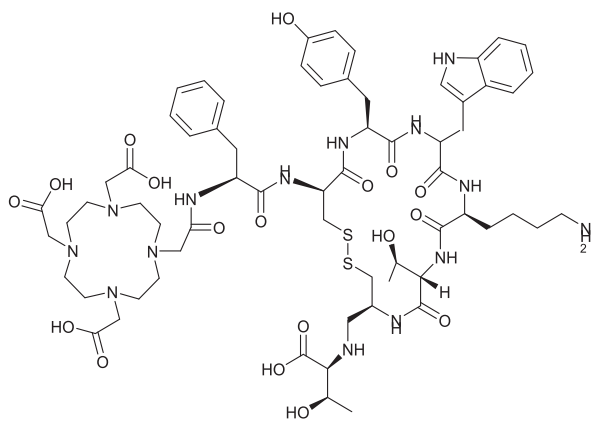

55

Fig. 30. Structures of **54** and **55**.

7.1. Tetraaza macrocycles

Kumar et al. reported a family of octahedral complexes based on the 6,12,5,11-tetraphenyl-di(2-pyridyl)[b,h][1,4,7,10]-N_4[12]annulene **60**, Fig. 34, left. The macrocycle adopted a saddled-shaped conformation. The complexes were screened for their antimicrobial activities against *E. coli, P. aeruginosa, B. cereus, S. aureus* and antifungal against *C. albicans*; the iron(II) complex out-performed the nickel(II) complex, showing best performance against *E. coli* [146].

The same group then reported the Fe(III) and Co(II) complexes **61** and **62** bearing a related tetraaza macrocycle, Fig. 34, right. Both complexes displayed promising antimicrobial activity as measured by the diameter of the inhibition zone, whilst in terms of antifungal activity (against the likes of *C. albicans*), the Fe(III) complex **61** proved to be superior [147].

A related type of type of macrocycle, namely a 14-membered tetraazamacrocycle, was coordinated with Fe(III) and Cr(III) to afford **63** and **64**, Fig. 35, and then Sangwan and Singh evaluated the antimicrobial activity of these complexes against the likes of *B. cereus* and *E. coli.* Results indicated good biocidal activity against bacteria and fungus, whilst antimicrobial activity was found to be related to the lipophilicity of the complex [148].

Chopra reported the Cr(III) (**65**, **66**), Fe(III) (**67**, **68**) and Co(III) (**69**, **70**) complexes of the macrocycles derived from the condensation of *o*-, *m*-diaminobenzene and ninhydrin, see Fig. 36; anti-fungal activity was noted for the Fe(III) complexes against *Fusarium oxysporium* [149].

Singh et al. prepared the macrocycle 5,6-bis-(4-fluorophenyl)-3,4,7,8-tetraazabicyclo[8.3.1]-tetradeca-1(13),4,6,10(14),11-pentaene-2,9-dione *via* the condensation reaction of 1,3-dicarbonyl-phenyl-dihydrazide with 4,4′-difluorobenzil. The macrocycle and the Co(II), Ni(II) and Cu(II) complexes thereof were screened *in vitro* for their potential antibacterial and antioxidant activity. The best antibacterial activity was displayed by the nickel system (as the acetate derivative) with minimum inhibitory concentrations (MICs) in the range 8–16 mg/L against *S. aureus*, *B. subtilis*, *E. coli*, *P. aeruginosa* and *S. typhi*. Against the cancer cell line SCC4, the cobalt complex (nitrate derivative) exhibited significant activity with a low IC_{50} at 31.1 μM over 72 h [150].

Krstić et al. reported the dinuclear complexes $[Zn_2(tpmc)(\mu\text{-}NO_3)](NO_3)_3\cdot CH_3OH$ **71** and $[Ni_2(tpmc)(NO_3)_2](NO_3)_2\cdot 3H_2O$ **72**, where tpmc = 1,4,8,11-tetrakis(2-pyridylmethyl)-1,4,8,11-tetraazacyclotetradecane **73**, and proposed the structures shown in Fig. 37. The report studied the biological activity of the two complexes against several bacterial strains and cancer cell lines. The zinc complex displaced better anti-bacterial activity than the nickel complex, whilst little activity was shown against the cancer cells MCF-7 and MDA-MB-231 [151].

Sakthivel et al. prepared 3-(2-hydroxy-3-methoxybenzylidene) pentane-2,4-dione *via* the Knoevenagel condensation of 2-hydroxy-3-methoxybenzaldehyde and acetylacetone. Further reaction with 1,2-phenyldiamine afforded the new macrocycle **74** (Fig. 38, left). Subsequent reaction with ethanolic solutions of the chlorides of cobalt(II), copper(II), nickel(II), manganese(II) and zinc(II) afforded metal complexes of the type [M(**74**)]Cl M = Co (**75**), Cu (**76**), Ni (**77**), Mn (**78**), Zn (**79**), whilst use of $VOSO_4$ led to $[VO(\mathbf{74})]SO_4$ (**80**).

The interaction of **74**–**80** with DNA was studied. From the data, it was proposed that such complexes intercalate with DNA *via* the aryl rings, and further studies (gel electrophoresis) indicated superoxide dismutase (SOD)-mimetic activity. The antibacterial and anticancer properties (against human breast and colon carcinoma cells) were evaluated. Results indicated that the copper, zinc and vanadium species with IC_{50} values of 22.4, 26.2 and 28.4 μg/mL (*versus* the human breast MCF7 cell line), respectively, exhibited the best antitumor activity. For the antibacterial studies (against *Salmonella typhi*, *Staphylococcus aureus*, *Escherichia coli*, *Bacillus subtilis* and fungi *Aspergillus niger*, *Aspergillus*

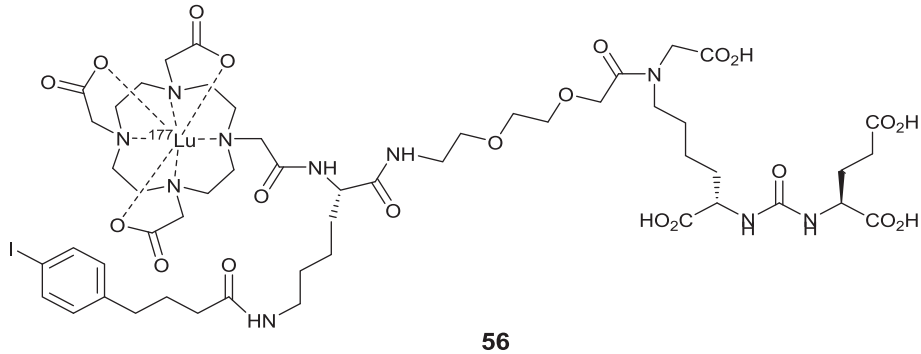

56

Fig. 31. *p*-Iodophenyl derivative **56**.

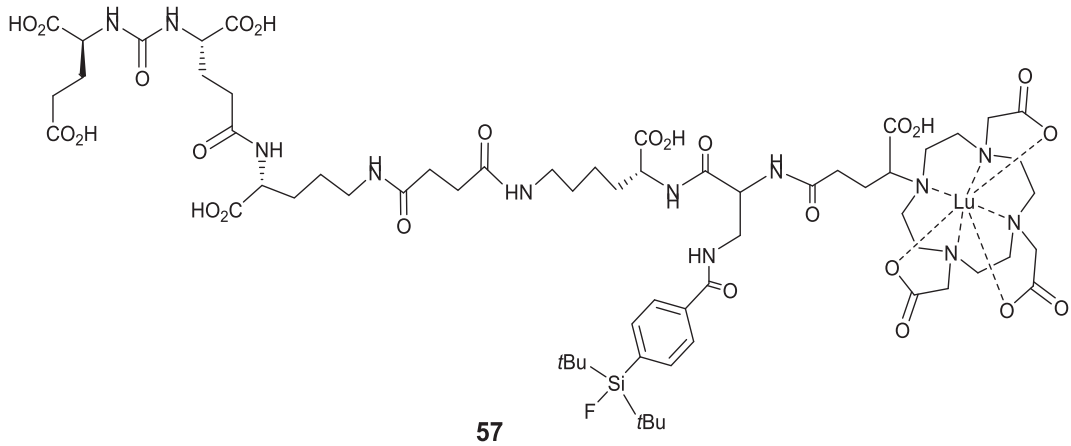

57

Fig. 32. Complex **57**.

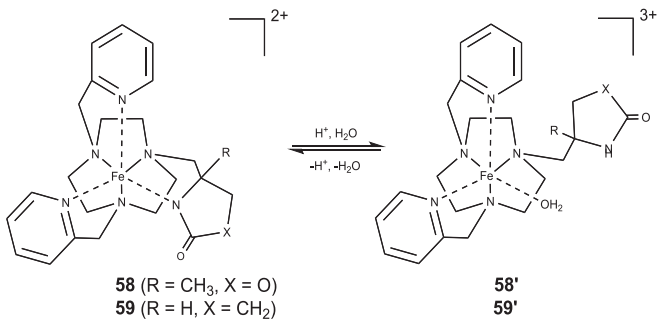

Fig. 33. Fe(III)-based MRI agents **58** and **59**.

flavus, *Candida Albicans* and *Rhizoctonia bataicola*), results (Tables 10 and 11) revealed that the metal complexes were only slightly better than the free macrocycle (*e.g.* for *E Coli* MIC values are 10–25 mg/mL for the metal complexes *versus* 45 mg/mL for the macrocycle) [152].

Thangavelu et al. have prepared the macrocycle **81** by the condensation of 3-(cinnamyl)-pentane-2,4-dione with two equivalents of 4-aminoantipyrine (Ampyrone) and subsequent treatment with 1,2-diaminobenzene, Fig. 39. Macrocycle **81** and its Cu(II) **82**, Co(II) **83**, Ni(II) **84** and Zn(II) **85** complexes were screened for their antimicrobial behavior and cytotoxicity. Against the bacteria *Staphylococcus aureus*, *Bacillus subtilis*, *Escherichia coli*, *Klebsiella pneumoniae* and *Salmonella typhi* and fungi *Aspergillus niger*, *Fusarium solani*, *Aspergillus flavus*, *Rhizoctonia bataticola* and *Candida albicans*, the metal complexes proved to be more active than the parent macrocycle. Cytotoxicity studies on human breast (MCF-7), cervical (HeLa), epithelioma (Hep-2) and normal human dermal fibroblast (NHDF) cell lines were also conducted, and the copper complex **82** was found to be more active than cisplatin (*e.g.* for Hep-2, $IC_{50} = 12 \pm 0.8$ μM *versus* 14 ± 1.0 μM for cisplatin) [153].

Sangwan and Singh reported the aza-macrocycle ($1^2Z,5^2Z,5^4E$)-$1^1,1^2,1^3,1^4,1^5,1^6,5^1,5^2,5^3,5^4,5^5,5^6$-dodecahydro-2,4,6,8-tetraaza-1-(2,4),5(4,2)-pyrimidine-3,7(1,2)-dibenzenacyclooctaphane-$1^6,5^6$-dione and the Co(II) **86**, Ni(II) **87** and Cu(II) **88** complexes thereof (Fig. 40). The resulting MX_2 type complexes (X = OAc) were screened for their antimicrobial efficacy. Both the cobalt and copper complexes exhibited good activity against Gram-positive bacterial and fungal cells respectively [154].

The complexes $[ML]Cl_2$ (Fig. 41), where M = Ni **89**, Cu **90** and L = dichloro-[2,4,9,13,15,20-hexamethyldibenzo-1,4,8,11-tetraazacyclotetradecatetraene]) have been reported by Vashistha and Kumar. Studies revealed that both complexes possessed antibacterial activity though to differing degrees against different pathogens. For example, **89** performed best against *P. aeruginosa* and *S. aureus*, and **90** against *B. cereus* [155].

More recently, Maurya et al. reported the use of cobalt complexes bearing 10-membered tetraazamacrocycles decorated with organotellurium. Studies revealed that such species could inhibit the bacterial strains *E. coli*, *P. aeruginosa,* and fungal strains *C. albicans, S. aureus, and*

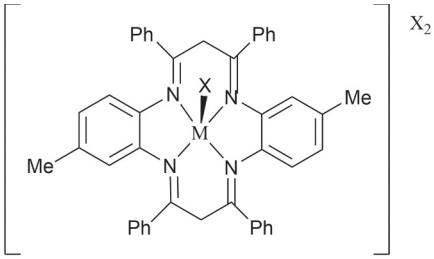

M = Fe (**63**), Cr (**64**)

Fig. 35. Complexes **63** and **64** (X = Cl^-, NO_3^-, CH_3COO^-).

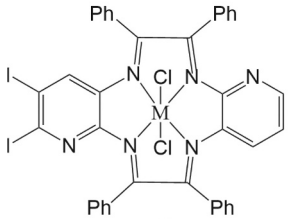

60

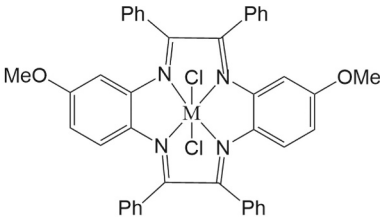

M = Fe (**61**), Co (**62**)

Fig. 34. Left: 6,12,5,11-Tetraphenyl-di(2-pyridyl)[b,h][1,4,7,10]-N_4[12]annulene **60**. Right: Fe(III) and Co(II) complexes **61** and **62**.

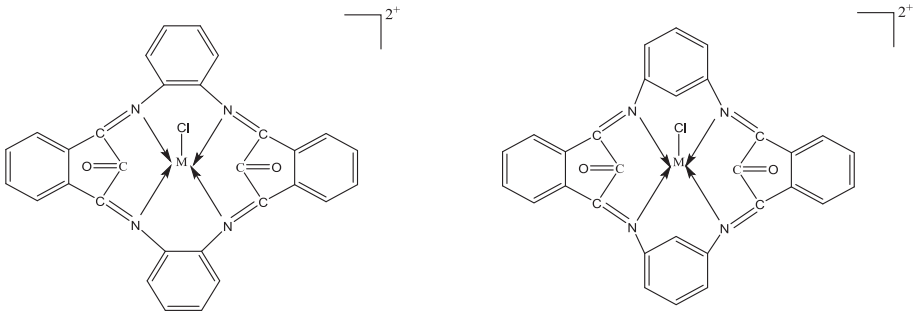

M = Cr (**65**), Fe (**67**), Co (**69**) M = Cr (**66**), Fe (**68**), Co (**70**)

Fig. 36. Complexes **65** to **70** (M = Cr(III), Fe(III), Co(III)).

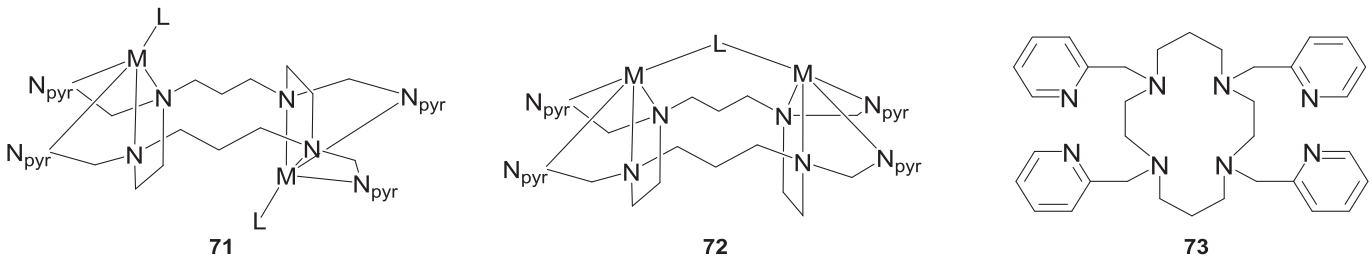

71 **72** **73**

Fig. 37. Left and Middle: 1,4,8,11-Tetrakis(2-pyridylmethyl)-1,4,8,11-tetraazacyclotetradecane complexes **71** and **72** (M = Ni, Zn; L = NO_3^-); Right: tpmc **73**.

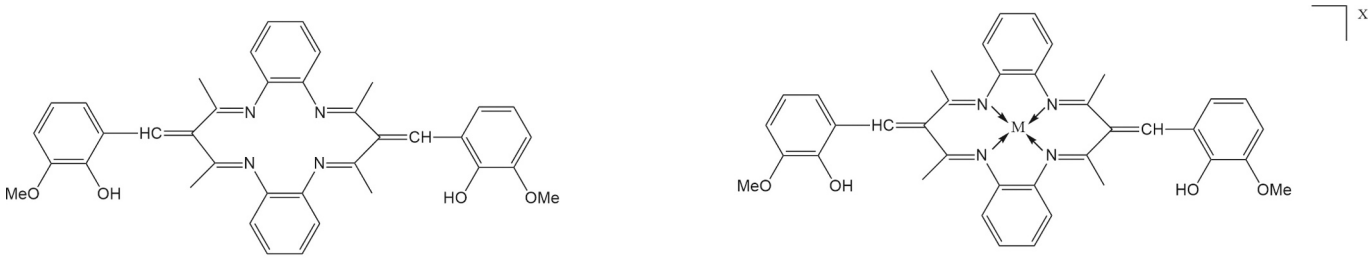

74

M = Cu, X = 2Cl (**75**)
M = Ni, X = 2Cl (**76**)
M = Co, X = 2Cl (**77**)
M = Mn, X = 2Cl (**78**)
M = Zn, X = 2Cl (**79**)
M = V, X = SO_4 (**80**)

Fig. 38. Macrocycle **74** and complexes **75–80**.

Table 10
Evaluation of macrocycle **74** and complexes **75–80** (*versus* Nystatin) against fungi (mg/mL).

Compound	MIC (mg/mL) *A. Niger*	MIC (mg/mL) *A. flavus*	MIC (mg/mL) *C. albicans*	MIC (mg/mL) *R. bataticola*
74	55	70	65	55
75	10	15	10	15
76	15	25	15	25
77	20	35	15	20
78	15	15	20	25
79	20	30	25	35
80	10	20	25	40
Nystatin	10	8	12	14

K. pneumonia [156].

7.2. Other N_4 macrocycles

El-Gammal et al. employed the [2 + 2] condensation of 1,4-phenylenediamine and 5,5-dimethyl-1,3-cyclohexanedione to afford the macrocycle **91**. The Cr(III) **92**, Fe(III) **93** and Mn(II) **94** complexes (Fig. 42) were prepared and these were screened for their antibacterial properties. Results revealed that both the parent macrocycle and its Cr(III) complex exhibited antibacterial activity on a par with the antibiotic ampicillin [157].

Chaturvedi et al. employed a template synthesis involving carbohydrazide, isatin (1H-indole-2,3-dione) and metal salts of Cr(III) **95–97** or Fe(III) **98–100** (each as the chloride, nitrate or acetate, see Fig. 43). The

Table 11
Evaluation of macrocycle **74** and complexes **75**–**80** (*versus* streptomycin) against bacteria (mg/mL).

Compound	MIC (mg/mL) *Escherichia coli*	MIC (mgM/mL) *Salmonella typhimurium*	MIC (mg/mL) *Staphylococcus aureus*	MIC (mg/mL) *Bacillus subtilis*
74	45	60	55	55
75	10	20	20	15
76	15	30	35	20
77	20	25	25	25
78	20	15	15	20
79	25	20	30	25
80	15	25	20	35
Streptomycin	14	18	12	10

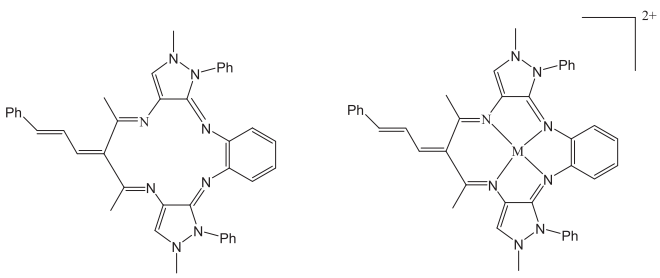

81 **82 - 85**

Fig. 39. Macrocycle **81** and complexes **82**–**85** thereof (M = Cu **82**, Co **83**, Ni **84**, Zn **85**).

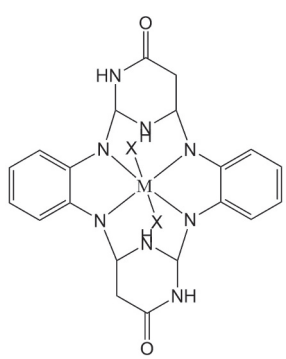

M = Co (**86**), Ni (**87**), Co (**88**)

Fig. 40. Complexes **86**–**88**.

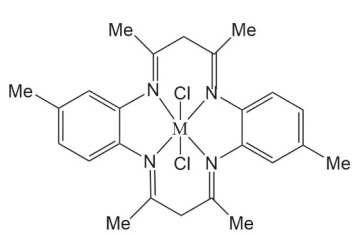

89 (M = Ni) and **90** (M = Cu)

Fig. 41. Complexes **89** and **90** (M = Cu(II), Ni(II)).

resulting complexes were screened against the bacteria *Staphylococcus aureus* (MTCC 96), *Bacillus subtilis* (MTCC 121)], *Escherichia coli* (MTCC 1652) and *Pseudomonas aeruginosa* (MTCC 741). Results revealed that against *S. aureus* and *B. subtilis*, the most active complex was the iron(III) acetate salt with an MIC of 8 μg/mL (see Table *12* where results are compared against the standard antibiotic Ciprofloxacin); the iron(III) chloride complex also exhibited an MIC of 8 μg/mL against *B. subtilis* [158].

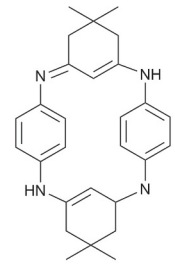

91

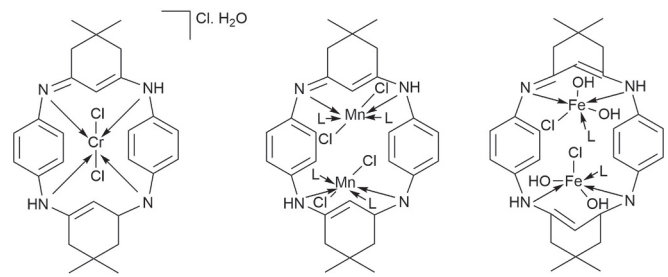

92 **93** **94**

Fig. 42. Macrocycle **91** and complexes **92**–**94** (L = H_2O).

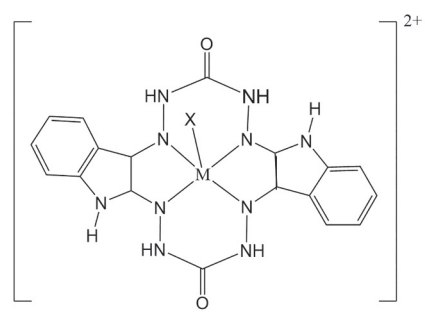

M = Cr(III); X = Cl (**95**), NO_3 (**96**), CH_3CO_2 (**97**)

M = Fe(III); X = Cl (**98**), NO_3 (**99**), CH_3CO_2 (**100**)

Fig. 43. Structure of complexes **95**–**100**.

Table 12
Macro dilution method values for MICs of **95–100**.

Compound	MIC (μg/mL) *Staphylococcus aureus*	MIC (μg/mL) *Bacillus subtilis*	MIC (μg/mL) *Escherichia coli*	MIC (μg/mL) *Pseudomonas aeruginosa*
95	32	32	Nil activity	128
96	64	32	128	>128
97	64	64	128	Nil activity
98	32	8	64	64
99	64	32	128	>128
100	8	8	64	32
Ciprofloxacin	5	5	5	5

7.3. N_5 coordination

A macrocycle prepared from the condensation reaction of 2,2-(piperazine1,4-diyl)dianiline and 2,6-diacetylpyridine was reacted with MBr_2 (M = Cd **101**, Zn **102**, Mn **103**) in the presence of sodium

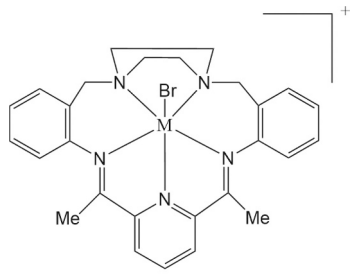

M = Cd (**101**), Zn (**102**), Mn (**103**)

Fig. 44. Complexes **101**–**103**. Note these structure are very similar to those shown in Fig. 23

Table 13
Cytotoxicity of compounds **101**–**103**.

Compound	IC_{50} (μM)	IC_{50} (μM)
	MCF-7	A548
101	6.43 ± 0.2	7.21 ± 0.33
102	8.96 ± 0.81	9.24 ± 0.82
103	10.41 ± 0.92	10.85 ± 0.93

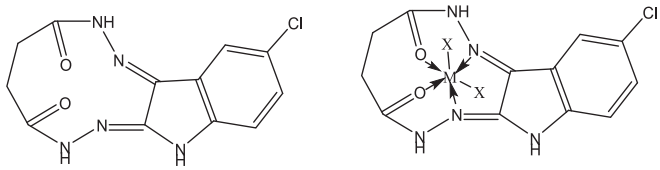

Fig. 45. Macrocyclic complexes derived from the condensation reaction of 5-chloroisatin and succinic acid dihydrazide. M = Co, X = Cl (**105**), NO_3 (**106**), OAc (**107**); M = Ni, X = Cl (**108**), NO_3 (**109**), OAc (**110**); M = Cu, X = Cl (**111**), NO_3 (**112**), OAc (**113**); M = Zn X = Cl (**114**), and macrocycle **104**.

Table 14
MIC results for complexes **105**–**114** *versus* ciprofloxacin.

Compound	MIC (μg/mL)	MIC (μg/mL)	MIC (μg/mL)	MIC (μg/mL)
	Bacillus subtilis	*Staphylococcus aureus*	*Pseudomonas aeruginosa*	*Escherichia coli*
105	>128	>128	>128	>128
106	32	16	64	128
107	32	>128	64	128
108	128	>128	128	64
109	>128	>128	>128	>128
110	>128	>128	>128	>128
111	>128	>128	>128	>128
112	8	8	8	128
113	16	16	128	32
114	8	8	32	64
Ciprofloxacin	5	5	5	5

perchlorate, and the resulting complexes (Fig. 44) were examined for their antibacterial behavior (against *Staphylococcus aureus*, *Escherichia coli*, *Klebsiella oxytoca*, *Salmonella typhimurium*, *Shigella dysenteriae Listeria monocytogenes* and *Bacillus subtilis*) and cytotoxicity (using human lung (A549) and breast (MCF-7)). Results (Table 13) revealed that the zinc complex exhibited best IC_{50} (*e.g.* for MCF-7, 6.43 ± 0.21 μM), and also had most impact on Gram-negative and Gram-positive bacteria; the most resistant bacteria were *S. aureus* (+) [159].

7.4. N_2O_2 coordination

Ali et al. investigated the coordination chemistry (Co(II), Ni(II), Cu (II), Zn(II)) of the macrocycle **104** derived from the condensation reaction of 5-chloroisatin and succinic acid dihydrazide (Fig. 45). The resulting complexes **105**–**114** were screened for their antibacterial (Table 14) and anticancer activity (Table 15), with the zinc and nickel complexes exhibiting the best anti-cancer activity against the SCC4 cell line with an IC_{50} of 41.4 μM and 45.4 μM (for the nickel acetate complex) respectively over 72 h (the value was 5 μM for cisplatin under the same conditions). The potential of the zinc complex was further illustrated from molecular docking studies where it was shown to exhibit a strong binding affinity toward epidermal growth factor receptor (EGFR) tyrosine tyrosine kinase. In terms of antibacterial performance, the complexes were screened against *B. subtilis*, *S. aureus*, *P. aeruginosa* and *E. coli* bacteria; the copper and zinc complexes performed best [160].

Table 15
Anticancer activity of complexes **105**–**114** *versus* cisplatin.

Compound	IC_{50} (μM)	MIC (μgM/mL)	MIC (μgM/mL)
	24 h	48 h	72 h
105	>100	97.2	95.5
106	>100	99.8	96.0
107	>100	>100	>100
108	>100	98.0	94.4
109	64.9	60.8	58.6
110	50.5	47.5	45.4
111	88.1	85.3	82.9
112	>100	99.6	96.2
113	97.6	95.0	93.6
114	46.9	43.0	41.4
Cisplatin	8	6	5

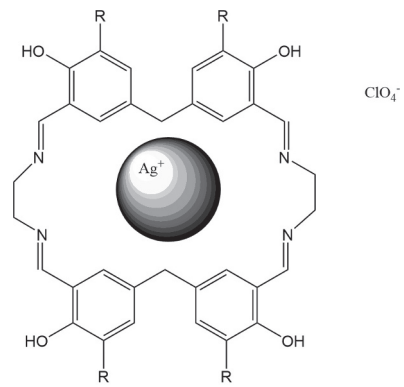

Fig. 46. Calix-salen-like molecules R = H **115**, OMe **116**, Br **117**, NO_2 **118**, *t*-Bu **119**.

7.5. Calix-salen-like macrocycles

Desai et al. employed silver ions as a template in the reaction of 5,5′-methylene-bis-salicylaldehyde with ethylene diamine to afford calix-salen-like molecules **115–119**, for which the silver ion resides in the cavity (Fig. 46) [161]. The anti-microbial/anti-cancer properties of the system were studied for various derivatives in which the bis-salicylaldehyde had been functionalized with either electron withdrawing or electron donating groups. Results (Table 16) revealed that the substituents greatly impacted on the behavior of the system, such that those bearing Br, NO_2 or *tert*-butyl substituents exhibited best antibacterial activity, the Br derivative the best fungicidal activity, whilst the Br derivative and the unsubstituted system were the best therapeutic agents (for anti-cancer properties, see Table 17).

Table 16
Antibacterial activity of compounds **115–119** *versus* ampicillin, chloramphenicol and ciprofoxacin.

Compound	MIC (μM) L132 cells	MIC (μM) HepG2 cells	MIC (μM) IMR32 cells	MIC (μM) MTCC 96	MIC (μM) MTCC 442	MIC (μM) MTC 441
115	261	261	326	653	130	653
116	226	113	226	226	282	282
117	185	231	92	116	231	116
118	211	211	66	132	211	211
119	63	101	202	101	101	252
ampicillin	286	–	286	716	286	716
chloramphenicol	155	155	155	155	155	155
ciprofoxacin	75	75	75	151	151	151

Table 17
Cytotoxicity of compounds **115**–**119** *versus* cisplatin over 24 h.

Compound	IC_{50} (μM) L132 cells	IC_{50} (μM) HepG2 cells	IC_{50} (μM) IMR32 cells
115	7.92 ± 0.64	7.15 ± 0.88	5.87 ± 0.91
116	9.34 ± 0.82	11.28 ± 1.09	7.11 ± 0.86
117	8.91 ± 1.2	8.39 ± 0.98	5.10 ± 0.82
118	16.38 ± 1.7	22.73 ± 1.3	20.61 ± 1.68
119	9.59 ± 0.95	11.62 ± 1.26	9.09 ± 1.08
Cisplatin	26.66 ± 1.8	23.66 ± 1.97	12.9 ± 1.72

7.6. Double layer Schiff bases

Our efforts in this area have centred around the use of Schiff-base complexes bearing macrocyclic ligands. For example, we recently reported the [2 + 2] **120**, [2 + 3] **121** and [2 + 4] **122** double layer Schiff-base macrocycles shown in Fig. 47. We employed **121** for the immobilization of palladium, and showed that this composite, in the presence of low concentrations of H_2O_2, exhibited excellent bactericidal activity against both *Escherichia coli* (Gram-negative bacterium) and *Staphylococcus aureus* (Gram-positive bacterium). Cytotoxicity tests carried out against HaCaT and Hep-G2 cell lines using the MTS assay revealed that the Pd composite is non-toxic even at high concentrations [162].

8. Anti-HIV activity

McKeating, Hannon et al. have employed a 'shape-fit' nucleic acid targeting approach which makes use of metallo-supramolecular triple stranded helicates (cylinders) based on Fe(II) **123**, Ni(II) **124** or Ru(II) **125**, Fig. 48. The potential of the cylinders to target the Trans Activation Response (TAR) region associated with the retrovirus human immunodeficiency virus type 1 (HIV-1) was explored. Best results were obtained using the Ni (**120**) and Ru (**121**)-based cylinders. These were able to inhibit formation of the virus-encoded Transactivator protein and thereby HIV infection. The cell viability values for these three complexes are given in Table 18 [163].

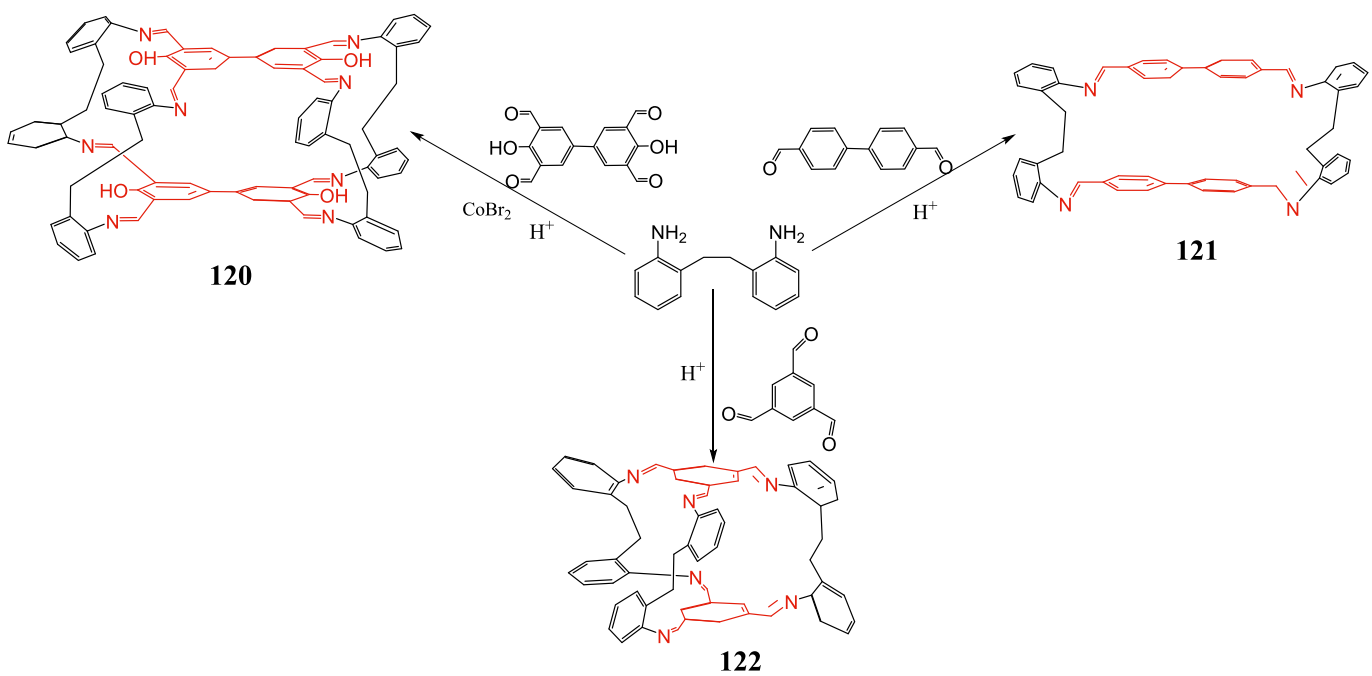

Fig. 47. Schiff base macrocycles **120** to **122**.

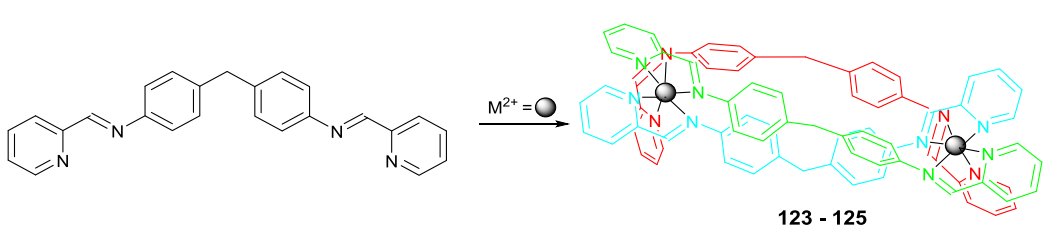

Fig. 48. Triple stranded helicates $[M_2L_3]^{4+}$ **123**–**125** (M = Fe, Ni, Ru).

Table 18
IC_{50} values for **123**–**125**.

Complex	IC_{50} 1G5	TZM.bI cells
123	55 ± 7	59 ± 19
124	>160	>100
125	51 ± 16	52 ± 13

9. *Mycobacterium tuberculosis*

Rutledge, Todd et al. have reported a series of cyclam-derived compounds that proved to be active against drug-resistant *Mycobacterium tuberculosis*. More specifically, studies focused on the use of a central cyclam core connected to two identical naphthalimide motifs *via* triazole linkers (Fig. 49). The nature of the metal present was also investigated, with variations including the use of Zn(II) **126**, Cu(II) **127**, Fe(II) **128**, Fe(III) **129**, Sm(III) **130**, Co(II) **131** and Mn(II) **132** salts. However, the studies revealed little change in antitubercular activity on changing the metal. Some antitubercular activity was maintained on replacing the naphthalimide with naphthalene-based pendent groups (*e.g.* in **133** and **134**, Fig. 49 middle). Moreover, when the naphthyl-containing system had the "reversed" triazole connectivity (Fig. 49,

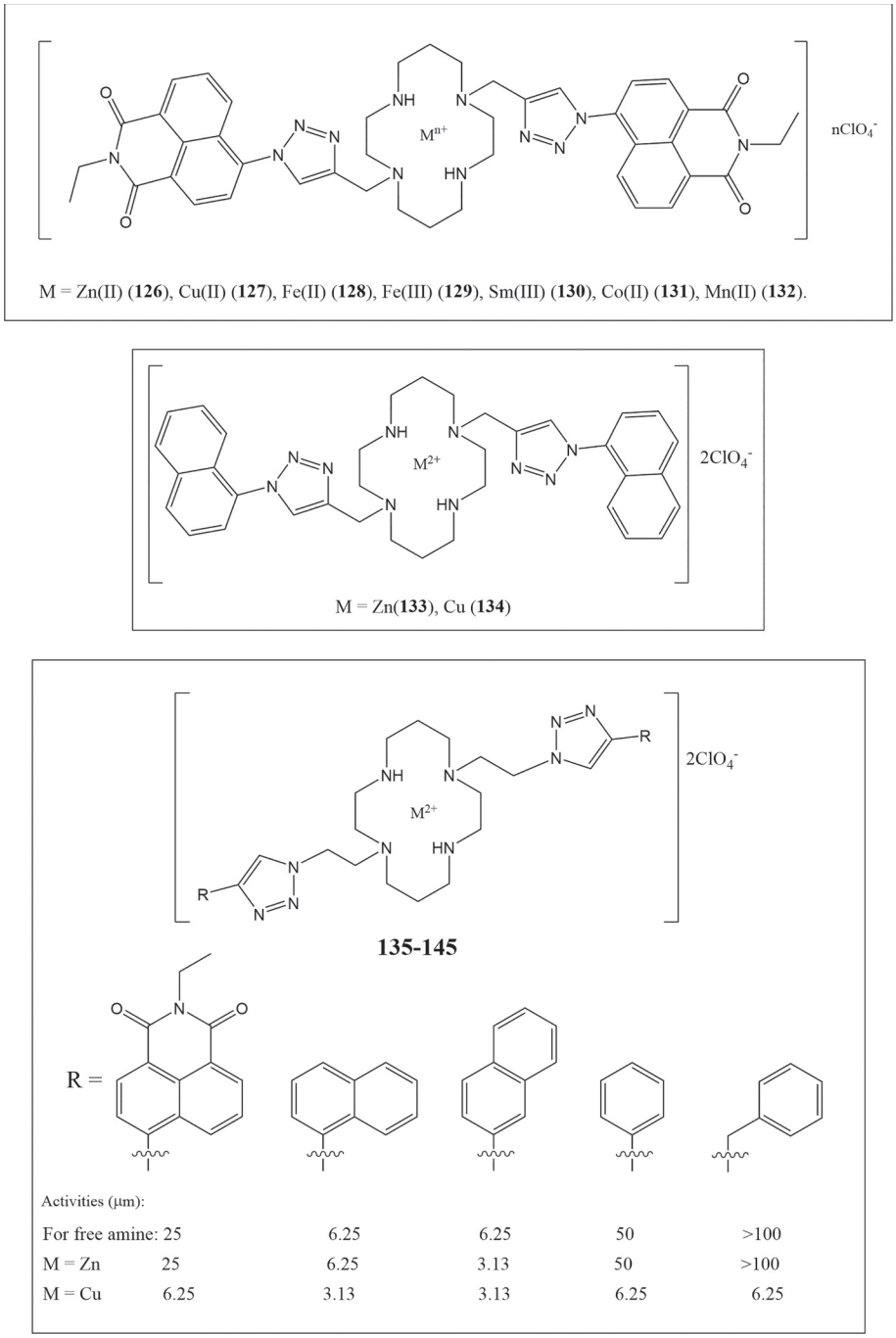

Fig. 49. Top, complexes **126–132**; middle: complexes **133** and **134**; bottom: variation of the linkers (M = Zn, Cu, Fe, Sm, Co, Mn) with activities for the free amines and their complexes **135–145** (where M = Zn, Cu).

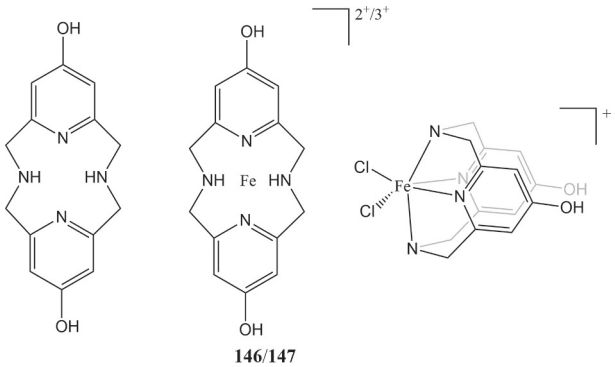

Fig. 50. Left: $^{OH}Py_2N_2$-type macrocycle; middle: Complexes **146** and **147**; right: binding mode of $^{OH}Py_2N_2$at Fe.

bottom), the results indicated increased antitubercular activity for the Zn(II) **126** and Cu(II) **127** complexes *versus* that of the parent compound. Other end groups were also trialed, including the likes of phenyl and benzyl, as well as 1–/2-naphthyl, and results revealed that the Cu(II) species tended to exhibit best antitubercular activity. Other *in vivo* studies revealed increased solubility for the $ZnCl_2$ derived complex which aided efficacy testing against *M. marinum* infection [164].

10. Other applications

10.1. Improvement of lens opacity

Wu, Green et al. have investigated the use of an $^{OH}Py_2N_2$-type macrocycle to tackle damage to the eye lens which occurs *via* oxidative stress. Multiple biological pathways appear to be involved in the protection process, including activating Nrf2 (nuclear factor erythroid-2-related factor 2) expression and Grx1 and 2 (Glutathione-dependent glutaredoxins) pathways, and increased levels of adenosine triphosphate. The ligand set also readily binds to Fe(II) **146** and Fe(III) **147** (Fig. 50). Interestingly, H_2O_2-induced lens opacity was reduced in the presence of $^{OH}Py_2N_2$ [165].

10.2. Alzheimer's disease

Gagey-Eilstein, Agasti et al. conjugated a number (six in all) of fluorophores with cucurbit[7]uril, *e.g.* Fig. 51. For the Q[7], the point of conjugation was ensured by first forming a monohydroxylated derivative, converting to an amine and then forming an *N*-hydroxysuccinimide derived species **148**. The system proved to be very good at not only detecting biomolecules, but could also identify folds and could even distinguish between amyloids originating from different sources with 100% success rate. Moreover, the system could identify Aβ-oligomers, which are thought to play a part in the neurodegeneration related to Alzheimer's disease [166].

10.3. Detection of antibiotics

Chen et al. made used of coordination polymers formed from tetramethylcucurbit[6]uril and alkaline earth metal salts in the presence of 4,4′-biphenyldisulfonic acid (as a structure inducer). The polymer formed when using $Ca(NO_3)_2$ was shown by using sensing experiments to be a good fluorescent probe for the detection of norfloxacin (a known antibiotic) [167].

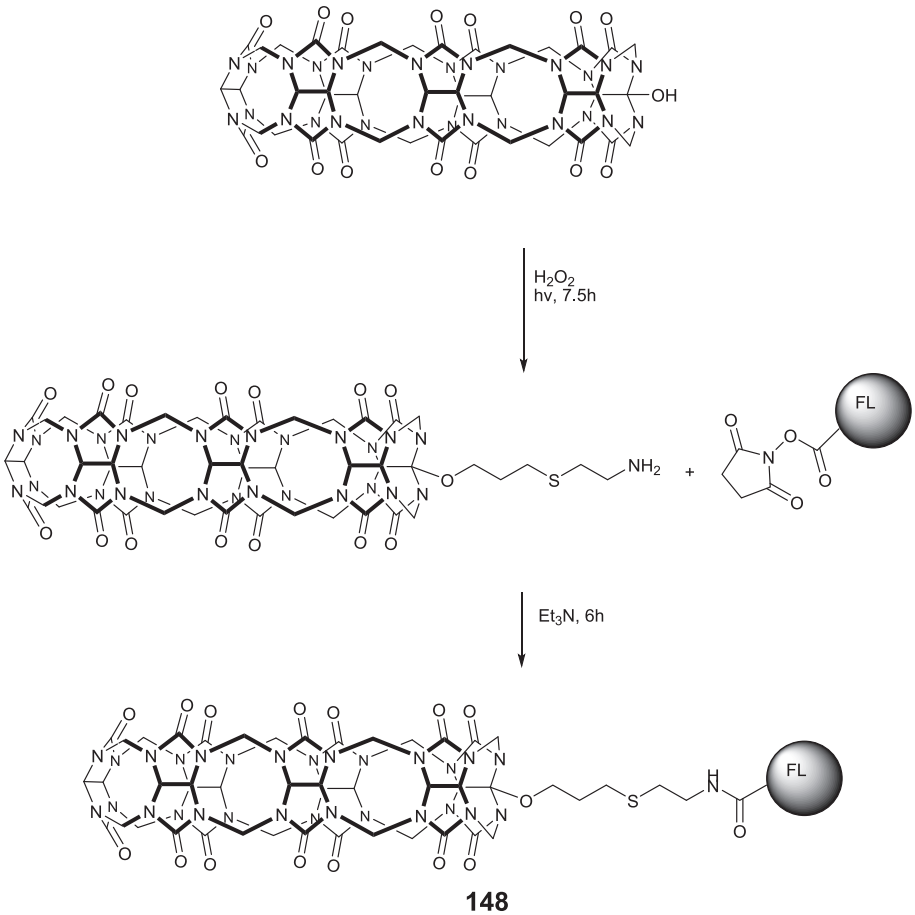

Fig. 51. Protocol for the conjugation of Q[7](OH) with fluorophores to form **148**.

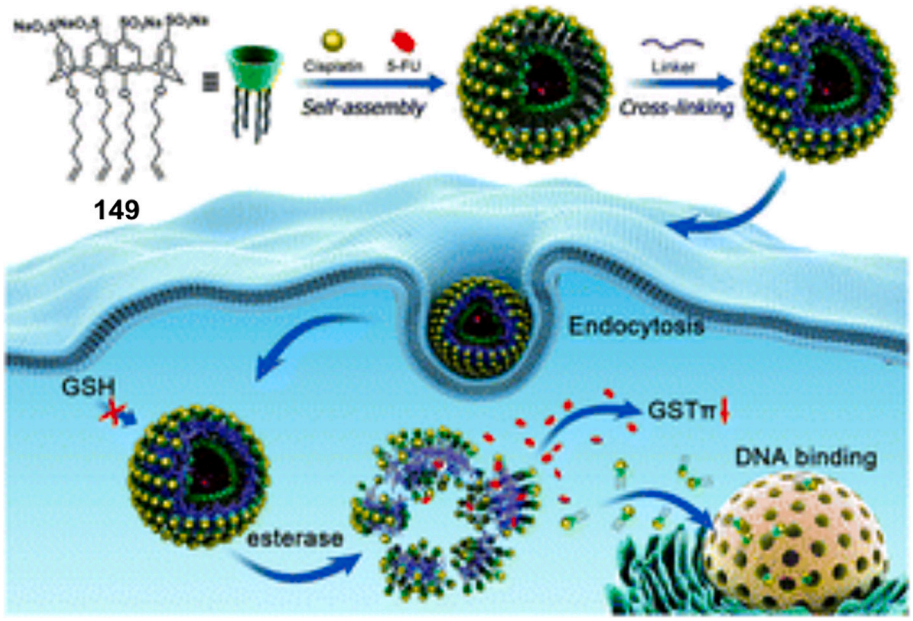

Fig. 52. Crossed-linked nanoparticles incorporating **149** and cytotoxicity studies thereof. Reproduced from reference 168 with permission from the Royal Society of Chemistry.

Table 19
Comparison of IC_{50} values and drug resistance.

Agent	IC_{50} A549	A549/CDDP	Resistance
Cisplatin	7.5 ± 0.5	37.6 ± 1.3	4.98
Pt·cCAV	25.7 ± 2.0	45.1 ± 0.5	1.76
Pt·cCAV$_{5\text{-FU}}$	18.6 ± 1.2	14.0 ± 2.2	0.75
Cisplatin + 5-FU	6.2 ± 0.7	21.0 ± 1.0	3.38

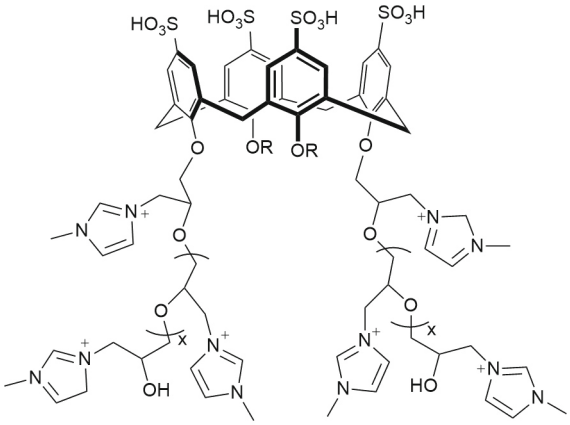

Fig. 53. Poly ionic liquid-grafted amphoteric calixarene **150** (x not defined; R = H).

11. Use of macrocycles in combination with nanoparticles

Numerous types of macrocycles have been utilized to modify the surface of nanoparticles with a view to subsequent use in medicine.

11.1. Calixarenes

11.1.1. Calix[4]arenes

For calix[4]arenes, these include the use of *p*-sulfonatocalix[4]arene, which following modification with 6-bromo-1-hexene to form the amphiphilic species **149**, was employed to protect cisplatin *via* the formation of a vesicle structure (Pt•cCAV), *i.e.* a guest-induced assembly. Synthetic studies indicated that the optimum ratio of calixarene to cisplatin was 1:1 [168]. Thiol-ene Click chemistry was employed to form cross-linked nanoparticles, with the latter exhibiting enhanced stability in blood environments, Fig. 52.

In the presence of 5-fluorouracil (5-FU), the nanoparticles were found to incorporate 13 wt% cisplatin and 19% 5-fluorouracil. This system together with the vesicle structure (*i.e.* Pt▪cCAV$_{5\text{-FU}}$) when screened against the human non-small cell lung cancer cell line A549 was found to increase the resistance of cisplatin (*versus* free cisplatin or cisplatin/5-fluorouracil) to detoxification. The cross-linked system exhibited the largest decrease in cell resistance relative to cisplatin with IC_{50} values of 18.6 ± 1.2 μM (against A549) and 14.0 ± 2.2 μM (against A549/CDDP), see Table 19. Studies suggested that any toxicity present was down to the guest (cisplatin) rather than to the host nanoparticle.

Further work explored the influence of loading the 5-fluorouracil within the nanoparticle on glutathione *S*-transferases expression (specifically π-glutathione *S*-transferase) and activity in A549/CDDP cells. Results indicated that the enzymatic activity was indeed reduced in the presence of the 5-fluorouracil loaded nanoparticle, and moreover that this system was more toxic to A549/CDDP cells *versus* A549 cells. Fluorescence studies indicated that the internalization of the loaded nanoparticle occurred *via* caveolin-mediated endocytosis, whilst flow cytometry and confocal laser scanning microscopy indicated a faster uptake for the loaded nanoparticle and accumulation in the cytoplasm, respectively.

Karimian, Kafil et al. combined *p*-sulfonatocalix[4]arene with excess 1-methyl-3-(oxirane-2-ylmethyl)–1H-imidazole-3-ium chloride to afford, following work up, the poly-ionic liquid-grafted amphoteric calixarene **150** (Fig. 53). This calixarene could then be used to coat Fe_3O_4 magnetic nanoparticles, and the system exhibited good biocompatibility. The drug co-delivery ability of the system was demonstrated using doxorubicin and methotrexate against MCF7 breast cancer cells (see Table 20) [169].

11.1.2. Calix[6]arenes

Bhasikuttan, Mohanty et al. have utilized silver nanoparticles coated

Table 20
Effect of drug (doxorubicin and methotrexate) dose against MCF7 breast cancer cells.

	DOX-MTX group	DOX-MTX/nanocarrier
Drug dose	Cell viability	Cell viability
0.312	69.270 ± 1.549	68.936 ± 2.679
0.625	60.299 ± 1.016	51.299 ± 2.227
1.250	50.799 ± 1.762	46.779 ± 3.609
2.500	41.609 ± 1.537	32.609 ± 2.620
5.000	27.733 ± 2.758	20.399 ± 2.208
10.000	21.606 ± 1.113	12.458 ± 2.115

with *p*-sulfonatocalix[6]arene **151** (bound *via* the upper rim SO_3^- moieties) to load the drug sanguinarine, Fig. 54. Studies revealed that the subsequent change in pK_a (from 7.7 to 10.1) was able to activate the iminium form of sanguinarine, which in turn led to an improvement in the antibacterial efficacy and reduced the minimum inhibitory concentration of the drug as evidenced for *Staphylococcus aureus* (Gram-positive), *Escherichia coli* (Gram-negative) bacteria and *Salmonella Oslo*, the latter being isolated from marine fish [170].

11.2. Cucurbiturils

In the case of Q[*n*]s, their use for a variety of applications has been

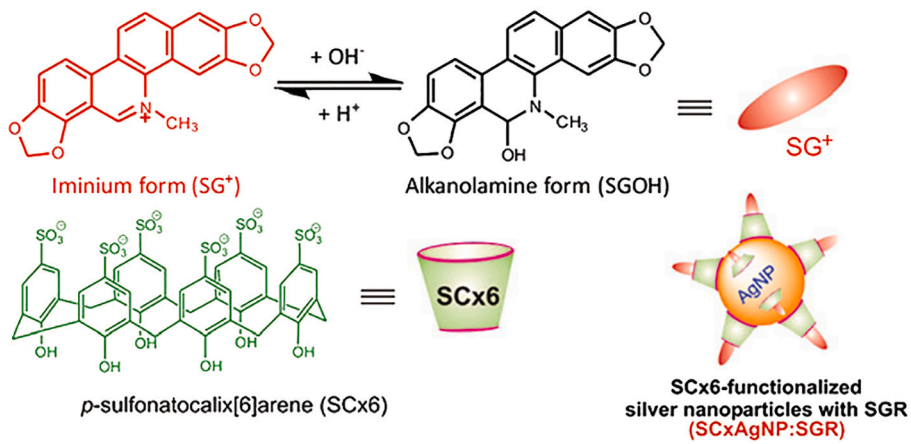

Fig. 54. Silver nanoparticles **151** coated with *p*-sulfonatocalix[6]arene as a carrier for the drug sanguinarine. Reproduced from reference 170 with permission from the Royal Society of Chemistry.

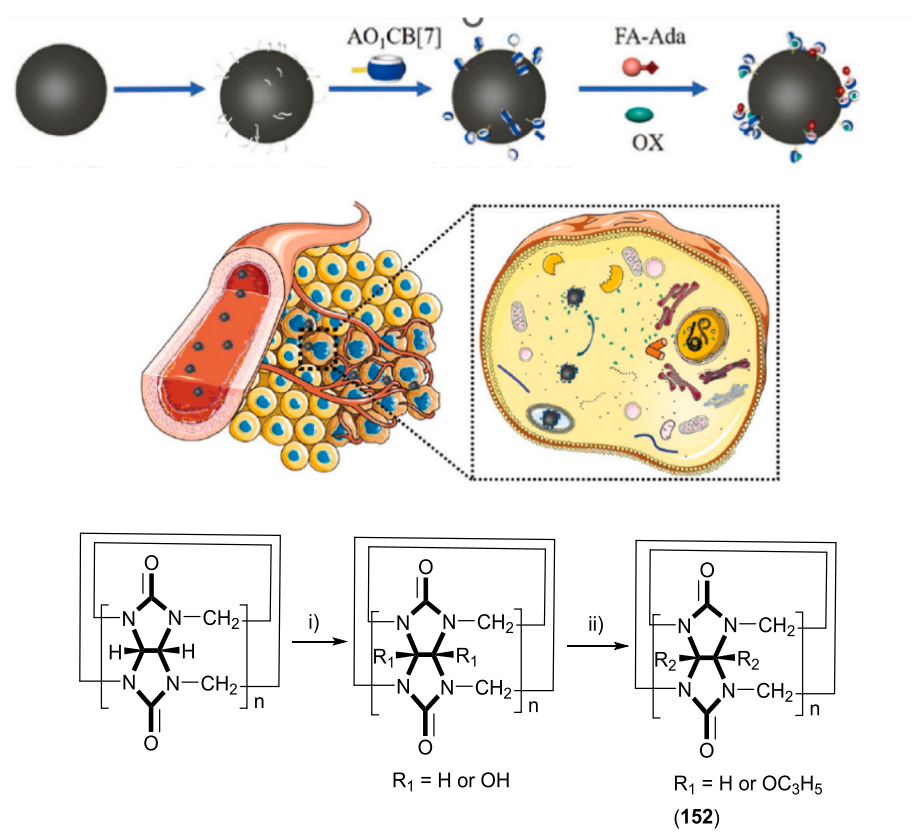

Fig. 55. Top: Design of the Fe_3O_4 nanoplatform (Reproduced from reference 171 with permission from the Royal Society of Chemistry); bottom: synthesis of **152**, i) $K_2S_2O_8$, K_2SO_4, 85 °C, H_2O, 12 h; ii) NaH, DMSO, 4 h, allyl bromide, 12 h.

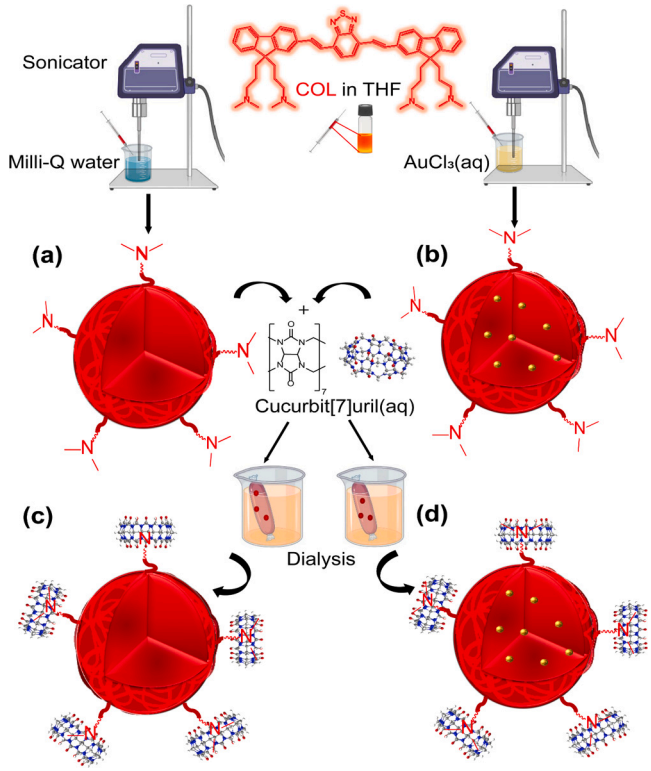

Fig. 56. Hybrid gold/conjugated oligomer nanoparticles in conjunction with Q[7] **153** for PDT and cellular imaging. (a) Conjugated oligomer nanoparticles; (b) Conjugated oligomer gold nanoparticles plus complexation of nanoparticle amine residues with Q[7]; (c) Q[7]@ Conjugated oligomer nanoparticles; (d) **153**. Reproduced from reference 175 with permission from the American Chemical Society (Copyright 2024).

reviewed [25,29,31,34,36,40].

11.2.1. *Cucurbit[7]uril*

Recent highlights include the report by Wang et al., who employed Q[7] in combination with superparamagnetic Fe_3O_4 (average size 7.40 nm) as part of a toolkit for MRI-image guided chemotherapy of cancer, Fig. 55 top [171]. In particular, a mono-*O*-allyl-Q[7] [172] (**152**, Fig. 55 bottom) was subject to a Click reaction with the thiol of the nanoparticle surface, and then *via* host-guest interactions, adamantanamine tags. By utilizing Q[7] host-guest interactions, oxaliplatin could also be loaded onto this system (as confirmed by FTIR spectroscopy; the cyclohexane peak at 3080 cm^{-1} was observed post-loading) with a loading efficiency of *ca.* 8% (confirmed by ICP-MS). *In vitro* and *in vivo* drug release was demonstrated in tumor cells with excess spermine present, *i.e.* the spermine displaced the oxaliplatin from the Q[7] cavity. At the concentration normally seen in tumor cells (1.0 mM), >70% release was observed over 72 h incubation; in the absence of spermine, the release of oxaliplatin was far lower. Whilst the toxicity of the system was enhanced against various cancer cell lines, the safety profile against non-cancerous cells was good. The increased targeting ability and therapeutic efficiency of this nanoparticle-based Q[7] system was also evident in studies on mice.

Wang et al. extended their Q[7] studies to the encapsulation of oxaliplatin by combining Q[7] with nano-graphene oxide. The host-guest properties of the Q[7] also allowed for the biocompatibility of the system to be boosted *via* adamantane substituted hyaluronic acid wrapping. The system could be co-loaded with the likes of chlorin e6, banoxantrone dihydrochloride together with the oxaliplatin. Subsequent *in vitro* and *in vivo* studies revealed remarkable antitumor efficacy as a result of the synergy of photothermal, photodynamic and chemotherapies [173].

Liang, Cheng et al. reported a drug release system in which Q[7], appended to a gold nano-star, was used to encapsulate camptothecin. The presence of the Q[7] led to improved aqueous stability for the

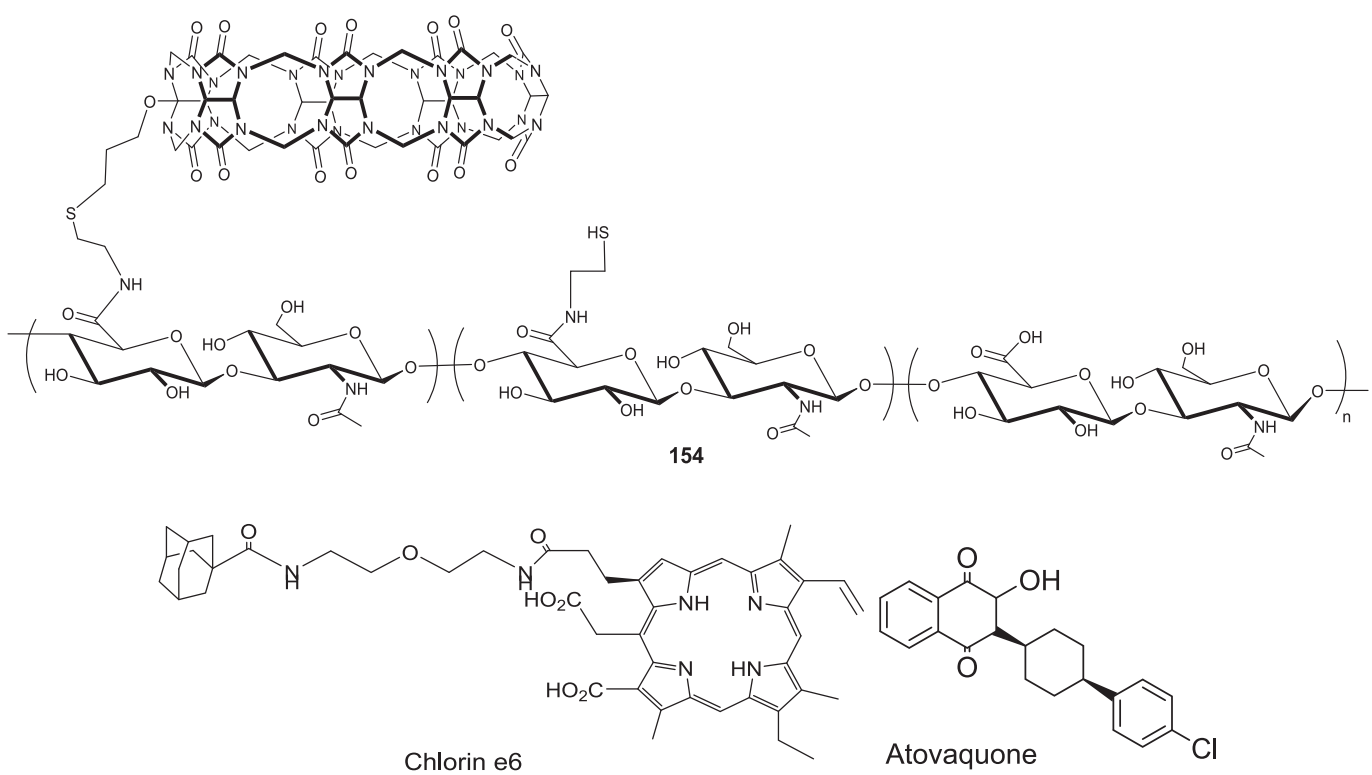

Fig. 57. Top: Q[7]-functionalized chain **154**; bottom left Chlorin e6 pegalated with adamantine; bottom right atovaquone.

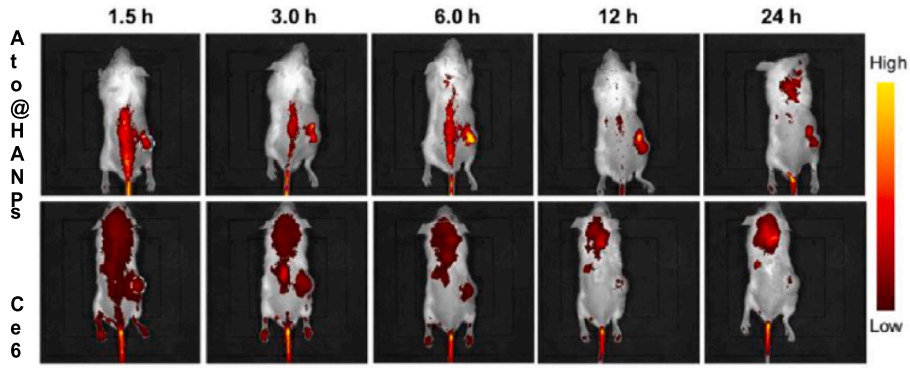

Fig. 58. *In-vivo* imaging using atovaquone-containing nanoparticles *versus* free Chlorin e6 for CT26-tumor bearing mice. Reproduced from reference 177 with permission from Elsevier.

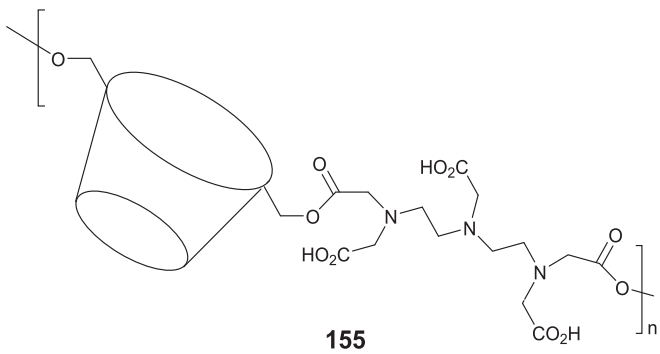

Fig. 59. Folic acid conjugated β-cyclodextrin polyester **155**.

system, and drug release proved possible by applying near-infrared (NIR) light irradiation. It was also found that the overheating was by virtue of the irradiation (photothermal therapy) together with the action of the drug (chemotherapy) allowed for a synergic cancer treatment [174].

Hybrid gold/conjugated oligomer nanoparticles have also been used in conjunction with Q[7] to afford **153** which was utilized for PDT and cellular imaging [175]. Work by Tuncel et al. showed that the dark cytotoxicity of the hybrid nanoparticles toward pathogens and breast cancer cells (MCF-7) was reduced upon addition of Q[7], Fig. 56. Moreover, the light induced cytotoxicity effects of the hybrid nanoparticles were maintained upon irradiation with either a laser (915 nm) or white light when applied to photothermal or photodynamic therapy respectively. It also proved possible to apply the system to cellular imaging.

Li, Wang et al. have utilized the conjugate formed between adamantane and lunimol, which is a known marker of use in biological systems, and also utilized the host-guest capability of the previously mentioned **5** (Fig. 10) to form supramolecular biocompatible nanoparticles. This system was found to be capable of deep tissue penetration and luminescent imaging using cell lines and mice peritonitis models by virtue of BRET (bioluminescence resonance energy transfer). The imaging performance proved to be better than that of luminol alone [176].

Wang et al. combined hyaluronic acid with Q[7] and employed the resulting Q[7]-functionalized chain **154** (Fig. 57, top) to encapsulate the photosensitizer Chlorin e6 (pegalated with adamantanes, Fig. 56, bottom left) at the same time as oxaliplatin (Fig. 2). It was found that the system self-assembled into nanoparticles, and the latter exhibited targeting ability and were capable of both PDT and chemotherapy. Moreover, by employing atovaquone (Fig. 57, bottom right), the therapeutic outcomes could be further improved as a result of limiting the oxygen consumption at the tumor [177]. The *in vivo* accumulation of atovaquone-containing nanoparticles was evaluated *versus* free Chlorin e6 for CT26-tumor bearing mice (Fig. 58). The data revealed a three times higher intensity for the nanoparticle system. It was also found that the nanoparticles were capable of better *ex vivo* imaging of organs at 24 h. We note that new directions in PDT have recently been reviewed

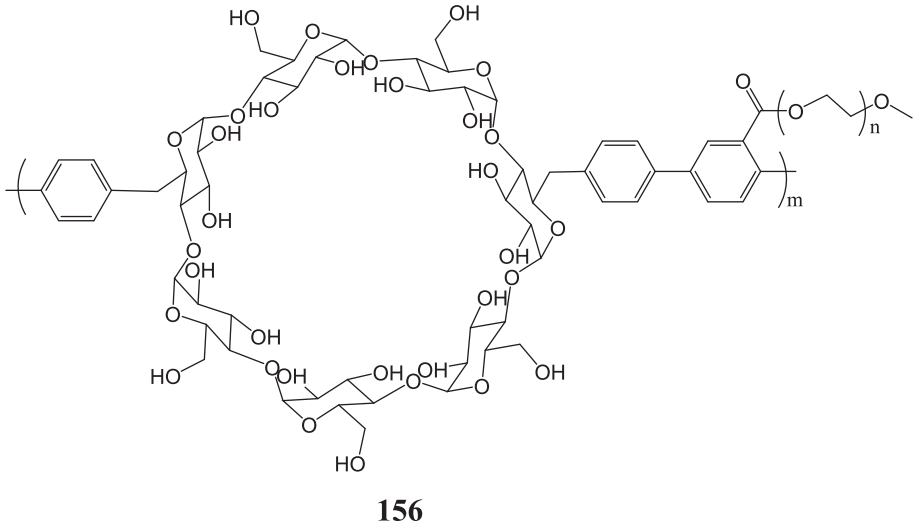

Fig. 60. Poly(*p*-phenylene-*co*-cyclodextrin-g-poly(ethylene glycol) polymer **156**.

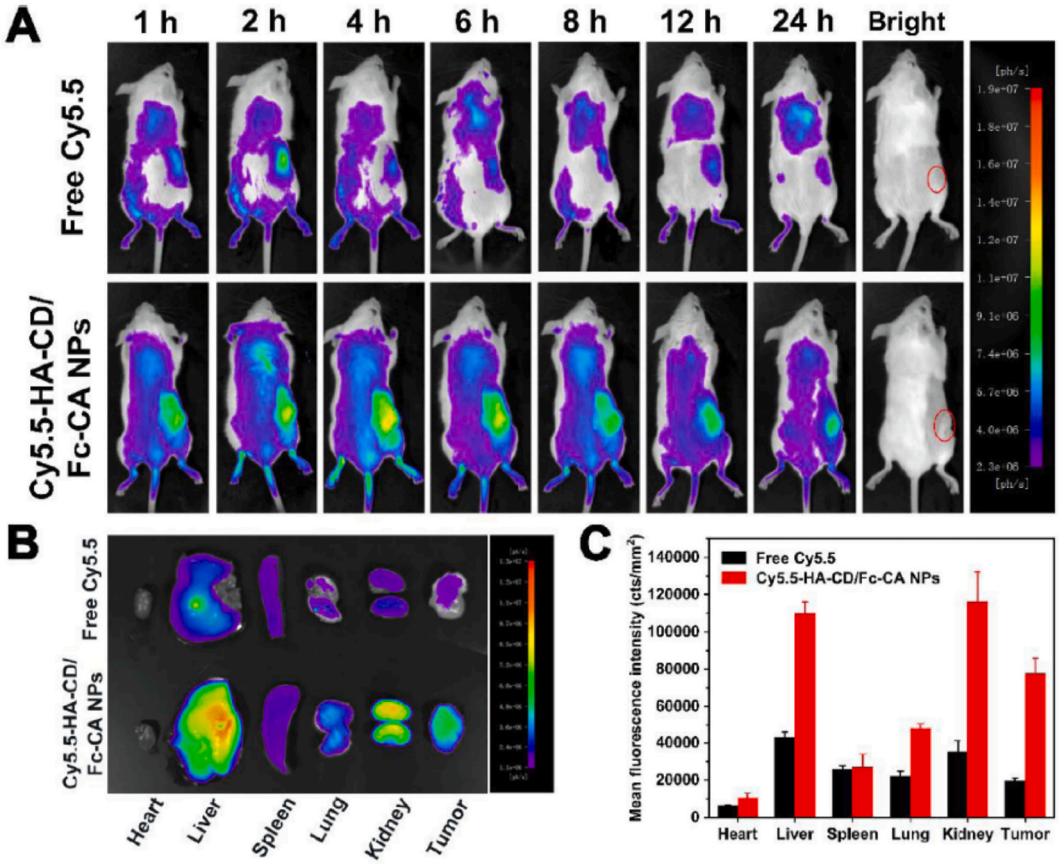

Fig. 61. A) *In-vivo* fluorescent images; B) *Ex-vivo* fluorescent images; C) Mean fluorescent intensities after 24 h. Reproduced from reference 184 with permission from Elsevier.

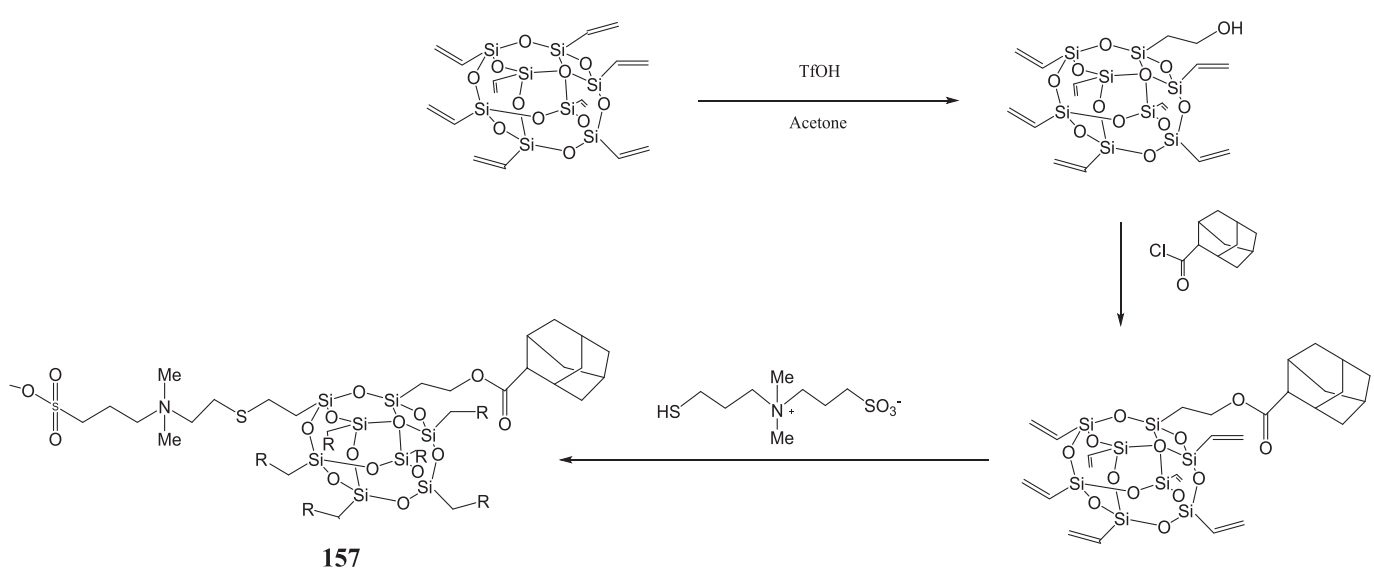

Fig. 62. Supramolecular amphiphilic zwitterionic complex **157** (R = $CH_2SC_3H_6N(CH_3)_2C_3H_6SO_3^-$).

[60,61].

11.2.2. Cucurbit[8]uril

The larger Q[8], in combination with Fe_3O_4 nanoparticles and a mesoporous silica core, has been employed by Chen, Di, Hu et al. for targeted drug release. The basis of the delivery system stems from the encapsulation of tryptophan by the Q[8], thereby forming the homo-ternary complex (Trp·Trp) ⊂ Q[8], and its stability in environments that overexpress indoleamine 2,3-dioxygenase 1. The area surrounding tumors represent such an environment, and this results in the transformation of tryptophan into *N*-formylkynurenine, and subsequent collapse of the delivery system. In turn, this can result in the release of any drug payloads stored within the mesoporous silica structure. Proof-of-principal was demonstrated using doxorubicin, whereby doxorubicin

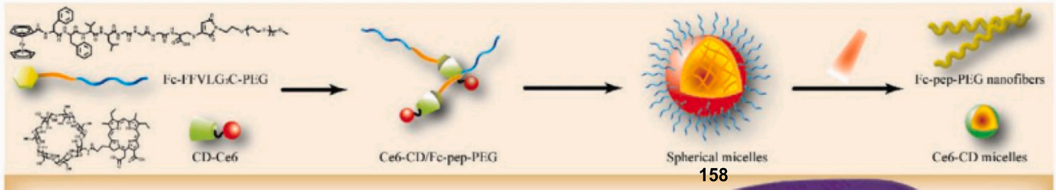

Fig. 63. Formation of spherical micelles **158** from chlorin e6-conjugated β-cyclodextrin and ferrocene-modified PEG conjugates and formation of nanofibers on reaction with reactive oxygen species. Reproduced from reference 186 with permission from Wiley.

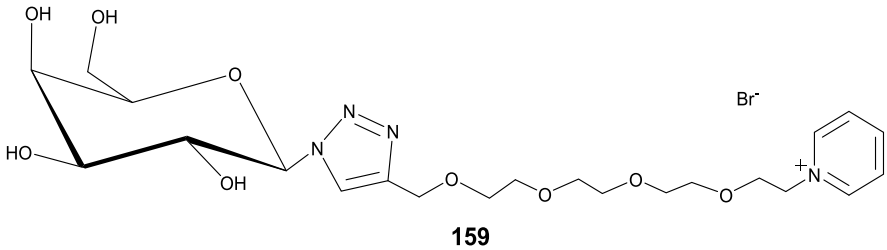

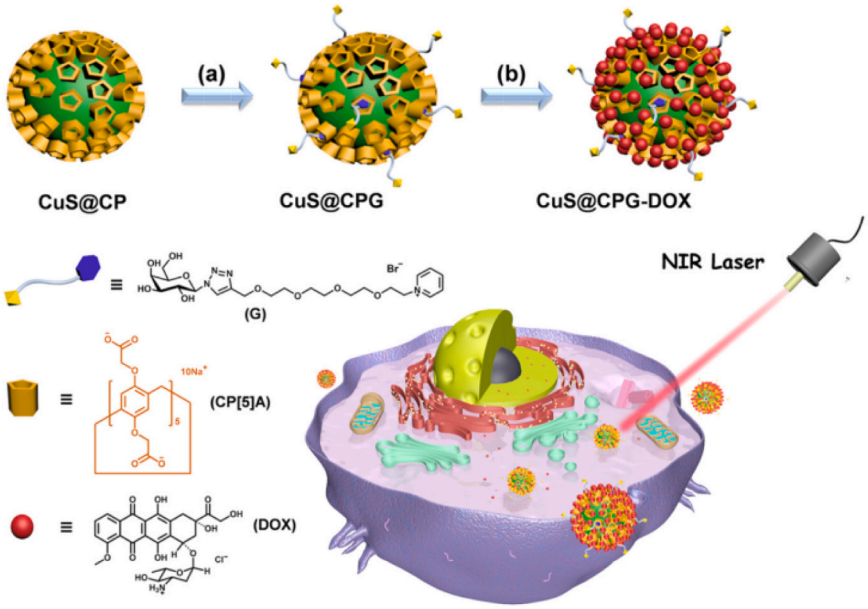

Fig. 64. Top galactose derivative **159**; bottom Targeting of liver cancer cells based on CuS nanoparticles decorated with carboxylatopillar[5]arenes. Reproduced from reference 187 with permission from the American Chemical Society (Copyright 2024).

leakage kinetics was increased in the presence of increased amounts of indoleamine 2,3-dioxygenase 1. In this delivery system, the loading capacity for doxorubicin was noted at 28.6% which is on a par with mesoporous silica [178].

11.2.3. Cyclodextrins

Work using cyclodextrins in combination with nanoparticles in the cancer therapy field was reviewed in 2021 [179,180].

Highlights include the work of Alam, Khoobi et al., who prepared an MRI contrast agent based on folic acid conjugated β-cyclodextrin polyester **155** (Fig. 59) coated gadolinium oxide nanoparticles. The presence of the polycyclodextrin environment greatly improved the toxicity (*i.e.* the biosafety), which was accomplished by masking the toxicity of the Gd_2O_3-based agent. For example, at concentration of up to 50 μg Gd (III)/mL, these coated nanoparticles exhibited little cytotoxicity against the normal human breast cell line MCF-10 A. The presence of the folic acid enabled enhanced intracellular uptake in cancer cells M109 *versus* 4 T1 cells. Moreover, the folic acid allowed for higher contrast enhancement in tumor areas *in vivo* when compared against the agent that lacked the presence of folic acid ligation [181].

Dong, Nie, Zhao, Wong et al. have also employed β-cyclodextrin to improve the water solubility of gold nanoparticles. Moreover, both the biocompatibility and the emission intensity (at *ca.* 600 nm) was greatly improved by the presence of the β-cyclodextrin. This allowed for the system to be taken up by gastric cancer cells (MGC-803) exhibiting red luminescence in the process. Using UV absorption spectra, the drug (doxorubicin) loading capability of the system was investigated, and it was found that 94 μg of DOX could be loaded per 1 mg of the β-cyclodextrin coated gold nanoparticles, a loading efficiency of 25% [182].

Timur, Yagci et al. prepared a polymer **156** incorporating β-cyclodextrin in the backbone (Fig. 60) and bearing poly(ethylene glycol), namely poly(*p*-phenylene-*co*-cyclodextrin-g-poly(ethylene glycol), where g = graft, and combined it with cysteamine treated gold nanoparticles. Subsequent studies on imaging quality and therapy efficiency (on U87 cells) revealed that the presence of the β-cyclodextrin-based polymer conjugated with gold nanoparticles allowed for more effective

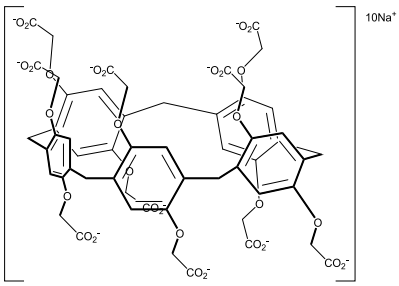

160

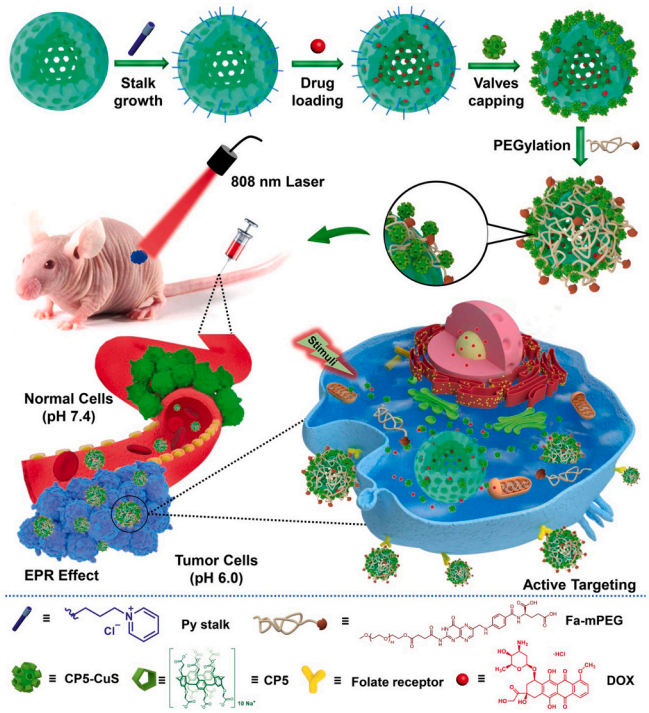

Fig. 65. Top: Carboxylated pillar[5]arene **160**; Bottom: CuS nanoparticle system functionalized with **160** capable of synergic chemo/photothermal therapy. Reproduced from reference 188 (Ma, Wang, Yang et al.) under license CC By 4.0.

imaging and targeting *versus* the unconjugated polymer. This conjugated system also led to enhanced radiosensitivity as evidenced for studies on U87 cells [183].

Zhao et al. have reported a nanoreactor, HA-CD/Fc-CA NPs, which utilizes a cyclodextrin-modified hyaluronic acid conjugate (HA-CD) together with a ferrocene-modified cinnamaldehyde prodrug (Fc-CA), that was responsive to pH and redox changes [184]. The system demonstrated minimal side effects during synergistic chemo/chemodynamic therapy and exhibited impressive tumor targeting ability. The underlying chemistry involved a ROS-generator *via* Fenton-type catalysis, aldehyde group protection and formation of a hydrophilic outer shell, and this allowed the system under acidic conditions to release cinnamaldehyde and ultimately to the generation of highly cytotoxic •OH. Results from *in vivo* real-time fluorescence imaging, suggested that the HA-CD/Fc-CA NPs were of an appropriate size to allow for efficient accumulation in tumor tissues. Further studies on 4T1 tumor bearing BALB/C mice revealed that the HA-CD/Fc-CA NPs exerted the greatest tumor suppression effects, superior to those observed for the constituent parts alone (Fig. 61).

Wang, Wu et al. employed Click chemistry and host-guest interactions to synthesize a supramolecular amphiphilic zwitterionic complex **157** incorporating polyhedral oligomeric silsesquioxane with appended adamantine-containing substituents and sulfobetaine substituents (Fig. 62), and star-shaped molecules of β-cyclodextrin-PLLA (PLLA = poly-L-lactic acid); the latter was formed *via* ring opening polymerization using $Sn(Oct)_2$ as catalyst. The system self-assembled into micellar nanoparticles, which were shown to be capable of both loading and releasing doxorubicin in a controlled fashion. The zwitterionic nature of the system aided its stability under extra- and intracellular pH conditions, including tumor sites. Indeed, accumulation and internalization were noted in the case of HeLa and MCF-7 tumor cells, for which an exciting anticancer therapeutic effect was observed [185].

Gao, Lu et al. have utilized the host-guest interaction between chlorin e6-conjugated β-cyclodextrin and ferrocene-modified PEG conjugates to form spherical micelles **158** that could transform their shape, Fig. 63. The micelles can access tumors *via* enhanced permeability and retention, and when at tumor sites, reactive oxygen species convert the ferrocene into water soluble ferrocenium, which results in dissociation of the PEGylated ferrocenium motif and formation of nanofibers *via* intermolecular hydrogen bonding resulting in increased retention in the tumor. During the process, and aided by laser irradiation, both O_2 and •OH were generated to the benefit of the photodynamic therapy, and this also maintained the supply of H_2O_2 allowing for the shape transformation and Fenton reaction. The Fenton chemistry was catalyzed by the retained ferrocene and resulted in beneficial chemodynamic therapy. By utilizing the above processes, the system was shown, both *in vitro* and *in vivo*, to be capable of producing potent immunogenetic cell death and *via* various mechanisms to the inhibition of primary tumors and bone metastases [186].

11.2.4. Pillar[n]arenes

Yu et al. decorated CuS nanoparticles with carboxylatopillar[5]arene and then used its host@guest chemistry to encapsulate the pyridinium salt moiety of the galactose derivative **159**, Fig. 64 top. The system could be further functionalized by making use of electrostatic interactions to

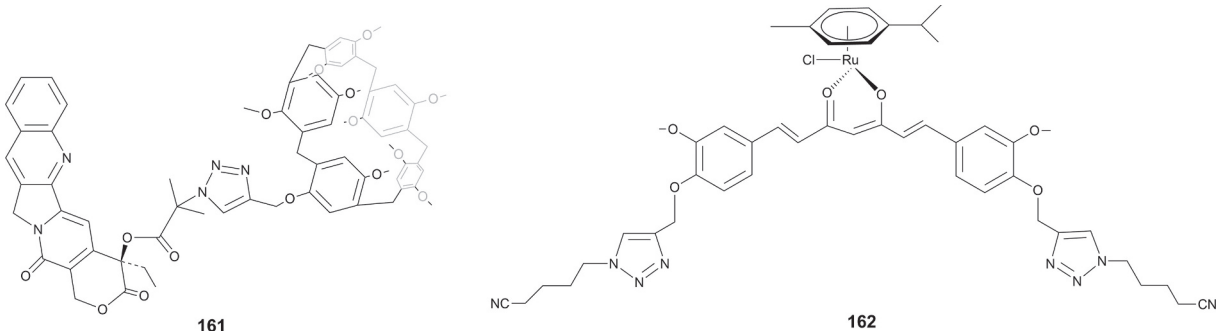

Fig. 66. Host **161** and guest **162**.

load doxorubicin (with up to 48.4% drug loading capacity). The various loadings allowed for the targeting of liver cancer cells, and its ability to absorb irradiation (from a laser at 808 nm) and convert it into heat to ablate cancer cells was demonstrated for HepG2 cells (Fig. 64 bottom). Moreover, on changing the pH (to an acidic environment), the system was able to release the doxorubicin. Both *in vitro* and *in vivo* studies demonstrated the excellent tumor inhibition ability of the system [187].

Ma, Wang, Yang et al. employed carboxylated pillar[5]arene **160** (Fig. 65 top) functionalized CuS nanoparticles combined with mesoporous silica nanoparticles that were modified with pyridinium groups and integrated this with folic acid bearing polyethylene glycol antennas to afford a system capable of synergic chemo/photothermal therapy. Doxorubicin could be loaded onto the silica nanoparticles, and release was triggered by stimulating the interaction between the pyridinium groups and the pillar[5]arene, with the latter components acting as a sort of nano-value. Good biocompatibility was observed for a variety of cells *via* MTT assays. The drug delivery capability of the platform was investigated by measuring the doxorubicin intensity in pre-incubated HeLa and A549 cells. Results revealed that the nanoparticles were internalized and that the doxorubicin upon release entered the cell nuclei. *In vivo* experiments on HeLa tumor-bearing xenograft nude mice revealed that use of the functionalized nanoparticles led to the tumors with the least weight/volume. Moreover, use of the nanoparticle scaffold led to increased drug accumulation at the tumor site than observed for use of doxorubicin alone, and this was aided by the presence of the targeting folic acid moieties [188].

Fan, Tian et al. prepared a supramolecule using host-guest chemistry, the host being pillar[5]arene-camptothecin **161** and the guest (p-cymene)Ru(dicyano-curcuminato)Cl **162** (Fig. 66), which self-assembles into micelles. The beauty of this system is that the metal present acts as a catalyst for hydrogen peroxide decomposition, which in turn means that in anaerobic (hypoxic) tumor environments, there is sufficient oxygen available for efficient *in vitro* and *in vivo* PDT and chemotherapy to take place [189].

11.2.5. Schiff base

The double Schiff-base **122** has been combined with silver nanoparticles using an *in-situ* reduction method, and the resulting Ag@**122** composite was found to exhibit good antibacterial properties against *Streptococcus sanguinis*, *Pseudomonas aeruginosa* and *Staphylococcus aureus*. Moreover, by employing Ag@**122** on a polymer film (polyethylene furanoate), bacterial growth could be inhibited [190].

12. Concluding remarks

The outputs described in this review underline the ability of both the supramolecular and coordination chemistry of macrocycles to impact on the efficiency of metal-based drug strategies. A summary of the diseases tackled by the metal-containing macrocyclic systems reported herein is shown in the introduction section in Chart 1, with cancer and antibacterial work the most studied fields. Much work has been done with the more established macrocycles, which pre-dates this review, and some of these systems have received FDA approval (*e.g.* **51** and **53**). Recent advances have tended to utilize newer additions to the macrocyclic family such as aza-containing macrocycles, cucurbit[*n*]urils ($n = 7$ or 8), Schiff-bases and to a lesser extent calixarenes, see Chart 2. This is likely to continue as synthetic methodologies improve and open-up new pathways for the functionalization of such macrocycles. For example, microwave technology and the use of solid support methodologies is leading to new macrocycle libraries [191].

It is evident from the examples herein that in many cases, the resulting macrocyclic/drug species were found to be better performing

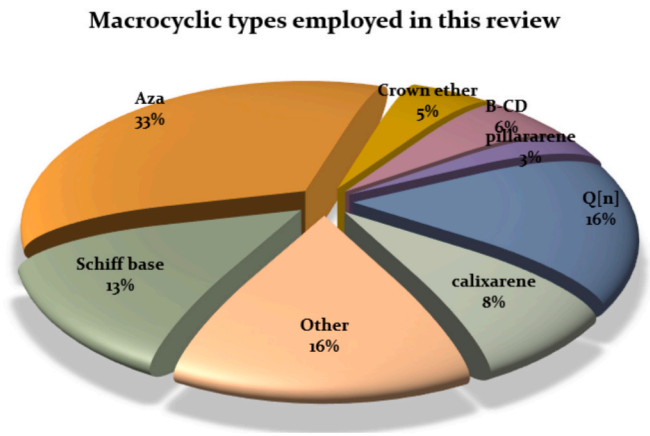

Chart 2. Breakdown of the macrocycles employed in the medicinal applications described in this review.

than the parent drugs, exhibiting better drug resistance properties, which has the potential to greatly improve treatments, whilst at the same time restricting side effects. For example, in the case of host-guest chemistry, calixarenes can increase the resistance of cisplatin to detoxification, whilst resulting host@guest complexes can exhibit stronger anticancer activity. For cucurbiturils, binding constants for the host@guest complexes allow such systems to act as biomarkers. These systems can also exhibit synergic PDT and chemotherapy effects. When employed as scaffolds for radiolabels, many macrocycles not only allow for good targeting, but also have impressive clearance rates.

Whilst there is great potential to employ both supramolecular and coordination chemistry of macrocyclic chemistry as a medicinal tool, current studies are mostly focusing on the systems that exploit the properties of the cavities present. In particular, many different sized cavities are available and these not only allow for drug selectivity, but also provide environments that increase the drug stability. This combined with the ability to functionalize the periphery of the macrocycle leads to increased targeted delivery.

Given this is a multi-disciplinary area, the best approach to tackle these health issues is to bring together groups with complementary expertise in areas such as organic, inorganic and medicinal chemistry. For example, our group has long-standing collaborations with organic calixarene (Saga, Japan) [192] and cucurbituril chemists (Guizhou, China) [193] and this has allowed us to utilize our coordination chemistry toolbox in the battle against a number of diseases. The field will also grow as new macrocycles are developed [194,195], and their coordination and/or supramolecular chemistry is explored.

Another future avenue, building on the lessons learned to-date, would be to explore the coordination chemistry of those macrocycles that have also received FDA approval or are currently in development. For example, will metalation of the likes of Plexixafor (Fig. 67, left) [196], Lorlatinib (Fig. 67, middle left) [197], Pacritinib (Fig. 67, middle right) [198], Zotiraciclib (Fig. 66, middle left) [199], have a positive impact on their performance or open-up their use for other treatments? A list of FDA approved macrocyclic drugs over the time period 1941 to 2022 has recently been published by Kihlberg et al. [200], whilst Kingwell has discussed the potential for macrocyclic drugs to push back on the Rule of 5 [201].

Given the increased global efforts in drug development, another important issue will be the adoption of positive regulation reforms/policies in various countries, particularly those with large markets. One example is provided by the National Medical Products Administration (NMPA) in China, who have adopted a series of mid- and long-term

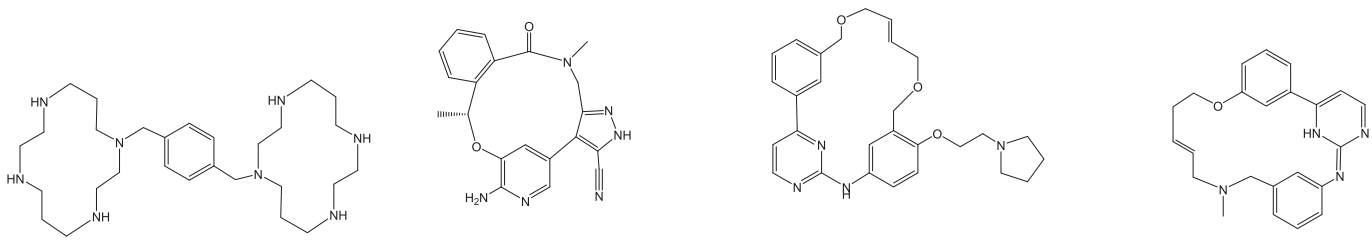

Fig. 67. FDA approved drugs (Plexixafor, Loriatinib and Pacritnib) and Zotiraciclib (in phase II trials).

development plans in order to stimulate domestic innovation (particularly for radiopharmaceuticals) [202].

Moreover, as we enter the AI age, the global pace of medical research is likely to increase yet further [203].

Declaration of competing interest

The authors declare that they have no known competing financial interests or personal relationships that could have appeared to influence the work reported in this paper.

Data availability

No data was used for the research described in the article.

Acknowledgements

CR thanks the EPSRC for funding (EP/X01374X/1).

References

[1] E.D. Agdeppa, M.E. Spilker, A review of imaging agent development, AAPS J. 11 (2009) 286–299. See for example (a).
[2] J. Wahsner, E.M. Gale, A. Rodríguez-Rodríguez, P. Caravan, Chemistry of MRI contrast agents: current challenges and new frontiers, Chem. Rev. 119 (2019) 957–1057.
[3] A.C. Sedgwick, J.T. Brewster II, P. Harvey, D.A. Iovan, G. Smith, X.-P. He, H. Tian, J.L. Sessler, T.D. James, Metal-based imaging agents: progress towards interrogating neurodegenerative disease, Chem. Soc. Rev. 49 (2020) 2886–2915.
[4] J.-G. Sun, P. Nie, P. Herdewijn, X.-J. Li, Exploring the synthetic approaches and clinical prowess of established macrocyclic pharmaceuticals, Eur. J. Med. Chem. 264 (2024) 116051.
[5] R. Paprocka, M. Wiese- Szadkowska, S. Janciauskiene, T. Kosmalski, M. Kuli, A., Helmin-Basa latest developments in metal complexes as anticancer agents, Coord. Chem. Rev. 452 (2022) 214307 (a).
[6] S. Sen, M. Won, M.S. Levine, Y. Noh, A.C. Sedgwick, J.S. Kim, J.L. Sessler, J. F. Arambula, Metal-based anticancer agents as immunogenic cell death inducers: the past, present, and future, Chem. Soc. Rev. 51 (2022) 1212–1233.
[7] R.L. Lucaciu, A.C. Hangan, B. Sevastre, L.S. Oprean, Metallo-drugs in cancer therapy: past, present and future, Molecules 27 (2022) 6485.
[8] D.M. Yufanyi, H.S. Abbo, S.J.J. Titinchi, T., Neville platinum(II) and ruthenium (II) complexes in medicine: antimycobacterial and anti-HIV activities, Coord. Chem. Rev. 414 (2020) 213285.
[9] T. Zhang, H. Lei, X. Chen, Z. Dou, B. Yu, W. Su, W. Wang, X. Jin, T. Katsube, B. Wang, H. Zhang, Q. Li, C. Di, Carrier systems of radiopharmaceuticals and the application in cancer therapy, Cell Death Dis. 10 (2024) 16.
[10] C.B. Scarim, R.L. de Farias, A.V. de Godoy Netto, C.M. Chin, J.L. dos Santos, F. R. Pavan, Recent advances in drug discovery against mycobacterium tuberculosis: metal-based complexes, Eur. J. Med. Chem. 214 (2021) 113166.
[11] D.M. Yufanyi, H.S. Abbo, S.J.J. Titinchi, T. Neville, Platinum(II) and ruthenium (II) complexes in medicine: Antimycobacterial and anti-HIV activities, Coord. Chem. Rev. 414 (2020) 213285.
[12] M. Tosato, V. Di Marco, Metal chelation therapy and Parkinson's disease: A critical review on the thermodynamics of complex formation between relevant metal ions and promising or established drugs, Biomolecules 9 (2019) 269.
[13] A. Frei, J. Zuegg, A.G. Elliott, M. Baker, S. Braese, C. Brown, F. Chen, C. G. Dowson, G. Dujardin, N. Jung, A.P. King, A.M. Mansour, M. Massi, J. Moat, H. A. Mohamed, A.K. Renfrew, P.J. Rutledge, P.J. Sadler, M.H. Todd, C.E. Willans, J. J. Wilson, M.A. Cooper, M.A.T. Blaskovich, Metal complexes as a promising source for new antibiotics, Chem. Sci. 11 (2020) 2627–2639.
[14] J.E. Waters, L. Stevens-Cullinane, L. Siebenmann, J. Hess, Recent advances in the development of metal complexes as antibacterial agents with metal-specific modes of action, Curr. Opin. Microbiol. 75 (2023) 102347.
[15] A. Evans, K.A. Kavanagh, Evaluation of metal-based antimicrobial compounds for the treatment of bacterial pathogens, J. Med. Microbiol. 70 (2021) 001363.
[16] B. Sharma, S. Shukla, R. Rattan, M. Fatima, M. Goel, M. Bhat, S. Dutta, R. K. Ranjan, M. Sharma, Antimicrobial agents based on metal complexes: present situation and future prospects, Int. J. Biomater. 2022 (2022) 6819080.
[17] W. Feng, M. Jin, K. Yang, Y. Pei, Z. Pei, Supramolecular delivery systems based on Pillararenes, Chem. Commun. 54 (2018) 13626–13640.
[18] D. Das, K.I. Assaf, W.M. Nau, Applications of Cucurbiturils in medicinal chemistry and chemical biology, Front. Chem. 7 (2019) 619.
[19] X. Yao, J. Mu, L. Zeng, J. Lin, Z. Nie, X. Jiang, P. Huang, Stimuli-responsive cyclodextrin-based nanoplatforms for cancer treatment and theranostics, Mater. Horiz. 6 (2019) 846–870.
[20] N. Song, X.-Y. Lou, L. Ma, H. Gao, Y.-W. Yang, Supramolecular nanotheranostics based on pillarenes, Theranostics 9 (2019) 3075–3093.
[21] J. Wankar, N.G. Kotla, S. Gera, S. Rasala, A. Pandit, Y.A. Rochev, Recent advances in host-guest self-assembled cyclodextrin carriers: implications for responsive drug delivery and biomedical engineering, Adv. Funct. Mater. 30 (2020) 1909049.
[22] E.B. Noruzi, M. Molaparast, M. Zarei, B. Shaabani, Z. Kariminezhad, B. Ebadi, V. Shafiei-Irannejad, M. Rahimi, J. Pietrasik, Para-sulfonatocalix[*n*]arene-based biomaterials: recent progress in pharmaceutical and biological applications, Eur. J. Med. Chem. 190 (2020) 112121.
[23] Y.-C. Pan, X.-Y. Hu, D.-S. Guo, Biomedical applications of calixarenes: state-of-the-art and perspectives, Angew. Chem. Int. Ed. 60 (2020) 2768–2794.
[24] R. Basilotta, D. Mannino, A. Filippone, G. Casili, A. Prestifilippo, L. Colarossi, G. Raciti, E. Esposito, M. Campolo, Role of calixarene in chemotherapy delivery strategies, Molecules 26 (2021) 3963.
[25] N. Barooah, J. Mohanty, A.C. Bhasikuttan, Cucurbituril-based supramolecular assemblies: prospective on drug delivery, sensing, separation, and catalytic applications, Langmuir 38 (2022) 6249–6264.
[26] D.N. Păduraru, A.-G. Niculescu, A. Bolocan, O. Andronic, A.M. Grumezescu, R. Bîrlă, An updated overview of cyclodextrin-based drug delivery systems for cancer therapy, Pharmaceutics 14 (2022) 1748.
[27] W.Y. Yi, F.L. Supian, M. Musa, N.F.D.A. Karim, A.F. Naim, Calixarenes as host molecules for drug carriers in the cosmetic and medical field, Macromol. Res. 30 (2022) 853–862.
[28] C. Wang, H. Li, J. Dong, J.Y. Chen, X. Luan, X. Li, X. Du, Pillararene-based supramolecular vesicles for stimuli-responsive drug delivery, Chem. Eur. J. 28 (2022) e202202050.
[29] Z. Wang, C. Sun, K. Yang, X. Chen, R. Wang, Cucurbituril-based supramolecular polymers for biomedical applications, Angew. Chem. Int. Ed. Eng. 61 (2022) e202206763.
[30] M. Yadav, D. Yadav, D.P. Singh, J.K. Kapoor, Pharmaceutical properties of macrocyclic Schiff base transition metal complexes: urgent need in today's world, Inorg. Chim. Acta 246 (2023) 121300.
[31] H. Yin, Q. Cheng, D. Bardeland, R. Wang, Challenges and opportunities of functionalized cucurbiturils for biomedical applications, JACS Au 3 (2023) 2356–2377.
[32] M. Mourer, J.-B. Regnouf-de-Vains, R.E. Duval, Functionalized calixarenes as promising antibacterial drugs to face antimicrobial resistance, Molecules 28 (2023) 6954.
[33] S. Paul, R.S. Jeyaprakash, A. Pal, H. Venkatachalam, B. Srinivas, Calixarenes and their relevance in anticancer drug development, Med. Chem. 19 (2023) 939–945.
[34] S. Shukla, B. Sagar, A.K. Sood, A. Gaur, S. Batra, S. Gulati, Supramolecular chemotherapy with cucurbit[*n*]urils as encapsulating hosts, ACS Appl. Bio Mater. 6 (2023) 2089–2101.
[35] G.V. Zyryanov, D.S. Kopchuk, I.S. Kovalev, S. Santra, A. Majee, B.C. Ranu, Pillararenes as promising carriers for drug delivery, Int. J. Mol. Sci. 24 (2023) 5167.
[36] O.A.A. Alabrahim, S.A. Fahmy, H.M.E. Azzazy, Stimuli-responsive cucurbit[*n*] uril-based supramolecular nanocarriers for delivery of chemotherapeutics, ACS Appl. Nano Mater. 6 (2023) 3139–3158.
[37] W. Yang, W. Zhang, J. Chen, J. Zhou, Mono-functionalized pillar[*n*]arenes: syntheses, host-guest properties and applications, Chin. Chem. Lett. 35 (2024) 108740.
[38] A.-N. Lazar, F. Perret, M. Perez-Lloret, M. Michaud, A.W. Coleman, Promises of anionic calix[*n*]arenes in life science: state of the art in 2023, Eur. J. Med. Chem. 264 (2024) 115994.
[39] R. Li, N. Liu, R. Liu, X. Jin, Z. Li, Calixarene: A supramolecular material for treating Cancer, Curr. Drug Deliv. 21 (2024) 184–192.

[40] M. Alešković, M. Šekutor, Overcoming barriers with non-covalent interactions: supramolecular recognition of adamantyl cucurbit[*n*]uril assemblies for medical applications, RSC Med. Chem. 15 (2024) 433–471.
[41] R. Pinalli, A. Pendrini, E. Dalcanale, Biochemical sensing with macrocyclic receptors, Chem. Soc. Rev. 47 (2018) 7006–7026.
[42] O.S. Fenton, K.N. Olafson, P.S. Pillai, M.J. Mitchell, R. Langer, Advances in biomaterials for drug delivery, Adv. Mater. 30 (2018) e1705328.
[43] M.M. Welling, A.W. Hensbergen, A. Bunschoten, A.H. Velders, M. Roestenberg, F. W.B. van Leeuwen, An update on radiotracer development for molecular imaging of bacterial infections, Clin. Translat. Imaging 7 (2019) 105–124.
[44] S.A. Fahmy, J. Brussler, M. Alawak, M.M.H. El-Sayed, U. Bakowsky, T. Shoeib, Chemotherapy based on supramolecular chemistry: A promising strategy in cancer therapy, Pharmaceutics 11 (2019) 292.
[45] X.-Y. Lou, Y.P. Li, Y.-W. Yang, Gated materials: installing macrocyclic Arenes-based supramolecular nanovalves on porous nanomaterials for controlled cargo release, Biotechnol. J. 14 (2019) 1800354.
[46] Z. Li, N. Song, Y.-W. Yang, Stimuli-responsive drug-delivery systems based on supramolecular Nanovalves, Matter 1 (2019) 345–368.
[47] C.-L. Deng, S.L. Murkli, L.D. Isaacs, Supramolecular hosts as *in vivo* sequestration agents for pharmaceuticals and toxins, Chem. Soc. Rev. 49 (2020) 7516–7532.
[48] C. Guo, A.C. Sedgwick, T. Hira, J.L. Sessler, Supramolecular fluorescent sensors: An historical overview and update, Coord. Chem. Rev. 427 (2021) 213560.
[49] N. Parmar, K. Bhatt, Exploring the expanding Frontiers: the promising role of supramolecules in advancing cancer and infectious disease therapy, Orient. J. Chem. 39 (2023) 1093–1100.
[50] B. Hazarika, V.P. Singh, Macrocyclic supramolecular biomaterials in anti-cancer therapeutics, Chin. Chem. Lett. 34 (2023) 108220.
[51] A. Gu, N.J. Wheate, Macrocycles as drug-enhancing excipients in pharmaceutical formulations, J. Incl. Phenom. Macrocycl. Chem. 100 (2021) 55–69.
[52] J. Zhou, L. Rao, G. Yu, T.R. Cook, X. Chen, F. Huang, Supramolecular cancer nanotheranostics, Chem. Soc. Rev. 50 (2021) 2839–2891.
[53] M.T. Manzari, Y. Shamay, H. Kiguchi, N. Rosen, M. Scaltriti, D.A. Heller, Targeted drug delivery strategies for precision medicines, Nat. Rev. Mater. 6 (2021) 351–370.
[54] Y. Liang, R. Fang, Q. Rao, An insight into the medicinal chemistry perspective of macrocyclic derivatives with antitumor activity: a systematic review, Molecules 27 (2022) 2837.
[55] F. Davis, S.P.J. Higson, Synthetic receptors for early detection and treatment of cancer, Biosensors 13 (2023) 953.
[56] S. Wu, M. Yan, M. Liang, W. Yang, J. Chen, J. Zhou, Supramolecular host-guest nanosystems for overcoming cancer drug resistance, Cancer Drug Resist 6 (2023) 805–827.
[57] B. Hazarika, V.P. Singh, Macrocyclic supramolecular biomaterials in anti-cancer therapeutics, Chin. Chem. Lett. 34 (2023) 108220.
[58] S. Peng, X. Yuan, H. Li, Y. Wei, B. Zhao, G. Ding, J. Bai, Recent progress in nanocarrier-based drug delivery systems for antitumour metastasis, Eur. J. Med. Chem. 252 (2023) 115259.
[59] Z. Zhang, H. Cui, T. Zhang, M. Zhang, L. Wu, X. Zhang, X. Zhou, X. Li, Y. Zhai, Z. Lu, C. Xu, C. Yin, J. Gao, Biomembrane and metal nanostructures for cancer theranostics: the state of the art in the combination of organic and inorganic chemistry, Mater. Des. 231 (2023) 112067.
[60] M. Warszyńska, P. Repetowski, J.M. Dąbrowski, Photodynamic therapy combined with immunotherapy: recent advances and future research directions, Coord. Chem. Rev. 495 (2023) 215350.
[61] K. Nisa, I.A. Lone, W. Arif, P. Singh, S.U. Rehman, R. Kumar, Applications of supramolecular assemblies in drug delivery and photodynamic therapy, RSC Med. Chem. 14 (2023) 2438–2458.
[62] J.-H. Tian, H. Xu, X.-Y. Hu, D.-S. Guo, Supramolecular fluorescence biosensing based on macrocycles, Supramol. Mater. 3 (2024) 100063.
[63] T.C. Johnstone, K. Suntharalingam, S.J. Lippard, The next generation of platinum drugs: targeted Pt(II) agents, nanoparticle delivery, and Pt(IV) prodrugs, Chem. Rev. 116 (2016) 3436–3486.
[64] V.K. Singh, V.K. Singh, A. Mishra, A.A. Varsha, G. Singh, A.K. Prasad, Singh., Recent advancements in coordination compounds and their potential clinical application in the management of diseases: An up-to-date review, Polyhedron 241 (2023) 116485.
[65] N. Vasan, J. Baselga, D.M. Hyman, A view on drug resistance in cancer, Nature 575 (2019) 299–309. See for example.
[66] R.A. Ward, S. Fawell, N. Floc'h, V. Flemington, D. McKerrecher, P.D. Smith, Challenges and opportunities in cancer drug resistance, Chem. Rev. 121 (2021) 3297–3351.
[67] T. Hu, H. Gong, J. Xu, Y. Huang, F. Wu, Z. He, Nanomedicines for overcoming cancer drug resistance, Pharmaceutics 14 (2022) 1606.
[68] X. Sun, P. Zhao, J. Lin, K. Chen, J. Shen, Recent advances in access to overcome cancer drug resistance by nanocarrier drug delivery system, Cancer Drug Resist 6 (2023) 390–415.
[69] P. Sa, S.K. Sahoo, F. Dilnawaz, Responsive role of nanomedicine in the tumor microenvironment and cancer drug resistance, Curr. Med. Chem. 30 (2023) 3335–3355.
[70] J. Zhou, G. Yu, F. Huang, Supramolecular chemotherapy based on host–guest molecular recognition: a novel strategy in the battle against cancer with a bright future, Chem. Soc. Rev. 46 (2017) 7021–7053.
[71] C.D. Gutsche, Calixarenes, Acc. Chem. Res. 16 (1983) 161–170.
[72] C. Wieser-Jeunesse, D. Matt, The development of platino-calixarenes, Platin. Met. Rev. 42 (1998) 11–16. See for example.
[73] N.J. Wheate, G.M. Abbott, R.J. Tate, C.J. Clements, R. Edrada-Ebel, B. F. Johnston, Side-on binding of p-sulphonatocalix[4]arene to the dinuclear platinum complex trans-$[\{PtCl(NH_3)_2\}_2\mu\text{-dpzm}]^{2+}$ and its implications for anticancer drug delivery, J. Inorg. Biochem. 103 (2009) 448–454.
[74] S.D. Brown, J.A. Plumb, B.F. Johnson, N.J. Wheate, Folding of dinuclear platinum anticancer complexes within the cavity of *para*-sulphonatocalix[4]arene, Inorg. Chim. Acta 393 (2012) 182–186.
[75] F.N. Pur, K.A. Dilmaghani, Calixplatin: novel potential anticancer agent based on the platinum complex with functionalized calixarene, J. Coord. Chem. 67 (2014) 440–448.
[76] C.T. Pang, A.J. Ammit, Y.Q.E. Ong, N.J. Wheate, *Para*-Sulfonatocalix[4]arene and polyamidoamine dendrimer nanocomplexes as delivery vehicles for a novel platinum anticancer agent, J. Inorg. Biochem. 176 (2017) 1–7.
[77] S.A. Fahmy, F. Ponte, M.K.A. El-Rahman, N. Russo, E. Sicilia, T. Shoeib, Investigation of the host-guest complexation between 4-sulfocalix[4]arene and nedaplatin for potential use in drug delivery, Spectrochim. Acta A Mol. Biomol. Spectrosc. 193 (2018) 528–536.
[78] X. Fan, X. Guo, Development of calixarene-based drug nanocarriers, J. Mol. Liq. 325 (2021) 115246.
[79] M. Li, L. Mao, M. Chen, M. Li, K. Wang, J. Mo, Characterization of an amphiphilic phosphonated calixarene carrier loaded with carboplatin and paclitaxel: A preliminary study to treat colon cancer *in vitro* and *in vivo*, Front. Bioeng. Biotechnol. 7 (2019) 238.
[80] S.A. Fahmy, F. Ponte, G. Grande, I.M. Fawzy, A.A. Mandour, E. Sililia, H.M. El-Said Azzazy, Synthesis, characterization and host-guest complexation of Asplatin: improved *in vitro* cytotoxicity and biocompatibility as compared to cisplatin, Pharmaceuticals 15 (2022) 259.
[81] Y. Li, S. Liu, M. Liang, Y. Cui, H. Zhao, Q. Gao, Glycocalixarene with luminescence for Warburg effect-mediated tumor imaging and targeted drug delivery, Chem. Commun. 57 (2021) 9728–9731.
[82] B.C. Gibb, R.G. Chapman, J.C. Sherman, Synthesis of hydroxyl-footed cavitands, J. Organomet. Chem. 61 (1996) 1505–1509.
[83] R. Kashapov, Y. Razuvayeva, A. Ziganshina, T. Sergeeva, S. Lukashenko, A. Sapunova, A. Voloshina, N. Kashapova, I. Nizameev, V. Salnikov, S. Ziganshina, B. Gareev, L. Zakharova, Supraamphiphilic systems based on metallosurfactant and calix[4]resorcinol: self- assembly and drug delivery potential, Inorg. Chem. 59 (2020) 18276–18286.
[84] X.-Y. Hu, J. Gao, F.Y. Chen, D.S. Guo, A host-guest drug delivery nanosystem for supramolecular chemotherapy, J. Control. Release 324 (2020) 124–133.
[85] J. Kim, I.-S. Jung, S.-Y. Kim, E. Lee, J.-K. Kang, S. Sakamoto, K. Yamaguchi, K. Kim, New cucurbituril homologues: syntheses, isolation, characterization, and X-ray crystal structures of cucurbit[*n*]uril ($n = 5$, 7, and 8), J. Am. Chem. Soc. 122 (2000) 540–541.
[86] S. Fink, K. Reddersen, C. Wiegand, P. Elsner, U.-C. Hipler, Evaluation of cell and hemocompatibility of Cucurbiturils, Eur. J. Pharm. Sci. 146 (2020) 105271.
[87] A.A. Aktanova, M.V. Bykova, O.S. Boeva, E.A. Pashkina, L.V. Grishina, V. A. Kozlov, Cucurbituril-based supramolecular complexes with platinum compounds influence expression of CTLA-4 on regulatory T cells, Med. Immunol. 25 (2023) 697–702.
[88] Y.Y. Chen, Z.W. Sun, Supramolecular chemotherapy based on the host-guest complex of lobaplatin-cucurbit[7]uril, ACS Appl. Bio. Mater. 3 (2020) 2449–2454.
[89] X. Huang, H. Zhou, R. Jiao, H.R. Liu, C.F. Qin, L.X. Xu, Y.Y. Chen, Supramolecular chemotherapy: host-guest complexes of heptaplatin-cucurbit[7]uril toward colorectal normal and tumor cells, Langmuir 37 (2021) 5475–5482.
[90] H. Chen, Y. Chen, H. Wu, J.-F. Xu, Z. Sun, X. Zhang, Supramolecular polymeric chemotherapy based on cucurbit[7]uril-PEG copolymer, Biomaterials 178 (2018) 697–705.
[91] J. Chen, S. Li, Z. Wang, Y. Pan, J. Wei, S. Lu, Q.-W. Zhang, L.-H. Wang, R. Wang, Synthesis of an AIEgen functionalized cucurbit[7]uril for subcellular bioimaging and synergistic photodynamic therapy and supramolecular chemotherapy, Chem. Sci. 12 (2021) 7727–7734.
[92] C. Jia, Y. Zhong, X. Zhang, X. Liao, Y. Li, B. Yang, C. Gao, Host–guest inclusion systems of nedaplatin with cucurbit[7]uril for improved in vitro antitumour activity, J. Incl. Phenom. Macrocycl. Chem. 97 (2020) 99–107.
[93] H. Chen, J. Zhang, Q. Yu, Y. Chen, Y. Tan, Hexanoate-cucurbit[7]uril: highly soluble with controlled release ability, Chem. Eur. J. 26 (2020) 9445–9448.
[94] E. Pashkina, A. Aktanova, I. Mirzaeva, E. Kovalenko, I. Andrienko, N. Knauer, N. Pronkina, V. Kozlov, The effect of cucurbit[7]uril on the antitumor and immunomodulating properties of oxaliplatin and carboplatin, Int. J. Mol. Sci. 22 (2021) 7337.
[95] H. Wu, H. Wang, F. Qi, T. Xia, Y. Xia, J.-F. Xu, X. Zhang, An activatable host−guest conjugate as a nanocarrier for effective drug release through self-inclusion, ACS Appl. Mater. Interfaces 13 (2021) 33962–33968.
[96] S. Datta, S.K. Misra, M.L. Saha, N. Lahiri, J. Louie, D. Pan, P.J. Stang, Orthogonal self-assembly of an organoplatinum(II) metallacycle and cucurbit[8]uril that delivers curcumin to cancer cells, Proc. Natl. Acad. Sci. 115 (2018) 8087–8092.
[97] F. Solis-Egana, N. Lavin-Urqueta, D.G. Díaz, N. Marino-Ocampo, M.A. Faúndez, D. Fuentealba, Supramolecular co-encapsulation of a photosensitizer and chemotherapeutic drug in cucurbit[8]uril for potential chemophototherapy, Photochem. Photobiol. Sci. 21 (2022) 349–359.
[98] X.-Y. Dai, B. Zhang, Q. Yu, Y. Liu, *In situ* coassembly induced mitochondrial aggregation activated drug-resistant tumor treatment, J. Med. Chem. 65 (2022) 7363–7370.

[99] S. Shukla, B. Sagar, A.K. Sood, A. Gaur, S. Batra, S. Gulati, Supramolecular chemotherapy with cucurbit[*n*]urils as encapsulating hosts, ACS Appl. Bio Mater. 6 (2023) 2089–2101.

[100] E.A. Pashking, L.V. Grishing, A.A. Aktanova, V.A. Kozlov, Antitumor activity of supramolecular complexes of cucurbituril with platinum(II) compounds, Inorg. Chim. Acta 522 (2021) 120370.

[101] T. Ogoshi, S. Kanai, S. Fujinami, T.-A. Yamagishi, Y. Nakamoto, *Para*-bridged symmetrical pillar[5]arenes: their Lewis acid catalyzed synthesis and host–guest property, J. Am. Chem. Soc. 130 (2008) 5022–5023.

[102] J. Chen, Q. Meng, J.L. Sessler, Y. Chai, Y. Zhang, X. Yuan, C. Li, Z. Meng, Y. Zhang, L. Guo, Supramolecular combination chemotherapy: a pH responsive co-encapsulation drug delivery system, Chem. Sci. 11 (2020) 6275–6282.

[103] G. Crini, Review: A history of Cyclodextrins, Chem. Rev. 114 (2014) 10940–10975.

[104] W. Chen, X. Li, C. Liu, J. He, M. Qi, Y. Sun, B. Shi, H. Sepehrpour, H. Li, W. Tian, P.J. Stang, β-Cyclodextrin modified Pt(II) metallacycle-based supramolecular hyperbranched polymer assemblies for DOX delivery to liver cancer cells, Proc. Natl. Acad. Sci. 117 (2021) 30942–30948.

[105] Y. Chen, Y. Yao, X. Zhou, C. Liao, X. Dai, J. Liu, Y. Yu, S. Zhang, Cascade-reaction-based nanodrug for combined chemo/starvation/chemodynamic therapy against multidrug-resistant tumors, ACS Appl. Mater. Interfaces 11 (2019) 46112–46123.

[106] C.J. Pedersen, Cyclic polyethers and their complexes with metal salts, J. Am. Chem. Soc. 89 (1967) 2495–2496.

[107] C.J. Pedersen, Cyclic polyethers and their complexes with metal salts, J. Am. Chem. Soc. 89 (1967) 7017–7036.

[108] B.A.J. Jansen, P. Wielaard, H. den Dulk, J. Brouwer, J. Reedijk, Oxa-aza crown ethers as ligands for mixed-ligand cisplatin derivatives and dinuclear platinum anticancer drugs, Eur. J. Inorg. Chem. 9 (2022) 2375–2379.

[109] D.S. Abou, N.A. Thiele, N.T. Gutsche, A. Villmer, H. Zhang, J.J. Woods, K. E. Baidoo, F.E. Escorcia, J.J. Wilson, D.L.J. Thorek, Towards the stable chelation of radium for biomedical applications with an 18-membered macrocyclic ligand, Chem. Sci. 12 (2021) 3733–3742.

[110] H. Meeres, P. Kunz, V. Radchenko, H. Yang, Synthesis of crown-1paMe, a novel dual modality Tb chelator, and preliminary labeling with 155Tb, J. Nucl. Chem. 63 (2022) 2472.

[111] D. Bauer, M. Blumberg, M. Köckerling, C. Mamat, A comparative evaluation of calix[4]arene-1,3-crown-6 as a ligand for selected divalent cations of radiopharmaceutical interest, RSC Adv. 9 (2019) 32357.

[112] L. Ma, L. Li, G. Zhu, Platinum-containing heterometallic complexes in cancer therapy: advances and perspectives, Inorg. Chem. Front. 9 (2022) 2424–2453.

[113] C.J. Adams, T.J. Meade, Gd(III)–Pt(IV) theranostic contrast agents for tandem MR imaging and chemotherapy, Chem. Sci. 11 (2020) 2524–2530.

[114] R. Oun, Y.E. Moussa, N.J. Wheate, The side effects of platinum-based chemotherapy drugs: a review for chemists, Dalton Trans. 47 (2018) 6645–6653.

[115] H. Schiff, Mittheilungen aus dem Universitätslaboratorium in Pisa: Eine neue Reihe organischer Basen, Justus Liebigs Ann. Chem. 131 (1864) 118–119.

[116] N.E. Borisova, M.D. Reshetova, Y.A. Ustynyuk, Metal-free methods in the synthesis of macrocyclic Schiff bases, Chem. Rev. 107 (2007) 46–79.

[117] J.P. Remiya, T.S. Sikha, B. Shyni, One-pot synthesis and characterization of Schiff base macrocyclic complexes as a potential bioactive core – a review, J. Coord. Chem. 74 (2021) 3081–3108.

[118] H. Zeynali, H. Keypour, L. Hosseinzadeh, R.W. Gable, The non-templating synthesis of macrocyclic Schiff base ligands containing pyrrole and homopiperazine and their binuclear nickel(II), cobalt(II) and mononuclear platinum(II) complexes: X-ray single crystal and anticancer studies, J. Mol. Struct. 1244 (2021) 130956.

[119] M.K. Pal, A.P. Wadawale, N. Chauhan, A.G. Majumdar, M. Subramanian, N. Bhuvanesh, S. Dey, Anticancer potential of Pd and Pt metallo-macrocycles of phosphines and 4,4´-dipyridyldiselenide, Polyhedron 211 (2022) 115547.

[120] G. Thiabaud, G. He, S. Sen, K.A. Shelton, W.B. Baze, L. Segura, J. Alaniz, R. M. Macias, G. Lyness, A.B. Watts, H.M. Kim, H. Lee, M.Y. Cho, K.S. Hong, R. Finch, Z.H. Siddik, J.F. Arambula, J.L. Sessler, Oxaliplatin Pt(IV) prodrugs conjugated to gadolinium-texaphyrin as potential antitumor agents, Proc. Natl. Acad. Sci. USA 117 (2020) 7021–7029.

[121] P. Xiao, C. Liu, T. Ma, X. Lu, L. Jing, Y. Hou, P. Zhang, G. Huang, M. Gao, A cyclodextrin-hosted Ir(III) complex for ratiometric mapping of tumor hypoxia *in vivo*, Adv. Sci. 8 (2021) 2004044.

[122] M. Aidi, H. Keypour, A. Shooshtari, M. Bayat, L. Hosseinzadeh, H.A. Rudbari, R. W. Gable, Coordination chemistry of some new Mn(II), Cd(II) and Zn(II) macrocyclic Schiff Base complexes containing a homopiperazine head unit, spectral, X-ray crystal structural, theoretical studies and anticancer activity, Inorg. Chim. Acta 490 (2019) 294–302.

[123] R. Kothari, A. Agrawal, Synthesis, molecular docking, antioxidant and anticancer activities of Tetraaza macrocyclic copper (II) complexes, Russ. J. Chem. 13 (2020) 1672–1684.

[124] Y. Fang, X. Lian, Y. Huang, G. Fu, Z. Xiao, Q. Wang, B. Nan, J.-P. Pellois, H.-C. Zhou, Investigating subcellular compartment targeting effect of porous coordination cages for enhancing cancer nanotherapy, Small 14 (2018) 1802709.

[125] Z. Xiao, H. Lin, H.F. Drake, J. Diaz, H.-C. Zhou, J.-P. Pellois, Investigating the cell entry mechanism, disassembly, and toxicity of the Nanocage PCC-1: insights into its potential as a drug delivery vehicle, J. Am. Chem. Soc. 145 (2023) 27690–27701.

[126] L.-D. Yu, Y.-J. Tong, N. Li, Y. Yang, P. Ye, G. Ouyang, F. Zhu, Calix[6]arene functionalized lanthanide metal–organic frameworks with boosted performance in identifying an anti-epidemic pharmaceutical, Chem. Commun. 58 (2022) 11697.

[127] C. Liu, Y. Xia, Z. Tao, X.-L. Ni, Host-guest interaction tailored cucurbit[6]uril-based supramolecular organic frameworks (SOFs) for drug delivery, Chin. Chem. Lett. 33 (2022) 1529–1532.

[128] J.-A. Fang, J.-L. Zhao, X. Liao, X. Zeng, S.-B. Su, Q.-Y. Luo, C. Redshaw, Z. Jin, A molecular tweezers-like calix[4]arene based alkaline earth metal cation (Ca^{2+}, Sr^{2+} & Ba^{2+}) chemosensor and its imaging in living cells and zebrafish, Inorg. Chem. 58 (2019) 14720–14727.

[129] K. Chen, Z.-Q. Zhu, M.-H. Zhang, C. Chen, J.-X. Liu, J.-X. Liu, C. Redshaw, 4,4'-Biphenyldisulfonic acid induced coordination polymers of symmetrical tetramethyl cucurbit[6]uril with alkaline-earth metals for detection of antibiotics, CrystEngComm 25 (2023) 961–970.

[130] M. Khatun, P. Ghorai, J. Mandal, S.G. Chowdhury, P. Karmakar, S. Blasco, E. Garcia-Espana, A. Saha, Aza-phenol based macrocyclic probes design for "CHEF-on" multi analytes sensor: crystal structure elucidation and application in biological cell imaging, ACS Omega 8 (2023) 7479.

[131] V.I.J. Jallinoja, C.H. Abbriano, K. Bhatt, A. Kaur, D.J. Schlyer, P.J. Yazaki, B. D. Carney, J.L. Houghton, Pretargeting with Cucurbituril–Adamantane Host–Guest Pair in Xenograft Models, J. Nucl. Med. 64 (2023) 1203–1209.

[132] E. Pauwels, F. Cleeren, G. Bormans, C.M. Deroose, Somatostatin receptor PET ligands: the next generation for clinical practice, Am. J. Nucl. Med. Mol. Imaging 8 (2018) 311–331.

[133] E.S. Mittra, Neuroendocrine tumor therapy: ^{177}Lu-DOTATATE, AJR 211 (2018) 278–285.

[134] Lutathera (Lutetium Lu 177 Dotatate) [Prescribing Information], Advanced Accelerator Applications USA, Millburn, NJ, USA, 2021. https://www.novartis.us/sites/www.novartis.us/files/lutathera.pdf (accessed on 2 August 2024).

[135] Netspot (Gallium Ga 68 Dotatate) [Prescribing Information], Advanced Accelerator Applications USA Inc., Millburn, NJ, USA, 2021. Available online: https://www.novartis.us/sites/www.novartis.us/files/netspot.pdf (accessed on 2 August 2024).

[136] Detectnet (Copper Cu 64 Dotatate) Injection [Prescribing Information], Curium US LLC, Maryland Heights, MO, USA, 2020. Available online: https://www.curiumpharma.com/wp-content/uploads/2020/09/copper-64-dotatate-injection-pi.pdf (accessed on August 2024).

[137] N.A. Thiele, V. Brown, J.M. Kelly, A. Amor-Coarasa, U. Jermilova, S. N. MacMillan, A. Nikolopoulou, S. Ponnala, C.F. Ramogida, A.K.H. Robertson, C. Rodriquez-Rodriquez, P. Schaffer, C. Williams Jr., J.W. Babich, V. Radchenko, J.J. Wilson, An eighteen-membered macrocyclic ligand for actinium-225 targeted alpha therapy, Angew. Chem. Int. Ed. Eng. 56 (2017) 14712–14717.

[138] A.P. King, N.T. Gutsche, N. Raju, S. Fayn, K.E. Baidoo, M.M. Bell, C.S. Olkowski, R.E. Swenson, F.I. Lin, S.M. Sadowski, S.S. Adler, N.A. Thiele, J.J. Wilson, P. L. Choyke, F.E. Escorcia, ^{225}Ac-MACROPATATE: A novel α-particle peptide receptor radionuclide therapy for neuroendocrine tumors, J. Nucl. Med. 64 (2023) 549–554.

[139] H. Yang, J.J. Wilson, C. Orvig, Y. Li, D.S. Wilbur, C.F. Ramogida, V. Radchenko, P. Schaffer, Harnessing **α**-emitting radionuclides for therapy: radiolabeling method review, J. Nucl. Med. 63 (2022) 5–13.

[140] M. Li, S. Wang, Q. Kong, X. Cheng, H. Yan, Y. Xing, X. Lan, D. Jiang, Advances in macrocyclic chelators for positron emission tomography imaging, View 4 (2023) 20230042.

[141] B.S. Lee, M.H. Kim, S.Y. Chu, W.J. Jung, H.J. Jeong, K. Lee, H.S. Kim, M.H. Kim, H.S. Kil, S.J. Han, Y.J. Lee, K.C. Lee, S.M. Lim, D.Y. Chi, Improving theranostic Gallium-68/Lutetium-177–labeled PSMA inhibitors with an albumin binder for prostate cancer, Mol. Cancer Ther. 20 (2021) 2410–2419.

[142] A. Wurzer, J.-P. Kunert, S. Fischer, V. Felber, R. Beck, F. de Rose, C. D'Alessandria, W. Weber, H.-J. Wester, Synthesis and preclinical evaluation of 177Lu-labeled radiohybrid PSMA ligands for endoradiotherapy of prostate cancer, J. Nucl. Med. 63 (2022) 1489–1495.

[143] J. Salaam, T. Fogeron, G. Pilet, R. Bolbos, C. Bucher, L. Khrouz, J. Hasserodt, Unprecedented relaxivity gap in pH-responsive Fe^{III}-based MRI probes, Angew. Chem. Int. Ed. 62 (2023) e202212782.

[144] Q.V. Le, J. Lee, S. Ko, H. Kim, T.Y. Vu, Y.S. Choe, Y.-K. Oh, G. Shim, Enzyme-responsive macrocyclic metal complexes for biomedical imaging, Bioeng. Transl. Med. 8 (2023) e10478.

[145] J.E. Waters, L. Stevens-Cullinane, L. Siebenmann, J. Hess, Recent advances in the development of metal complexes as antibacterial agents with metal-specific modes of action, Curr. Opin. Microbiol. 75 (2023) 102347.

[146] V.K. Vashistha, A. Kumar, P. Tevatia, D.K. Das, Synthesis, characterization, electrochemical and antimicrobial studies of Iron(II) and nickel(II) macrocyclic complexes, Russ. J. Electrochem. 57 (2021) 348.

[147] V. Sharma, V.K. Vasistha, D.K. Das, Biological and electrochemical studies of macrocyclic complexes of iron and cobalt, Biointerface Res. Appl. Chem. 11 (2021) 7393–7399.

[148] V. Sangwan, D.P. Singh, *In-vitro* DNA binding and antimicrobial studies of trivalent transition metal ion based macrocyclic complexes, Vietnam J. Chem. 57 (2019) 543–551.

[149] R.M. ne'e Chopra, Anti-fungal properties of synthesized complexes of trivalent transition metal ions derived from Indan-1,3-dione and diaminobenzene, Rasayan J. Chem. 11 (2018) 694–701.

[150] P. Jain, V. Singh, S. Ali, V. Tripathi, U. Saraswat, Synthesis molecular docking and biological activity of 5,6-bis-(4-fluorophenyl)-3,4,7,8-tetraazabicyclo[8.3.1]-tetradeca-1(13),4,6,10(14),11-pentaene-2,9-dione and its transition metal complexes, J. Saudi Chem. Soc. 22 (2018) 546–557.

[151] M. Krstić, B. Petković, M. Milčić, D. Mišić, J.F. Santibanez, Synthesis, characterization and biological study of new dinuclear zinc(II) and nickel(II) Octaaza macrocyclic complexes, Maced. J. Chem. Chem. Eng. 38 (2019) 1–11.

[152] A. Sakthivel, B. Thangagiri, N. Raman, J. Joseph, R. Guda, M. Kasula, L. Mitu, Spectroscopic, SOD, anticancer, antimicrobial, molecular docking and DNA binding properties of bioactive VO(IV), cu(II), Zn(II), co(II), Mn(II) and Ni(II) complexes obtained from 3-(2-hydroxy-3-methoxybenzylidene)pentane-2,4-dione, J. Biomol. Struct. Dyn. 39 (2021) 6500–6514.
[153] P. Rajakkani, A. Alagarraj, S.A.G. Thangavelu, Tetraaza macrocyclic Schiff base metal complexes bearing pendant groups: synthesis, characterization and bioactivity studies, Inorg. Chem. Commun. 134 (2021) 108989.
[154] V. Sangwan, D.P. Singh, Template-engineered metal macrocyclic complexes: synthesis and biological activity, J. Chin. Chem. Soc. 67 (2020) 1024–1031.
[155] V.K. Vashistha, A. Kumar, Kinetic and biological studies of nickel(II) and copper (II) macrocyclic complexes, Russ. J. Inorg. Chem. 66 (2021) 834–838.
[156] C. Maurya, S. Bajpai, P.K. Kushwaha, U. Chand, S. Singh, Synthesis, characterization and in vitro antimicrobial activity of Organotellurium decorated 10-membered Tetraazamacrocyclic complexes of cobalt(II), Asian J. Chem. 36 (2024) 1056–1060.
[157] O.A. El-Gammal, S.A. El-Brashy, G.M. Abu El-Reash, Macrocyclic Cr^{3+}, Mn^{2+} and Fe^{3+} complexes of a mimic SOD moiety: design, structural aspects, DFT, XRD, optical properties and biological activity, Appl. Organomet. Chem. 34 (2020) e5456.
[158] M. Kamboj, D.P. Singh, A.K. Singh, D. Chaturvedi, Molecular modeling, in-silico docking and antibacterial studies of novel template wangled macrocyclic complexes involving Isatin moiety, J. Mol. Struct. 1207 (2020) 127602.
[159] S. Hajari, H. Keypour, M.T. Rezaei, S.H.M. Farida, R.W. Gable, New 15-membered macrocyclic Schiff Base ligand; synthesis some Cd(II), Mn(II) and Zn(II) complexes, crystal structure, cytotoxicity, antibacterial and antioxidant activity, J. Mol. Struct. 1251 (2022) 132049.
[160] S. Ali, V. Singh, P. Jain, V. Tripathi, Synthesis, antibacterial, anticancer and molecular docking studies of macrocyclic metal complexes of Dihydrazide and Diketone, J. Saudi Chem. Soc. 23 (2019) 52–60.
[161] H. Roy, M. Deolalkar, A. Desai, Synthesis of calix-salen silver corates for evaluation of their antimicrobial and anticancer activities. ACS, Omega 4 (2019) 21346–21352.
[162] K. Wang, K. Chen, T.J. Prior, X. Feng, C. Redshaw, Pd-immobilized Schiff Base double-layer macrocycle: synthesis, structures, peroxidase mimic activity, and antibacterial performance, ACS Appl. Mater. Interfaces 14 (2022) 1423–1433.
[163] L. Cardo, I. Nawroth, P. Cail, J. McKeating, M. Hannon, Metallo supramolecular cylinders inhibit HIV-1 TAR-TAT complex formation and viral replication in cellulo, Sci. Rep. 8 (2018) 13342.
[164] M. Spain, J.K.H. Wong, G. Nagalingam, J.M. Batten, E. Hortle, S.H. Oehlers, X. F. Jiang, H.E. Murage, J.T. Orford, P. Crisologo, J.A. Triccas, P.J. Rutledge, M. H. Todd, Antitubercular bis-substituted cyclam derivatives: structure/activity relationships and *in vivo* studies, J. Med. Chem. 61 (2018) 3595–3608.
[165] J. Zhang, Y. Yu, M.A. Mekhail, H. Wu, K.N. Green, A macrocyclic molecule with multiple antioxidative activities protects the lens from oxidative damage, Front. Chem. 10 (2022) 996604.
[166] N.D. Saha, S. Pradhan, R. Sasmal, A. Sarkar, C.M. Berač, J.C. KÖlsch, M. Pahwa, S. Show, Y. Rozenholsc, Z. TopÇu, V. Alessandrini, J. Guibourdenche, V. Tsatsaris, N. Gagey-Eilstein, S.S. Agasti, Cucurbit[7]uril macrocyclic sensors for optical fingerprinting: predicting protein structural changes to identifying disease-specific amyloid assemblies, J. Am. Chem. Soc. 144 (2022) 14363–14379.
[167] K. Chen, Z.-Q. Zhu, M.-H. Zhang, X. Yang, J. Li, C. Chen, C. Redshaw, 4,4′-Biphenyldisulfonic acid induced coordination polymers of symmetrical tetramethyl cucurbit[6]uril with alkaline-earth metals for detection of antibiotics, CrystEngComm 25 (2023) 961–970.
[168] X. Dai, X. Zhou, C. Liao, Y. Yao, Y. Yu, S. Zhang, A nanodrug to combat cisplatin-resistance by protecting cisplatin with *p*-sulfonatocalix[4]arene and regulating glutathione S-transferases with loaded 5-fluorouracil, Chem. Commun. 55 (2019) 7199–7202.
[169] M. Rahimi, R. Karimian, E.B. Noruzi, K. Ganbarov, M. Zarei, F.S. Kamounah, B. Yiusefi, M. Bastami, M. Yousefi, H.S. Kafil, Needle-shaped amphoteric calix[4] arene as a magnetic nanocarrier for simultaneous delivery of anticancer drugs to the breast cancer cells, Int. J. Nanomedicine 14 (2019) 2619–2636.
[170] C. Mehra, R. Gala, A. Kakatkar, V. Kumar, R. Khurana, S. Chatterjee, N.N. Kumar, N. Barooah, A.C. Bhasikuttan, J. Mohanty, Cooperative enhancement of antibacterial activity of sanguinarine drug through p-sulfonatocalix[6]arene functionalized silver nanoparticles, Chem. Commun. 55 (2019) 14275–14278.
[171] L. Yue, C. Sun, C.H.T. Kwong, R. Wang, Cucurbit[7]uril-functionalized magnetic nanoparticles for imaging-guided cancer therapy, J. Mater. Chem. B 8 (2020) 2749–2753.
[172] Y. Ahn, Y. Jang, N. Selvapalam, G. Yun, K. Kim, Supramolecular Velcro for reversible underwater adhesion, Angew. Chem. Int. Ed. 52 (2013) 3140–3144.
[173] Y.-F. Ding, C.H.T. Kwong, S. Li, Y.-T. Pan, J. Wei, L.-H. Wang, G.S.P. Mok, R. Wang, Supramolecular nanomedicine derived from cucurbit[7]uril-conjugated nano-graphene oxide for multi-modality cancer therapy, Biomater. Sci. 9 (2021) 3804–3813.
[174] P. Xu, Q. Feng, X. Yang, S. Liu, C. Xu, L. Huang, M. Chen, F. Liang, Y. Cheng, Near infrared light triggered cucurbit[7]uril-stabilized gold nanostars as a supramolecular nanoplatform for combination treatment of cancer, Bioconjug. Chem. 29 (2018) 2855–2866.
[175] M. Özkan, S.E. Hadi, I. Tunc, Y. Midilli, B. Ortac, D. Tuncel, Cucurbit[7]uril-capped hybrid conjugated oligomer-gold nanoparticles for combined photodynamic-photothermal therapy and cellular imaging, ACS Appl. Polym. Mater. 2 (2020) 3840–3849.
[176] J. Chen, Q. Huang, Q. Wang, Y. Ding, S. Lu, L.-H. Wang, S. Li, R. Wang, Supramolecular Luminol–AIEgen nanoparticles for deep-tissue-inflammation imaging, ACS Appl. Nano Mater. 5 (2022) 5993–6000.
[177] Y.-F. Ding, X. Xu, J. Li, Z. Wang, J. Luo, G.S.P. Mok, S. Li, R. Wang, Hyaluronic acid-based supramolecular nanomedicine with optimized ratio of oxaliplatin/chlorin e6 for combined chemotherapy and O_2-economized photodynamic therapy, Acta Biomater. 164 (2023) 397–406.
[178] H. Qiao, J. Jia, H. Shen, S. Zhao, E. Chen, W. Chen, B. Di, C. Hu, Capping silica nanoparticles with tryptophan-mediated cucurbit[8]uril complex for targeted intracellular drug delivery triggered by tumor-overexpressed IDO1 enzyme, Adv. Healthc. Mater. 8 (2019) 1900174.
[179] S. Gandhi, P. Shende, Cyclodextrins-modified metallic nanoparticles for effective cancer therapy, J. Control. Release 339 (2021) 41–50.
[180] A. Karthic, A. Roy, J. Lakkakula, S. Alghamdi, A. Shakoori, A.O. Babalghith, T. Bin Emran, R. Sharma, C.M.G. Lima, B. Kim, M.N. Park, S.Z. Safi, R.S. de Almeida, H.D.M. Coutinho, Cyclodextrin nanoparticles for diagnosis and potential cancer therapy: a systematic review, Front. Cell Dev. Biol. 10 (2022) 984311.
[181] T. Mortezazadeh, E. Gholibegloo, N.R. Alam, S. Dehghani, S. Haghgoo, H. Ghanaati, M. Khoobi, Gadolinium (III) oxide nanoparticles coated with folic acid-functionalized poly(β-cyclodextrin-co-pentetic acid) as a biocompatible targeted nanocontrast agent for cancer diagnostic: *in vitro* and *in vivo* studies, Magn. Reson. Mater. Phys. Biol. Med. 32 (2019) 487–500.
[182] Y. Wang, H. Guo, Y. Zhang, F. Tai, Y. Wang, Q. Dong, Y. Nie, Q. Zhao, W.-Y. Wong, Achieving highly water-soluble and luminescent gold nanoclusters modified by β–cyclodextrin as multifunctional nanoprobe for biological applications, Dyes Pigments 157 (2018) 359–368.
[183] F.B. Barlas, E. Aydindogan, M. Arslan, S. Timur, Y. Yagci, Gold nanoparticle conjugated poly(p-phenylene-β-cyclodextrin)-graft-poly(ethylene glycol) for theranostic applications, J. Appl. Polym. Sci. 136 (2019) 47250–47257.
[184] X. Xu, Z. Zeng, J. Chen, B. Huang, Z. Guan, Y. Huang, Z. Huang, C. Zhao, Tumor-targeted supramolecular catalytic nanoreactor for synergistic chemo/chemodynamic therapy via oxidative stress amplification and cascaded Fenton reaction, Chem. Eng. J. 390 (2020) 124628.
[185] L. Fan, X. Wang, Q. Cao, Y. Yang, D. Wu, POSS-based supramolecular amphiphilic zwitterionic complexes for drug delivery, Biomater. Sci. 7 (2019) 1984–1994.
[186] Y. Qin, F. Tong, W. Zhang, Y. Zhou, S. He, R. Xie, T. Lei, Y. Wang, S. Peng, Z. Li, J. Leong, H. Gao, L. Lu, Self-delivered supramolecular nanomedicine with transformable shape for ferrocene-amplified photodynamic therapy of breast cancer and bone metastases, Adv. Funct. Mater. 31 (2021) 210464.
[187] Q.-L. Li, Y. Sun, L. Ren, X. Wang, C. Wang, L. Li, Y.-W. Yang, X.-H. Yu, J.-H. Yu, Supramolecular nanosystem based on pillar[*n*]arenes-capped CuS nanoparticles for targeted chemophotothermal therapy, ACS Appl. Mater. Interfaces 10 (2018) 29314–29324.
[188] J. Yang, D. Dai, X. Lou, L. Ma, B. Wang, Y.W. Yang, Supramolecular nanomaterials based on hollow mesoporous drug carriers and macrocycle-capped CuS nanogates for synergistic chemo-photothermal therapy, Theranostics 10 (2020) 615–629.
[189] C. Liu, M. Li, P. Li, Y. Bai, J. Pang, L. Fan, W. Tian, Ruthenium(II)-coordinated supramolecular metallodrug complex realizing oxygen self-supply in situ for overcoming hypoxic tumors, Adv. Funct. Mater. 31 (2021) 2105837.
[190] K. Wang, C. Redshaw, X. Zhao, A. Wang, K. Chen, Y. Qiao, Silver nanoparticle-immobilized Schiff-Base macrocycles as nanozymes with peroxidase mimic activity for antibacterial films, ACS Appl. Nano Mater. 7 (2024) 16274–16282.
[191] D. Sun, Recent advances in macrocyclic drugs and microwave-assisted and/or solid-supported synthesis of macrocycles, Molecules 27 (2022) 1012.
[192] C. Wu, C.-Z. Wang, Q. Zhu, X. Zeng, C. Redshaw, T. Yamato, Click synthesis of a quinoline-functionalized hexahomotrioxacalix[3]arene: A turn-on fluorescent sensor for Fe^{3+}, Sensors Actuators B Chem. 254 (2018) 52–58. See for example.
[193] M. Liu, R. Cen, J.-H. Lu, T.-H. Meng, C.-R. Li, C. Redshaw, T.J. Prior, Z. Tao, X. Xiao, Novel carbon dots based on cucurbit[6]uril for recognizing *L*-Tryptophan and Capecitabine, Mat. Chem. Front. 6 (2022) 2859–2868. See for example.
[194] D.G. Jimenez, V. Poongavanam, J. Kihberg, Macrocycles in drug discovery – learning from the past for the future, J. Med. Chem. 66 (2023) 5377–5396.
[195] L. Wang, J. Han, R. Pan, X. Yuan, Y. You, X. Cen, Q. Zhang, Q. Ge, H. Cong, M. Liu, Synthesis of hybrid thiohemicucurbiturils, Tetrahedron Lett. 101 (2022) 153918. See for example.
[196] Plexixafor (Brand Name Mozobil) Was Developed by AnorMED (Purchased by Genzyme) and Is Utilized to Mobilize Hematopoietic Stem Cells, 2024.
[197] Loriatinib (Brand Name Lorbrena) Was Developed by Pfizer and Is Employed as an Anti-cancer Drug, 2024.
[198] Pacritnib (Brand Name Vonjo) Was Developed by CTI Biopharm and Is Used to Treat Myelofibrosis, 2024.
[199] Zotiraciclib (Also Known as TG02, SB1317) Has Being Evaluated by Adastra Pharmaceuticals for Brain Cancers, 2024.
[200] D.G. Jimenez, V. Poongavanam, J. Kihlberg, Macrocycles in drug discovery – learning from the past for the future, J. Med. Chem. 66 (2023) 5377–5396.
[201] K. Kingswell, Macrocycle drugs serve up new opportunities, Natl. Rev. 22 (2023) 771–773.
[202] S. An, L. Wang, F. Xie, D. Jiang, G. Huang, J. Liu, X. Ma, W. Wei, Pathway to approval of innovative radiopharmaceuticals in China, J. Nucl. Med. 65 (2024) 72S–76S.
[203] P.J. Salveson, A.P. Moyer, M.Y. Said, G. Gökçe, X. Li, A. Kang, H. Nguyen, A. K. Bera, P.M. Levine, G. Bhardwaj, D. Bake, Expansive discovery of chemically diverse structured macrocyclic oligoamides, Science 384 (2024) 420–428.